Trust & Quality

Inspecta

INSPECTA

TECHNICAL REPORT

SKB

Probabilistic analysis of BWR canister inserts for spent nuclear fuel in the case of an earthquake induced rock shear load

Report No.: 50014130-1

Revision No.: 5

Inspecta

TECHNICAL REPORT

Report No.: 50014130-1   Revision No.: 5

Date	Our project No.
2014-03-13	50014130
Approved by	**Organizational unit**
Keivan Ashhami	Inspecta Technology AB
Customer	**Customer reference**
SKB	Mikael Jonsson

Summary

In this report a probabilistic analysis of canister inserts for spent nuclear fuel, that is subjected to an earthquake induced rock shear through a deposition hole, is presented. The analysis is performed using BWR data (canister insert geometry and material data). First, the important parameters that influence the calculated failure probabilities are identified. Then, a probabilistic analysis is performed for a postulated defect in the region of the insert that experiences the highest impact of a shear movement. These results are subsequently scaled so that results representative for an entire insert are obtained.

A large benefit when conducting a probabilistic analysis is the fact that it is possible to investigate the dependence of the different probabilistic parameters included in the analysis. Several sensitivity studies are presented in order to investigate what parameter that contributes the most to the calculated probability. Also a comparison is made using defect distributions and fracture toughness data from PWR-inserts.

The main conclusions from this study are:
- If the bentonite density is treated as a probabilistic parameter, its importance decreases as compared with the deterministic damage tolerance analysis.
- The shear plane position has no dominant contribution in the probabilistic analysis.
- Assumptions regarding the shear displacement have a large impact on the analysis.
  - When the shear displacement is treated as a deterministic parameter, the fracture toughness and defect size contributes the most to the calculated probabilities.
  - When the shear displacement is treated as a probabilistic parameter, the shear displacement and defect size contributes the most to the calculated probabilities.
- The probability of global plastic collapse is much smaller than the probability of initiation of crack growth and the probability of 2 mm stable crack growth.
- The probability of failure of an insert, using a rock shear displacement of 5 cm, is between $5.8 \cdot 10^{-4}$ and $2.2 \cdot 10^{-3}$.
- The calculated probabilities are much lower using defect distributions and fracture toughness data from PWR-inserts as compared to BWR-inserts.

Report title	
Probabilistic analysis of BWR canister inserts for spent nuclear fuel in the case of an earthquake induced rock shear load	**Index terms**

Work carried out by	Distribution
Peter Dillström, Lars Alverlind	☒ No distribution without permission from the customer or Inspecta Technology AB.
Work verified by	☐ Limited internal distribution in Inspecta Technology AB.
Andrey Shipsha	☐ Unrestricted distribution.

Table of content *Page*

1   INTRODUCTION

Nuclear waste in Sweden is handled by the Swedish Nuclear Fuel and Waste Management Co, SKB. Several decades of research and development has led SKB to put forward the KBS-3 method for the final stage of the spent nuclear fuel management. In this method, copper canisters with a cast iron insert containing spent nuclear fuel are surrounded by bentonite clay and deposited in saturated, granitic rock, see Fig. 1-1.
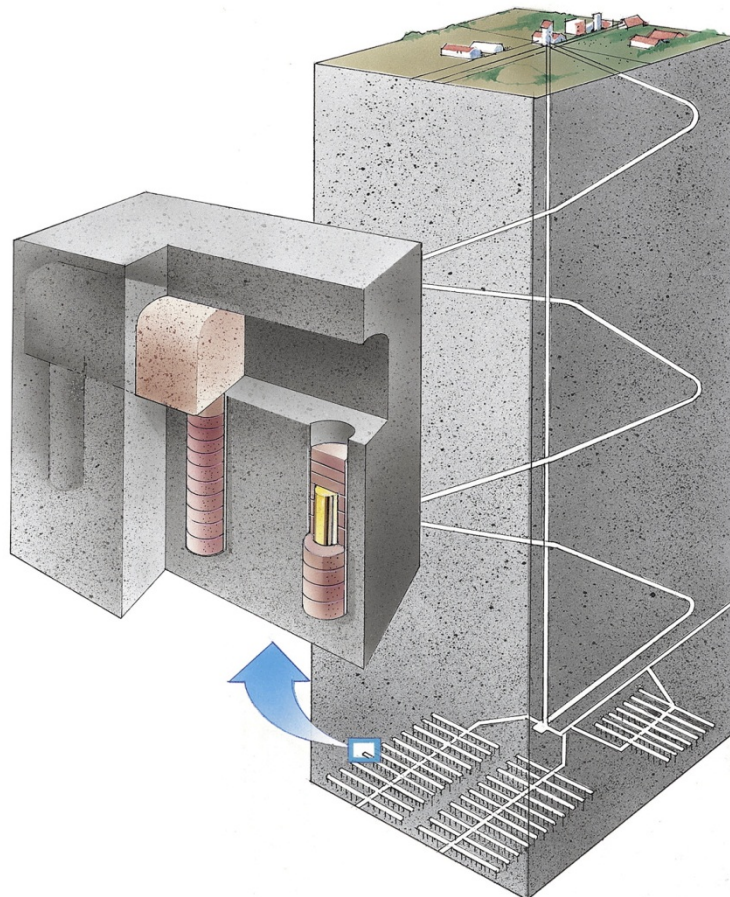
Figure 1-1. SKB has applied for building a deep repository for all spent nuclear fuel.

The primary safety function of the KBS-3 system is to completely contain the spent nuclear fuel within copper canisters over the entire assessment period. Should a canister be damaged, the secondary safety function is to retard any releases from the canisters. This report concerns one aspect of the containment function related to the cast iron insert.

The canister consists of a pressure-bearing insert of nodular iron with a steel lid, Fig. 1-2. The insert contains channels for the fuel assemblies, 12 in the BWR version and 4 in the PWR version. The insert is surrounded by an outer corrosion barrier of copper. More detailed information about the canister geometry is given in [1]. In the repository, the canisters will be mechanically loaded by the hydrostatic pressure and the swelling pressure from the surrounding bentonite. During the extreme time scales, several ice ages are expected resulting in an additional pressure on the canister. The maximum pressure for the KBS-3 canisters is 45 MPa [1].

Figure 1-2. Canister for final repository of spent nuclear fuel.

For the licensing procedures of repositories for spent nuclear fuel safety analyses are performed. Among other items it is required to obtain an estimate of the probability of mechanical failure of canisters by considering the effects of a possible ice load and also the possibility of shearing of the bedrock. A probabilistic analysis of canister inserts subjected to a maximum hydrostatic pressure during an ice load has been presented earlier [2].

In the present report a probabilistic analysis of canister inserts for spent nuclear fuel, subjected to an earthquake induced rock shear through a deposition hole is presented. The analysis is performed using BWR data (canister insert geometry and material data) as given in Sect. 2. The first part of the study is a probabilistic analysis done for a postulated defect in the region of the insert that experiences the highest impact of a shear movement (presented in Sect. 5-7). These results are subsequently scaled so that results representative for an entire insert are obtained (presented in Sect. 8).

2 PARAMETERS TO BE INCLUDED IN THE ANALYSIS

When performing a probabilistic analysis of the BWR canister inserts subjected to a shear load, the important parameters that influence the calculated failure probabilities should be identified. Within this project, a pilot study was performed [3], and it was decided that the following parameters should be investigated further.

The BWR insert material data (nodular cast iron)
- Fracture toughness
- Yield stress
- Ultimate tensile strength
- Elongation at fracture

Defects and nondestructive testing
- BWR defect distribution of crack like defects
- Probability of detecting a defect

The surrounding bentonite
- Type of bentonite
- The bentonite density

Loading
- The size of the rock shear displacement
- The velocity of the rock shear displacement
- The angle of the rock shear plane
- The position of the rock shear plane
- The thickness of the ice sheet

These parameters are described in more detail below.

2.1 The insert material – Fracture toughness

SKB has, over the years, performed several tests to determine the fracture toughness of the insert. The test series conducted in 2003-2004, which was used in the probabilistic analysis with an isostatic pressure load [2], are not characteristic of the insert fracture toughness experienced today. The most representative test series for the BWR inserts was conducted in 2009, and evaluation of this test series are found in [4]. In these cases the fracture mechanics tests exhibited very ductile behavior with rising J_r-curves. In this study, fracture toughness data at 0°C will be used and both initiation values (J_{Ic}) and value at 2 mm stable crack growth (J_{2mm}) are presented in [4]. These data are taken from the inserts I54, I55 and I57 and a total of 25 values are used in the data evaluation. Regarding the fracture toughness in the ductile region a normal distribution is commonly used [5].

Initiation fracture toughness data to be used in the probabilistic analysis [4]:
- Mean value = 34.4 kN/m
- Standard deviation = 4.15 kN/m
- Distribution = Normal [5] (see Fig. 2-1)

Figure 2-1. Initiation fracture toughness data and chosen distribution.

Fracture toughness data at 2 mm stable crack growth to be used in the probabilistic analysis [4]:
- Mean value = 90.8 kN/m
- Standard deviation = 7.87 kN/m
- Distribution = Normal [5] (see Fig. 2-2)
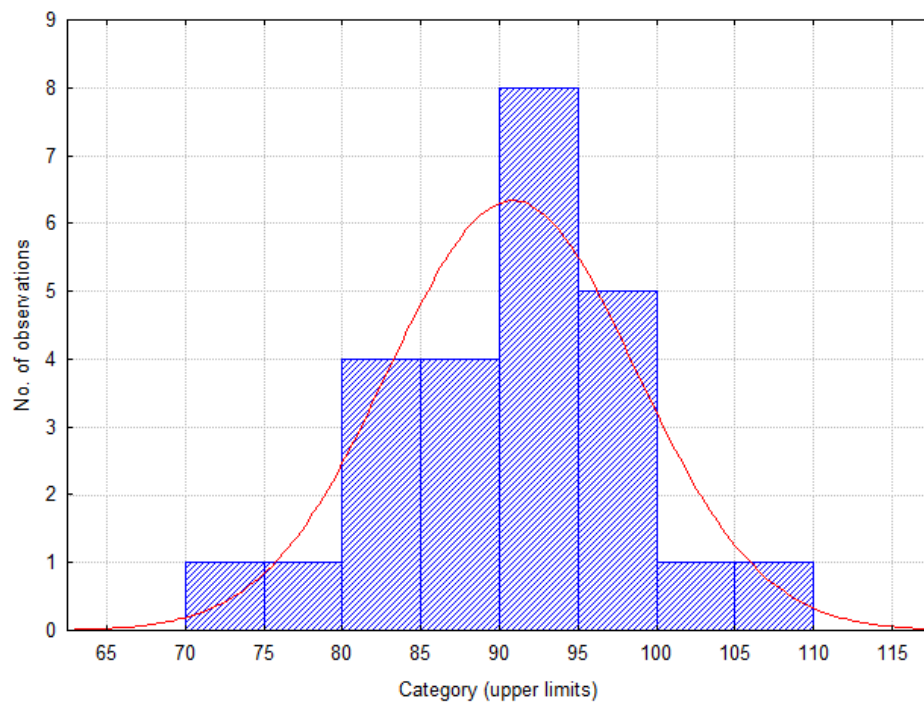
Figure 2-2. Fracture toughness data and chosen distribution at 2mm stable crack growth.

2.2   The insert material – Yield stress and ultimate tensile strength

SKB has, over the years, performed many tensile (and compression) tests of the insert. The test series conducted in 2003-2004, which was used in the probabilistic analysis with an isostatic pressure load [2], are not characteristic of the insert today. More recent tests show that the scatter of the tensile data has reduced considerably. The most representative test series for the BWR inserts are data from the inserts I53, I54, I55, I56, I57 and I63 (manufactured in 2007). A summary of the test results and an analysis of these data are given in [6]. For the probabilistic analysis, room temperature data are used (more pessimistic than using data at 0°C). Also data from tensile tests of the middle section (in the axial direction) of the inserts are used (this part of the insert has large tensile stress/strains in the case of a shear load), giving a total of 36 values that are used in the data evaluation. The tensile data given in Table 2 in [6] are engineering stress/strain data and these data are converted to true stress/strain data that are used in the FE-analysis of an earthquake induced rock shear displacement.

Yield stress data to be used in the probabilistic analysis (true stress):
- Mean value = 280.4 MPa
- Standard deviation = 6.77 MPa
- Distribution = Normal [5] (see Fig. 2-3)
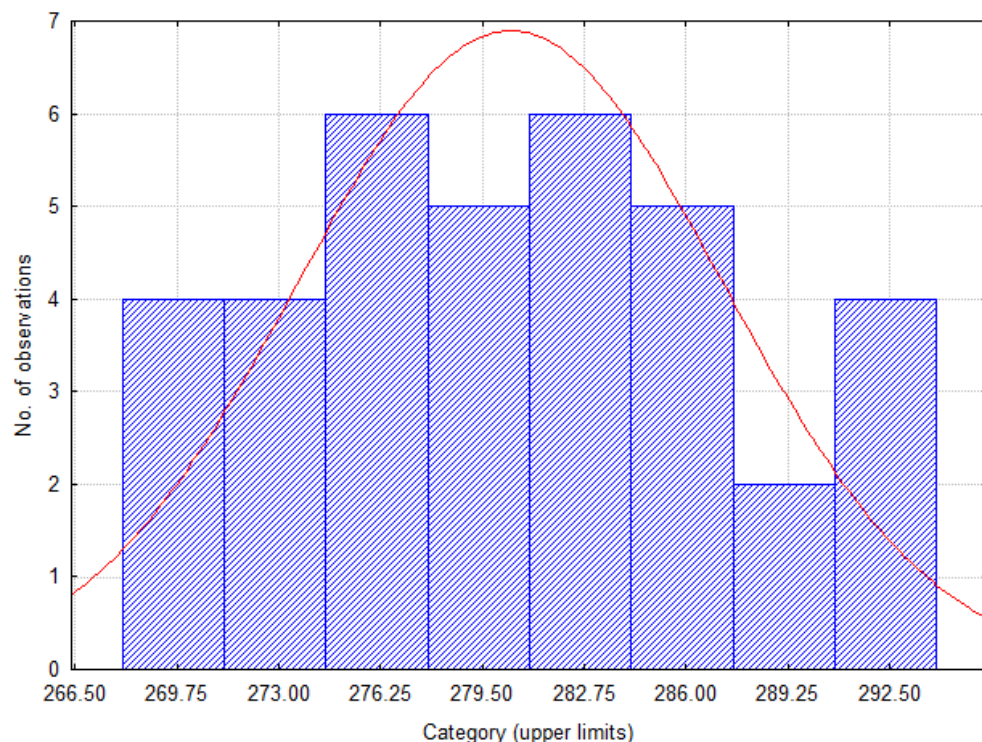
Figure 2-3. Yield stress data and chosen distribution.

Ultimate tensile strength data to be used in the probabilistic analysis (true stress):
- Mean value = 448.8 MPa
- Standard deviation = 6.39 MPa
- Distribution = Normal [5] (see Fig. 2-4)

Ultimate tensile strength is given at 12.1% true strain (the mean value from the data).
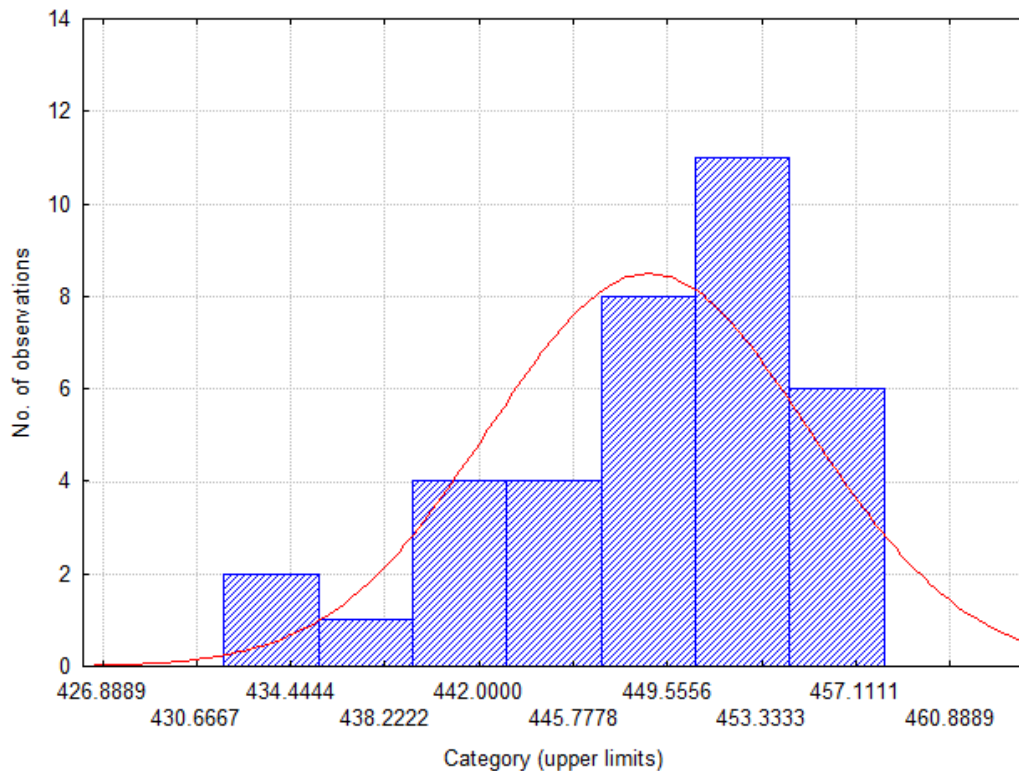
Figure 2-4. Ultimate tensile strength data and chosen distribution.

In order to perform the FE-analysis, a complete (true) stress/strain-curve is needed. The mean value curve is given in Table 2-1. In the FE-analysis, other values for the stress/strain-curve are also needed as given in Sect. 3.4.1 (by using a linear scaling procedure as defined in [7]).

Table 2-1. Mean value stress/strain-curve for the nodular cast iron material.

True strain, ε_{true} [%]	True stress, σ_{true} [MPa]
0.0000	0.0000
0.16900	280.40
1.9800	322.60
3.9200	361.00
5.8300	392.30
7.7000	414.60
9.5300	431.50
12.100	448.80

In Table 2-1 true stress versus true strain are given for the nodular cast iron material. The finite element code ABAQUS, which was used for the calculations, needs data for true stress (σ_{true}) versus true plastic strain (ε_{pl}). The latter are calculated using the relation $\varepsilon_{pl} = \varepsilon_{true} - \sigma_{true}/E$.

2.3 The insert material – Elongation at fracture

As stated above, the most representative test series for the BWR inserts are data from the inserts I53, I54, I55, I56, I57 and I63. A summary of the test results and an analysis of these data are given in [6].

Elongation at fracture data to be used in the probabilistic analysis (true strain):

- Mean value = 14.8%
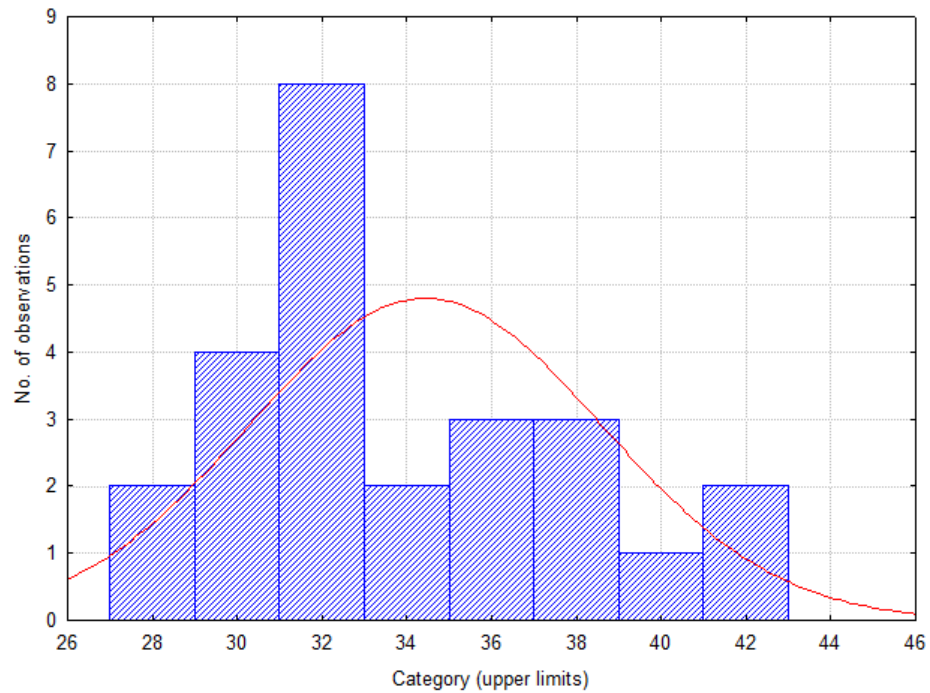- Standard deviation = 1.57%
- Distribution = Normal [5] (see Fig. 2-5)
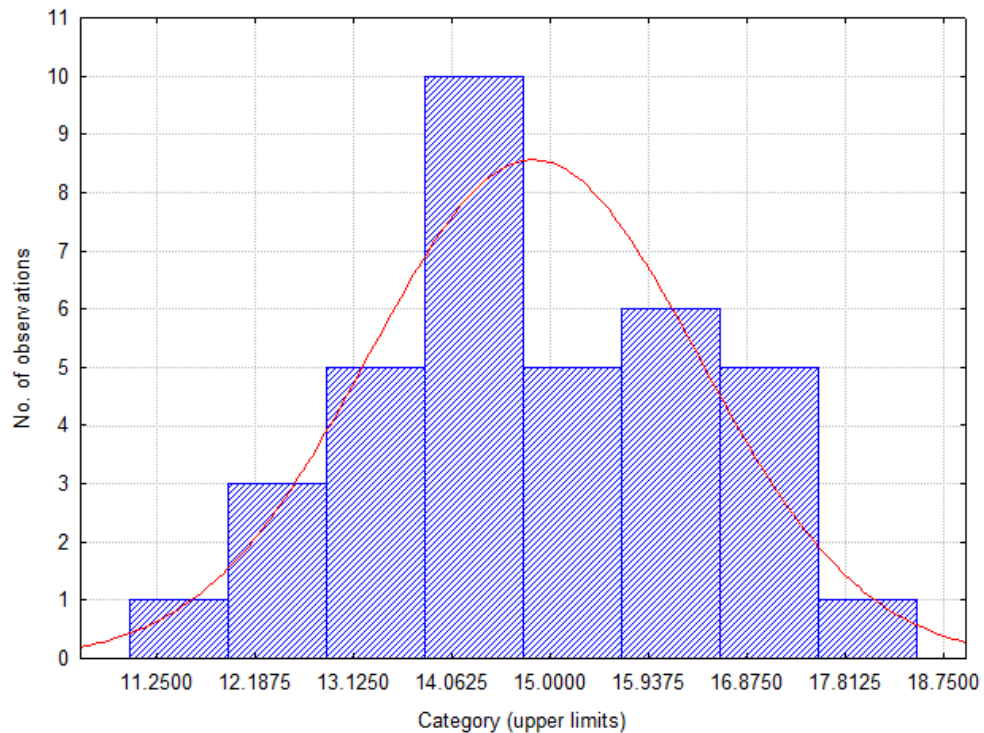
Figure 2-5. Elongation at fracture data and chosen distribution.

2.4 The insert material – Defect depth distribution of crack like defects

SKB has, over the years, performed many tensile (and compression) tests of the different inserts. SKB has also conducted an extensive fractographic and metallographic study on broken test specimens to check for defects. The test series conducted in 2003-2004, from which results were used in the probabilistic analysis with an isostatic pressure load [2], are not characteristic of the insert today. More recent tests show that the number of large defects has reduced considerably.

SKB has performed a new investigation using fracture surfaces on broken test specimens of the inserts I53, I54, I55, I56, and I57 [8-10]. These defect data are used to develop a new defect distribution that more realistically reflects the nodular cast iron material of today. This is presented in [11] and summarized below.

In this investigation all the defects were identified as being either porosity defects or graphite/dross defects. For all the defects an ellipse was drawn surrounding the defect and the major and minor axis of the ellipse were measured. Porosity defects were not considered to be crack like defects. However, graphite/dross defects were considered to be crack like defects.

To check these assumptions the size of porosity defects (given as defect area) were plotted against the elongation at fracture for the test specimens where porosity defects were found on the fracture surface (Figure 2-7). Also, the size of graphite/dross defects (given as defect area) was plotted against the elongation at fracture for the test specimens where graphite/dross defects were found on the fracture surface (Figure 2-7).
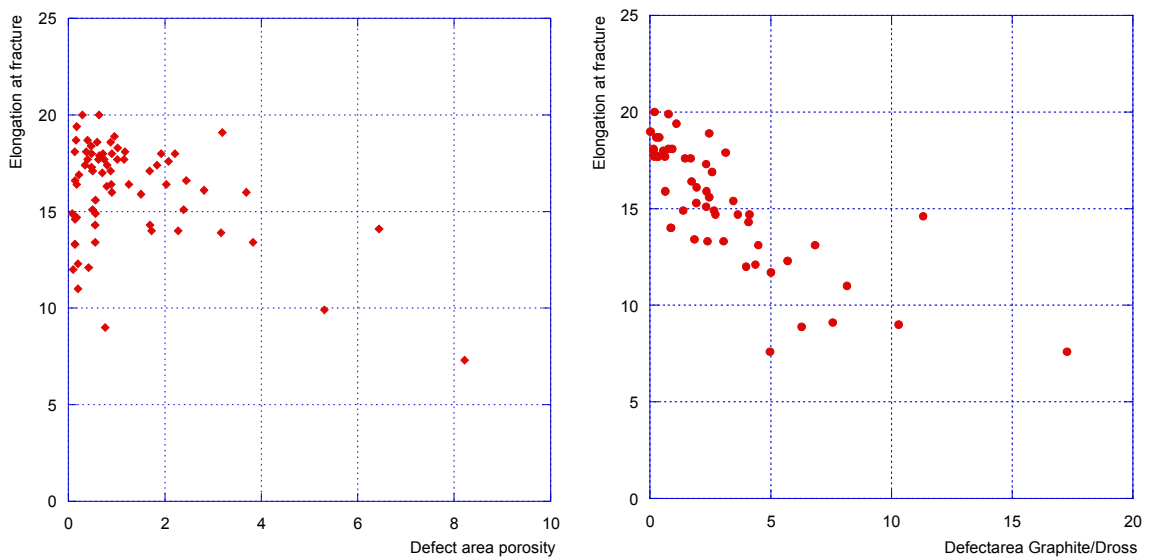
Figure 2-7. The elongation at fracture plotted against the defect area for porosity defects or the defect area for graphite/dross defects.

As shown in Figure 2-7, the area for porosity defects has a weak correlation with the elongation at fracture. The area for graphite/dross defects has a much better correlation with the elongation at fracture. This indicates that graphite/dross defects should be included when developing a new defect distribution for crack like defects (a simplification of what can be seen on the fracture surfaces). This type of defect was also considered relevant when a defect distribution was developed for the probabilistic analysis with an isostatic pressure load [2].

In the probabilistic analysis, a crack-like defect is postulated to exist in the region of the insert that experiences the highest impact of a shear movement. The size (depth) of this defect is characterized by an exponential distribution (same assumption as in the earlier study [2]). In order to simplify the analysis it was assumed that the defect is surface breaking, which is more severe than a subsurface defect and therefore a pessimistic assumption (the *J*-value for a surface breaking defect is approximately twice as large as a subsurface defect of the same size).

Defect depth distribution to be used in the probabilistic analysis:

- Defect geometry = a semi-elliptical surface defect
- Defect length/depth = 6

  This assumption is also used in the deterministic damage tolerance analysis [4], which makes it easy to compare results from deterministic and probabilistic analyses. The data given from [8-10] shows that the defect length/depth actually varies between 1.0 and 4.7, so this is a pessimistic assumption.

- Defect depth (mean value) = 1.3 mm
- Defect depth distribution = Exponential (see Fig. 2-8)
- The model assumes the existence of one crack-like defect; a simple scaling argument is applied to consider the number of defects at the surface of the insert, see Sect. 8.
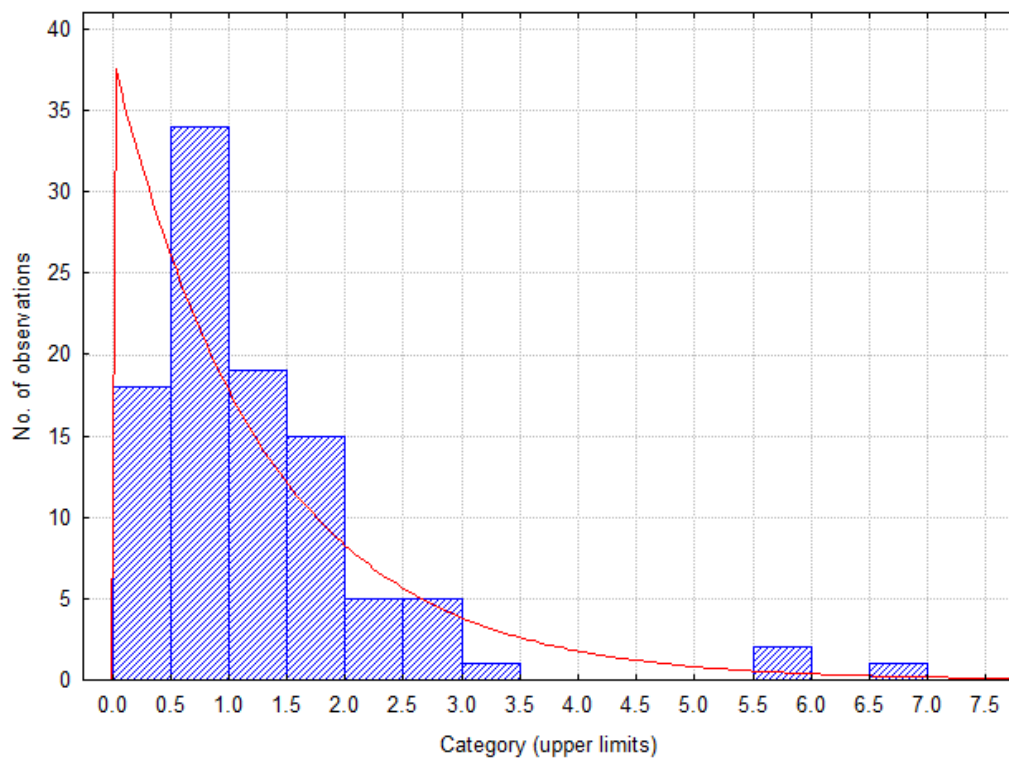
Figure 2-8. Defect (depth) data and the chosen exponential distribution.

The choice of defect depth distribution is quite important when performing a probabilistic analysis; therefore a sensitivity analysis will be performed using either a lognormal or a Weibull defect depth distribution (as recommended in [5]). A comparison between the three distributions is shown in Figure 2-9.
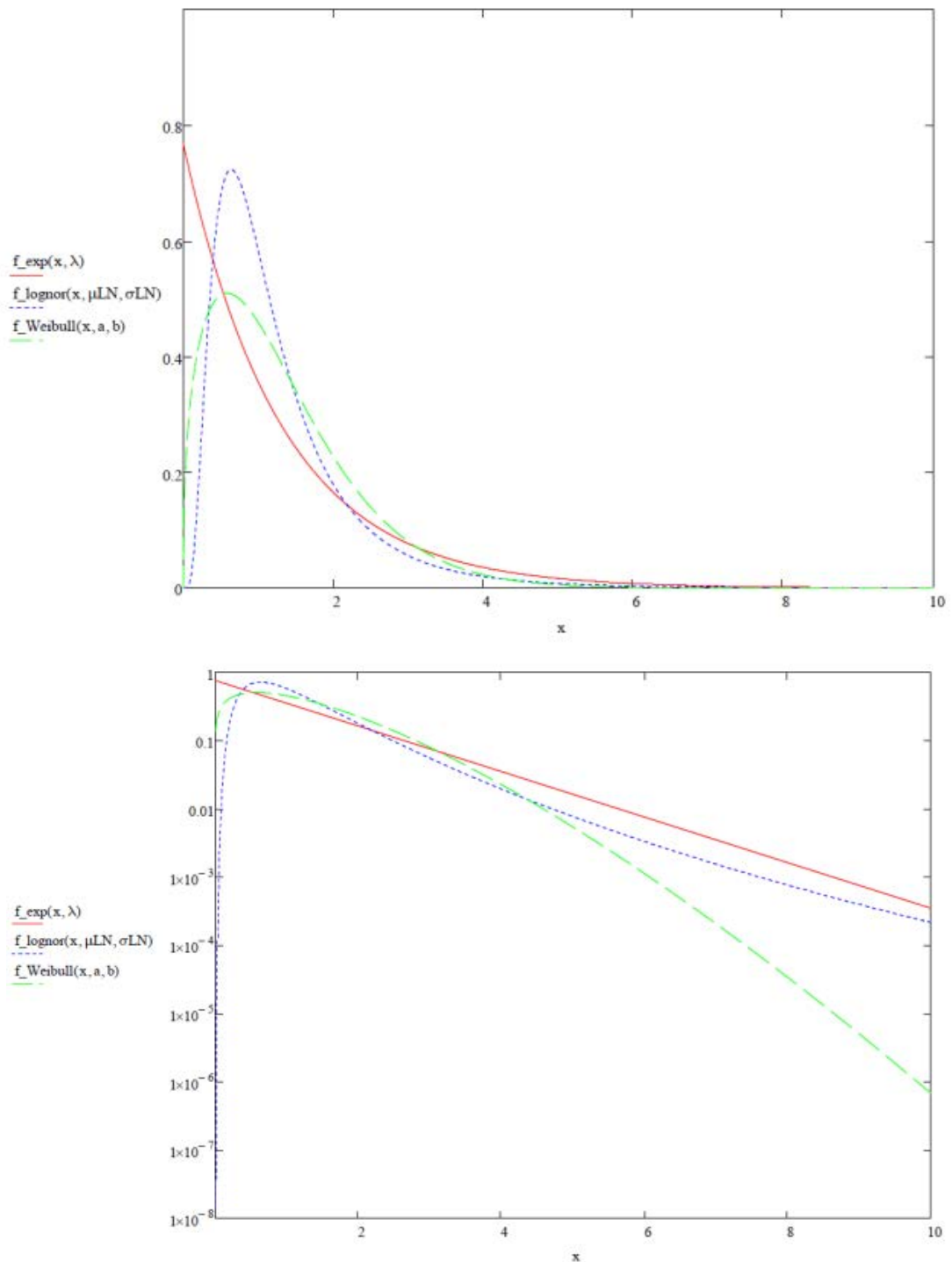
Figure 2-9.   A comparison between exponential, lognormal and Weibull defect depth distribution (linear and logarithmic scale).

As shown in Fig. 2-9, there is only a minor difference between the exponential and lognormal distribution for defects larger than ~1 mm (depth), but a major difference for defects smaller than ~1 mm. The largest difference between the Weibull distribution and the others are that the Weibull distribution differs for defects larger than ~6 mm. However, in practice, the Weibull distribution is seldom used to model crack like defects in materials that does not behave in a brittle manner.

Note: The data on fracture surfaces of the broken test specimens [8-10] has some errors; these are going to be corrected in an upcoming revision of these reports. However, since the difference is small, this will have no significance to the calculation presented in this report.

2.5   The probability of detecting a defect

The effectiveness of the inspection is an important parameter in a probabilistic analysis. A quantitative measure of inspection effectiveness is needed in order to calculate the risk reduction related to inspection. The detection probability is typically presented in the form of POD functions/curves, which describe the detection probability as a function of the defect depth or length.

At present, there is not enough knowledge about the quality of the NDT systems used by SKB. This does not mean that the selected systems are of poor quality, it only means that it has not been quantified. It was therefore decided not to include this parameter in the probabilistic analysis.

Later, when more information is available, it is possible to check the impact of various POD curves on the results. Combined with data on defect distributions, this could yield interesting information about the usefulness of different types of NDT-systems, for how rejection criteria of inserts could be formulated etc.

2.6   The type of bentonite

As all mechanical loads on the canister is transferred through the bentonite buffer, the material properties of bentonite gives important conditions for the analysis of the canister. The design analysis [1] presents the assumptions used in the analysis of the rock shear load. Regarding the type of bentonite, the Na-bentonite which is installed in the repository is later expected to be converted to Ca-bentonite. The properties of the two types of bentonite are different and affect the analysis of the insert and it is pessimistic to use data for Ca-bentonite. In the design analysis it is therefore assumed that all bentonite is converted to Ca-bentonite.

Since all the bentonite is assumed to have been converted to Ca-bentonite this parameter is not considered in the probabilistic analysis.

2.7   The bentonite density

In the design analysis [1], assumptions regarding the bentonite are given. It is stated that the analyzes are completed in the density range 1950 kg/m^3 to 2050 kg/m^3. When the design analysis summarizes the damage tolerance analysis in the form of acceptable defect sizes [1], the density 2050 kg/m^3 is used (which of course is a pessimistic assumption).

In the global FE-analysis [7], the results are related to the bentonite density but the primary characteristics are actually bentonite stiffness and shear strength. These in turn depends on the type of bentonite, density and the current strain rate. Ca-bentonite has higher shear strength than Na-bentonite and shear strength increases with increasing density and increasing strain rate. In the global FE-analysis [7], this has been taken into account by adopting the characteristics of the corresponding Ca-bentonite.

In the production report for the buffer [12], the design basis for the buffer and an explanation of the expected initial state is given. In the report, an evaluation of bentonite properties in a water saturated state is also given. This analysis assumes that the dominant parameter is the variation of the deposition hole diameter (experiences from the Prototype Repository show that the diameter of the deposition hole varies according to a normal distribution). When describing the statistic distribution of a deposition hole drilled in the final repository it is reasonable to assume a mean value of the diameter of 1750 mm and, based on the current experiences, assume a standard deviation of 2.02 mm [12]. Given the conditions of the analysis, the installed bentonite dry density is calculated to be 1577 kg/m^3 (with a standard deviation of 4.72 kg/m^3). The analysis then gives the resulting bentonite density at water saturation to be 2010 kg/m^3 (with a standard deviation of 3.04 kg/m^3). These results should not be considered to be the design condition of the buffer but it may be used as an example of a realistic statistical distribution of the bentonite density. Finally, it should be noted that the above reported density values apply to the cases included in that study [12]. One can, for example, adapt the manufacture of bentonite to obtain an average density of 2000 kg/m^3 (if desired).

Within the project, it was decided that the bentonite density should be treated as a deterministic parameter. It was also decided that it is of interest to study the influence of this parameter and therefore to include the bentonite density in different sensitivity analysis (assumptions regarding data to be used in the analysis are found below).

Bentonite density data to be used in the probabilistic analysis (sensitivity analysis, alternative 1, using data from the production report for the buffer [12]):
- Mean value = 2010 kg/m^3
- Standard deviation = 3.04 kg/m^3
- Distribution = Normal

Bentonite density data to be used in the probabilistic analysis (sensitivity analysis, alternative 2, using a uniform density distribution):
- Mean value = 2000 kg/m^3
- Lower limit = 1950 kg/m^3
- Upper limit = 2050 kg/m^3
- Distribution = Uniform

2.8   The size of the rock shear displacement

The sizes of rock fracture shear movements that are of interest are in the interval 0-10 cm. The upper limit of 10 cm is determined by the fact that larger movements can be excluded in fractures intersecting canisters in the layout for the Forsmark site analyzed in SR-Site. In the safety assessment SR-Site ([23], section 10.4.5), it was demonstrated that the mean number of canisters, out of the total of 6000, that are expected to experience shear movements exceeding 5 cm is less than 0.1. This estimate was, furthermore, based on several pessimistic assumptions. It is a result of the deposition strategy applied in the repository layout used in SR-Site, where several measures are taken to avoid deposition in positions intersected by large fractures thus avoiding detrimental shear movements. Shear movements exceeding 5 cm are thus rare and according to Figure 7-1 in [24] none of the 6000 canister will experience a shear movement exceeding 10 cm for the types of earthquakes that could occur in a one million year perspective at the Forsmark site.

There are two problems with treating this entity as a probabilistic parameter:

1) The real property of interest is the likelihood that a canister experiences a shear movement of a certain size during the one million years the safety assessment considers.

2) This entity was not available as a distribution from SKB when the analysis was undertaken.

According to SKB, it is possible to derive such a distribution. It is, however, a complex task and the basis for its derivation (the understanding of how large earthquakes generate shear movements in fractures intersecting the canister) is still evolving.

Therefore, it was decided that the rock shear displacement should be treated as a deterministic parameter and to calculate most of the probabilities as a function of shear displacements in the interval 0-10 cm. The types of results this yields can later, in other studies, be combined with estimates of fracture shear movements in the repository during the one million years assessment interval, to yield meaningful results for the safety assessment.

In addition, exponential distributions of fracture shear movement sizes with mean values in the range 0.2-3 cm are used for test purposes in a sensitivity analysis in this work.

Rock shear displacement data to be used in a sensitivity analysis:

- Mean value = in the range 0.2 cm to 3 cm.
- Distribution = Exponential

2.9 The velocity of the rock shear displacement

In the design analysis [1], assumptions are presented regarding the rock shear displacement and the following deterministic damage tolerance analysis of the same load case [4]. Studies presented in section 5.4.5 of [24] show that 1 m/s is an upper bound on shear velocities at canister deposition positions for the types of earthquakes that may occur at the Forsmark site. For the reference case the rock shear displacement is therefore assumed to have a velocity of 1 m/s [1]. To check this assumption, a sensitivity analysis was performed, using the velocity 0.1 m/s, which resulted in slightly lower stresses and strains.

Since the assumption regarding the velocity of the rock shear displacement does not affect the analysis to any significant degree, this parameter is not considered in the probabilistic analysis of shear load (all the global FE-analyses are performed with a shear velocity of 1 m/s).

2.10 The angle of the rock shear plane

In the design analysis [1], assumptions are presented regarding the rock shear displacement and the following deterministic damage tolerance analysis of the same load case [4]. The majority of the calculations have been carried out with a shear plane that is perpendicular to the canister axis (also some sensitivity analysis using other angles). When the design analysis summarizes the damage tolerance analysis in the form of acceptable defect sizes [1] the shear plane is assumed to be located perpendicular to the canister axis.

The angle of the rock shear plane is determined by the nature of the several fracture sets at the rock site in question, and of rejection criteria used when selecting deposition positions. For the KBS-3 repository at the Forsmark site analyzed in SR-Site, typically half of the deposition positions experiencing shear movements of 5 cm or larger are intersected by fractures belonging to a horizontal fracture set [14]. Since it was demonstrated in the design analysis [1] that a horizontal fracture orientation is the worst case for the canister, it will be pessimistically assumed that all fractures are horizontal.

Angle of the rock shear plane to be used in the probabilistic analysis:
- The shear plane angle should be perpendicular to the canister axis (in all analyses).

2.11 The position of the rock shear plane

In the design analysis [1], assumptions are presented regarding the rock shear displacement and the following deterministic damage tolerance analysis of the same load case [4]. The analysis is carried out so that the shear plane hits the center of the canister or at a distance of three-quarters of the canister (from the base of the canister). When, in the design analysis, the damage tolerance analysis is summarized in the form of acceptable defect sizes [1, 4], it is assumed that the shear plane hits the canister at a distance of three-quarters of the canister (the design case).

Going back to the design criteria for the repository [13] it is stated that the shear plane position will affect the analysis of shear load (but it says nothing about which positions are most realistic for the repository). However, it is quite obvious that all positions are in principle equally likely and that assumption should be used in a probabilistic analysis.

Shear plane position (in the axial direction) to be used in the probabilistic analysis:
- Mean value = the center of the canister
- Lower limit = the base of the canister
- Upper limit = the top of the canister
- Distribution = Uniform

2.12 The thickness of the ice sheet

When the shear load occurs, the ice sheet may have a certain thickness. This is implied in both the design analysis [1] and in the design criteria for the repository [13]. There is no indication of a realistic ice thickness associated with shear [1, 13]. However, SKB has pointed out that uncertainties in the ice thickness do not need to be further investigated within this project. This is because the combination of a hydrostatic pressure load caused by the ice sheet and a rock shear load are less likely (and the combined load case gives smaller tensile stresses in the insert).

SKB has also pointed out that the assumptions made in the calculations that determine the shear movements in fractures intersecting deposition holes require that the ice has disappeared. To be consistent throughout the analysis process, a zero ice thickness in the probabilistic analysis should therefore be assumed (and this parameter is therefore not considered in the analysis.).

3 PROBABILISTIC ANALYSIS IN THE CASE OF A ROCK SHEAR LOAD

3.1 Definition of critical event

To carry out a probabilistic analysis of a rock shear load, a critical event has to be defined. For example, it may be a fracture/failure that is linked to the presence of crack-like defects; the definition of failure may then correspond to the initiation of crack growth, or that a certain amount of stable crack growth is obtained. Another form of critical event may be a global collapse of the insert. Below, a number of critical events that are relevant to a rock shear load are discussed.

3.1.1 Initiation of crack growth

If it is assumed that there exist crack-like defects in the insert, there is also a risk that these cracks begin to grow with increasing load. The parameter used to predict this growth is called stress intensity factor (linear case) or J-integral (nonlinear case). A critical defect size can be calculated using the criterion $J = J_{Ic}$. Here, J is the applied J-value given by a nonlinear FE-analysis, J_{Ic} is a material parameter known as the fracture toughness and shows how resistant the material is to the initiation of crack growth. The critical event thus becomes:

$$J = J_{Ic} \tag{3.1}$$

and the limit state function is given as:

$$g_{initiation} = J_{Ic} - J . \tag{3.2}$$

3.1.2 Stable crack growth

For materials that do not have a brittle fracture behavior, the condition $J = J_{Ic}$ only shows an initiation of stable crack growth under increasing load. This means that the use of J_{Ic} underestimates the real fracture behavior of the material. A more realistic criterion for material that has a ductile fracture behavior is to accept a certain amount of stable crack growth, such as 2 mm stable growth that is accepted by SSM [15] for a ductile material (the limit of 2 mm comes from the fact that it is often difficult to obtain valid tests for more stable growth than 2-3 mm). A fracture toughness value which includes 2 mm of stable crack growth is usually referred to as J_{2mm}. The critical event thus becomes:

$$J = J_{2mm} \tag{3.3}$$

and the limit state function is given as:

$$g_{2mm} = J_{2mm} - J . \tag{3.4}$$

3.1.3 Global plastic collapse

The rock shear load is a case with a displacement controlled loading, which imposes certain difficulties when defining a global collapse of the canister/insert. To overcome this problem, an engineering collapse condition was defined in the design analysis [1]. This condition coupled tensile tests that gave a critical stress measure (σ_{crit}), to the effective stresses (σ_{eff}) that was obtained from FE-analysis of the rock shear load. In principle, one could instead use a more direct condition between a critical strain measure (ε_{crit}) from the tensile tests (as given in Sect. 2.3) and the effective strain (ε_{eff}) that is obtained from FE-analysis of the rock shear load. The critical event thus becomes:

$$\varepsilon_{eff} = \varepsilon_{crit} \tag{3.5}$$

and the limit state function is given as:

$$g_{collapse} = \varepsilon_{crit} - \varepsilon_{eff} . \tag{3.6}$$

3.2   Theoretical background

In this study, different limit state functions, $g(X)$, are defined in Section 3.1. To calculate the probability of initiation, fracture or plastic collapse, a multi-dimensional integral has to be evaluated:

$$P_f = \Pr[g(X) < 0] = \int_{g(X)<0} f_X(x)dx . \tag{3.7}$$

The set where the above analysed event is fulfilled, is formulated as $g(X) < 0$, and is called the failure set. The set where $g(X) > 0$ is called the safe set. $f_X(x)$ is a known joint probability density function of the random vector X. This integral is very hard (impossible) to evaluate by numerical integration if there are many random parameters. In the calculations, all the random parameters are treated as not being correlated with one another (this assumption is investigated and discussed in Sect. 7.4). The parameters can follow almost any distribution.

As mentioned above, the failure probability integral is very hard to solve using numerical integration. Instead, the following numerical algorithms are used in this study [5]:
-    Simple Monte Carlo Simulation (MCS), only used to check the results using the other methods.
-    First-Order Reliability Method (FORM)
-    Monte Carlo Simulation with Importance Sampling (MCS-IS)

3.2.1   Probability calculation using Simple Monte Carlo Simulation (MCS)

MCS is a simple method that uses the fact that the failure probability integral is interpreted as a mean value in a stochastic experiment. An estimate is therefore given by averaging a suitably large number of independent outcomes (simulations) of this experiment.

The basic building block of this sampling is the generation of random numbers from a uniform distribution (between 0 and 1). Once a random number u, between 0 and 1, has been generated, it is used to generate a value of the desired random variable with a given distribution. A common method is the inverse transform method. Using the cumulative distribution function $F_X(x)$, the random variable would then be given as:

$$x = F_X^{-1}(u) . \tag{3.8}$$

To calculate the failure probability, one performs N deterministic simulations and for every simulation checks if the component analysed has failed (i.e. if $g(X) < 0$). The number of failures is N_F, and an estimate of the mean probability of failure is:

$$P_{F,MCS} = \frac{N_F}{N} . \tag{3.9}$$

An advantage with MCS, is that it is robust and easy to implement into a computer program, and for a sample size $N \rightarrow \infty$, the estimated probability converges to the exact result. Another advantage is that MCS works with any distribution of the random variables and there is no restriction on the limit state functions.

However, MCS is inefficient when calculating failure probabilities, since most of the contribution to P_F is in a limited part of the integration interval. Within this project, Simple Monte Carlo Simulation was only used to check the results of using the other methods.

3.2.2   Probability calculation using Monte Carlo Simulation with Importance Sampling (MCS-IS)

MCS-IS is an algorithm that concentrates the samples in the most important part of the integration interval. Instead of sampling over the entire probability density functions (MCS), one samples around the most probable point of failure (MCS-IS). This point, called MPP, is generally evaluated using information from a FORM analysis (see Section 3.2.3 below).

3.2.3   Probability calculation using the First-Order Reliability Method (FORM)

FORM (First-Order Reliability Method) or SORM (Second-Order Reliability Method) uses a combination of both analytical and approximate methods, when estimating the probability of failure [5].

First, all the variables are transformed into equivalent normally distributed variables in standard normal space (i. e. with mean = 0 and standard deviation = 1). This means that the original limit state surface $g(x) = 0$ then becomes mapped onto the new limit state surface $g_U(u) = 0$.

Secondly, the shortest distance between the origin and the limit state surface (in a transformed standard normal space U) is calculated. The answer is a point on this surface, called the most probable point of failure (MPP), design point or β-point. The distance between the origin and the MPP is called the reliability index β_{HL} (see figure 3-1).
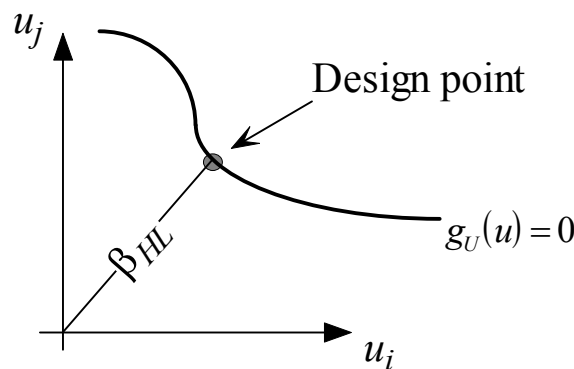
Figure 3-1. The definition of design point / MPP and reliability index β_{HL}.

In [5] a linearization of the limit state function is used to calculate the MPP.

$$y_{i+1} = \frac{1}{\left|\nabla g_U(y_i)\right|^2} \cdot \left[\nabla g_U(y_i) \cdot y_i - g_U(y_i)\right] \cdot \nabla g_U(y_i)^T \,,$$
(3.10)

where y_i is the current approximation to the MPP and $\nabla g_U(y_i)$ is the gradient of the limit state function. This algorithm, generally called the Rackwitz & Fiessler (R & F) algorithm, is commonly used when evaluating P_F, mainly because it is very easy to implement and it converges fast in many cases. However, the R & F algorithm converges extremely slowly in some cases or oscillates about the solution without any convergence at all. Therefore, the R & F algorithm was not chosen in this case.

Instead, a modified Rackwitz & Fiessler algorithm was chosen. It works by "damping" the gradient contribution of the limit state function and this algorithm is very robust and converges quite fast for most cases. In this algorithm one defines a search direction vector d_i:

$$d_i = \frac{1}{\left|\nabla g_U(y_i)\right|^2} \cdot \left[\nabla g_U(y_i) \cdot y_i - g_U(y_i)\right] \cdot \nabla g_U(y_i)^T - y_i \,.$$
(3.11)

A new approximation to the MPP can then be calculated:

$$y_{i+1} = y_i + s_i \cdot d_i \,.$$
(3.12)

The step size s_i was selected such that the inequality $m(y_i + s_i d_i) < m(y_i)$ holds, where $m(y_i)$ is the merit function:

$$m(y_i) = \frac{1}{2} \cdot \left|y_i\right|^2 + c \cdot \left|g_U(y_i)\right|,$$
(3.13)

in which c is a parameter satisfying the condition $c > \left|y_i\right|/\left|\nabla g_U(y_i)\right|$ at each step i. This algorithm is globally convergent, i. e., the sequence is guaranteed to converge to a minimum-distance point on the limit state surface, provided $g_U(u)$ is continuous and differentiable.

Finally, the failure probability is calculated using an approximation of the limit state surface at the most probable point of failure. Using FORM, the surface is approximated to a hyperplane (a first order / linear approximation). It is also possible to use a second order / quadratic approximation to a hyperparaboloid (SORM approximation, see figure 3-2).
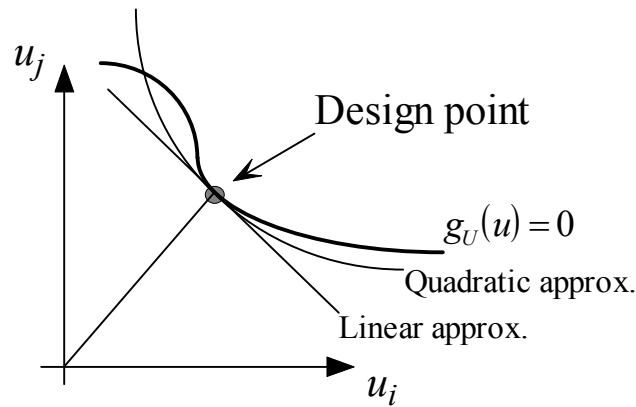
Figure 3-2.   Schematic difference between a linear and a quadratic approximation of the limit state surface.

The probability of failure is given as [5]:

$$P_{F,FORM} = \Pr\left[g_{Linear}(u) < 0\right] = \Phi(-\beta_{HL}),$$ (3.14)

$$P_{F,SORM} = \Pr\left[g_{Quadratic}(u) < 0\right] \approx \Phi(-\beta_{HL}) \cdot \prod_{i=1}^{N-1}\left(1 - \kappa_i \cdot \beta_{HL}\right)^{-1/2},$$ (3.15)

where $\Phi(u)$ is the cumulative distribution function in standard normal space and κ_i are the principal curvatures of the limit state surface at the most probable point of failure (MPP).

FORM or SORM are, as regards CPU-time, extremely efficient as compared to MCS. A disadvantage is that the random parameters must be continuous, and every limit state function must also be continuous (using the given implementation).

3.2.4   Sensitivity study – What parameter contributes the most to the calculated probabilities

In this study, a more formal sensitivity analysis is also presented. The purpose is to investigate what parameter that contributes the most to the calculated probability. To answer this, one may use the gradient computation that is readily available in any probability analysis using FORM.

However, the simplest approach is to investigate the relative importance of the basic standard normal random variables that is given in a FORM analysis. These are given by means of the vector α^* defined as:

$$\alpha^* = \frac{y^*}{\|y^*\|}$$ (3.16)

where y^* denotes the coordinates of the design point in the standard normal space. The ordering of the elements in α^* indicates the relative importance of the random variables in the standard normal space.

Since y^* is the coordinate of the design point (or the most probable point of fracture), then $\left\| y^* \right\|$ is equivalent to the design point β and related to the probability of fracture as given in Eqn. (3.14), i.e. $P_f = \Phi(-\beta)$ when using a FORM approximation. This means that there is a nonlinear relation between the importance factors and how they contribute to the calculated fracture probability. These importance factors should therefore be used to get a qualitative understanding of the different parameter's/variable's relative importance in a probabilistic analysis. To get a quantitative understanding, a more formal sensitivity analysis should be used; such an analysis is presented below.

3.2.5   Sensitivity study – What parameter change, has the most influence on the calculated probabilities

Above, the importance factors were defined. The purpose was to show what parameter that contributes the most to the calculated fracture probability. Another aspect of a probabilistic analysis is to define what happens to the calculated fracture probability if a small change in the input data is introduced, i.e. what parameter change has the most influence on the calculated fracture probability.

Of interest is therefore the sensitivity of the reliability index β with respect to parameters θ entering the definition of the limit state function g. The sensitivity of β is given by:

$$\frac{d\beta}{d\theta} = \frac{1}{\left\| \nabla G \right\|} \frac{dg}{d\theta} \ . \tag{3.17}$$

When doing a FORM analysis, the probability of failure (fracture) is given as $P_f = \Phi(-\beta)$ and differentiated with respect to θ:

$$\frac{dP_f}{d\theta} = \frac{d}{d\theta}\Phi(-\beta) = \frac{d}{d\theta}\big(1 - \Phi(\beta)\big) = -\frac{d\beta}{d\theta}\frac{d}{d\beta}\Phi(\beta) = -\frac{d\beta}{d\theta}\varphi(\beta) \ , \tag{3.18}$$

where $\varphi()$ is the probability density function.

The sensitivity of the probability of failure (fracture) P_f with respect to parameters θ is then given by:

$$\frac{dP_f}{d\theta} = -\varphi(\beta)\frac{1}{\left\| \nabla G \right\|}\frac{dg}{d\theta} \ , \tag{3.19}$$

where $\left\| \nabla G \right\|$ and $dg/d\theta$ is easily computed in any FORM analysis.

This sensitivity study tries to answer the question: What parameter change has the most influence on the calculated fracture probability? One investigates a change in the given mean values and in the given values for the standard deviation. The results are normalised (against the fracture probability) to get a better understanding of the interaction between the calculated sensitivities.

3.3   Steps in a probabilistic analysis

Described below are the steps that must be implemented (completed) before a probabilistic analysis can begin.

1)   Define the critical events to be included in the analysis.

Within this project three critical events are defined in Section 3.1. The chosen events are:

i) Initiation of crack growth.

ii) 2 mm stable crack growth.

iii) Global plastic collapse.

2)   Define the limit state functions corresponding to the given critical events.

The limit state functions are also defined in Section 3.1.

3)   Determine which parameters that should be probabilistic in the analysis.

The important parameters that influence the calculated failure probabilities are identified and described in Section 2.1-2.12.

4)   Define distributions that describe the probabilistic parameters.

The selected distributions are defined in Section 2.1-2.12.

5)   Perform global FE-analyses.

First global FE-analyses are performed, including bentonite and boundary conditions between the buffer and the rock, to get the displacements, strains and stresses in the canister. These analyses are reported in [7] and the results are used as input to new global FE-analyses performed within this project (see Section 4.1).

6)   Perform local FE-analyses.

Using the results from the new global FE-analyses, local FE-analyses are performed (see Section 4.2). These calculations uses sub-models that contain different defects (surface cracks).

7)   Evaluate the governing parameters of the selected critical events.

Three critical events are defined. The governing parameter for both *initiation of crack growth* and *2 mm stable crack growth* are the *J*-values given from the local FE-analysis of sub-models that contain surface cracks. The governing parameter for *global plastic collapse* is the strain values given from global FE-analysis of the canister insert. Both the *J*-values and the strains are tabulated in appendix A-B.

8)   Compile the results.

Compile the results in order to approximate the limit state surfaces needed for the probabilistic analyzes. The limit state surfaces are approximated using cubic spline interpolation which gives continuous and smooth surfaces. The more FE-analyses performed under paragraph 5-6, the better approximation is obtained.

9)   Perform probabilistic analyses of BWR canister inserts in the case of an earthquake induced rock shear load.

Report No.: 50014130-1   Revision No.: 5

3.4   Chosen parameters for the global FE-analyses

In order to perform the probabilistic analysis, a number of global and local FE-analyses has to be performed. The results from these FE-analyses are used to define the limit state functions corresponding to the selected critical events. The following table summarizes whether the different parameters (as defined in Section 2.1-2.12) affect the number of FE-analyses.

Table 3-1.   Summary of the different parameters influence on the number of FE-analyses that has to be performed.

Parameter	Affecting the number of global FE-analyses	Affecting the number of local FE-analyses	No impact on the number of FE analyses
Fracture toughness of the insert			X
Yield stress and ultimate tensile strength of the insert	X	X	
Elongation at fracture of the insert			X
Defect depth distribution of crack like defects		X	
POD-curve			X
Type of bentonite			X
Bentonite density	X	X	
Size of the rock shear displacement			X
Velocity of the rock shear displacement			X
Angle of the rock shear plane			X
Position of the rock shear plane	X	X	
Thickness of the ice sheet			X

Note: The size of the rock shear displacement does not affect the number of FE analyses, since for every analysis all the chosen displacements are included in the analysis.

The number of global FE-analyses is thus dependent on the yield stress and ultimate tensile strength of the insert, bentonite density and the shear plane position in the axial direction. The number of local FE-analyses is also dependent on the number of defect geometries to be included in the analysis (this should be chosen to cover the selected defect distributions for crack-like defects).

3.4.1   Chosen values for the yield stress and the ultimate tensile strength

A summary of the test results, for the yield stress and the ultimate tensile strength, is presented in section 2.2:

- The yield stress has a mean value of 280.4 MPa (true stress) and a standard deviation of 6.77 MPa. Investigating the data [6] one finds that the minimum value is 270.5 MPa (equivalent to minus 1.5 standard deviations) and the maximum value is 291.6 MPa (equivalent to plus 1.7 standard deviations).

- The ultimate tensile strength has a mean value of 448.8 MPa (true stress) and a standard deviation of 6.39 MPa. Investigating the data [6] one finds that the minimum value is 432.1 MPa (equivalent to minus 2.6 standard deviations) and the maximum value is 457.5 MPa (equivalent to plus 1.4 standard deviations).

It was decided that at least 3 combinations, of each parameter, should be included in the FE-analysis. Using the information above, the mean value plus/minus five standard deviations was considered to be sufficient:

- The yield stress (true stress): 246.6, 280.4 and 314.2 MPa
- The ultimate tensile strength (true stress): 416.8, 448.8 and 480.8 MPa

It could also be of some interest to do a sensitivity check using even smaller values for the yield stress and the ultimate tensile strength (mean value plus/minus ten standard deviations).

3.4.2   Chosen values for the bentonite density

In the case of the bentonite density, 3 combinations are included. Given the data used in the damage tolerance analysis [4], the following values were chosen:

- The bentonite density: 1950, 2000 and 2050 kg/m^3

3.4.3   Chosen values for the position of the rock shear plane

Also in the case of the position of the rock shear plane at least 3 combinations should be included. Based on the experience from earlier performed deterministic analyzes of the shear load [1, 4, 16], the following values were chosen (positioned from the base of the insert):

- The shear plane position in the axial direction: Mid (50%), 3/4 (75%) and 9/10 (90%)

3.4.4   Chosen values for the defect geometry

The number of defect geometries to be included in the analysis should be chosen to cover the selected defect distributions for crack-like defects (see Sect. 2.5). Based on the experience from probabilistic analyzes performed by Inspecta Technology the following values were chosen:

- Defect geometry: A semi-elliptical surface defect
- Defect length/depth: 6
- The defect depth: 1, 5, 10 and 20 mm

3.4.5   Number of global and local FE-analyses

Given the chosen parameter values above, a total of 3·3·3·3 = 81 <u>global FE-analyses</u> are needed to completely define the limit state functions corresponding to the selected critical events. This does not mean that 81 FE-models are needed to perform the global FE-analyses. The number of FE-models depends only on the shear plane position in the axial direction, i.e. it requires only three global FE-models. These models are then used with different assumptions regarding yield stress, ultimate tensile strength and bentonite density.

The number of local FE-analyses is controlled by the number of defect geometries to be analyzed. For every global analysis, four local FE-analyses are performed (using sub-models that contain surface cracks). Then, a total of 81·4 = 324 <u>local FE-analyses</u> are needed to completely define the limit state functions corresponding to the selected critical events.

Within the project, it was realised that the number of global FE-analyses needed to completely define the limit state functions were too many given the time constraints on the project. Therefore, it was decided that a subset of 43 global FE-analyses should be performed (see Table 3-2). This choice was made using a design of experiments approach. The purpose was to achieve a sufficiently accurate approximation of the different limit state functions.

In Table 3-2 below, the definition of the different values used are as follows:

- *The yield stress (true stress):*
  Low = 246.6 MPa
  Mean = 280.4 MPa
  High = 314.2 MPa
  Special case = 212.7 MPa (mean value minus ten standard deviations)

- *The ultimate tensile strength (true stress):*
  Low = 416.8 MPa
  Mean = 448.8 MPa
  High = 480.8 MPa
  Special case = 384.9 MPa (mean value minus ten standard deviations)

- *The shear plane position in the axial direction:*
  Mid (50%)
  3/4 (75%)
  9/10 (90%)

- *The bentonite (buffer) density:*
  Low = 1950 kg/m^3
  Mean = 2000 kg/m^3
  High = 2050 kg/m^3

These global analyses can also be summarized in a calculation matrix as given in Table 3-3.

Table 3-2. Definition of values used in the global FE-analysis (43 cases).

Case	Shear plane location	Insert yield stress	Insert ultimate tensile strength	Buffer density
N1b	50%	mean	mean	low
N2b	75%	mean	mean	low
N3b	90%	mean	mean	low
N4b	50%	mean	mean	mean
N5b	75%	mean	mean	mean
N6b	90%	mean	mean	mean
N7b	50%	mean	mean	high
N8b	75%	mean	mean	high
N9b	90%	mean	mean	high
N10b	50%	212.7 MPa	mean	mean
N11b	50%	212.7 MPa	384.9 MPa	mean
N12b	50%	low	low	low
N13b	50%	high	low	low
N14b	50%	low	high	low
N15b	50%	high	high	low
N16b	90%	low	low	low
N17b	90%	high	low	low
N18b	90%	low	high	low
N19b	90%	high	high	low
N20b	75%	low	mean	mean
N21b	75%	high	mean	mean
N22b	75%	mean	low	mean
N23b	75%	mean	high	mean
N24b	50%	low	low	high
N25b	50%	high	low	high
N26b	50%	low	high	high
N27b	50%	high	high	high
N28b	90%	low	low	high
N29b	90%	high	low	high
N30b	90%	low	high	high
N31b	90%	high	high	high
N36b	75%	low	low	low
N37b	75%	high	low	low
N38b	75%	low	high	low
N39b	75%	high	high	low
N40b	75%	low	low	high
N41b	75%	high	low	high
N42b	75%	low	high	high
N43b	75%	high	high	high
N44b	90%	low	low	mean
N45b	90%	high	low	mean
N46b	90%	low	high	mean
N47b	90%	high	high	mean

Table 3-3. Calculation matrix for the global FE-analysis as given in Table 3-2.

Bentonite density	The shear plane position in the axial direction		
	50%	75%	90%
1950	N1b N12b N13b N14b N15b	N2b N36b N37b N38b N39b	N3b N16b N17b N18b N19b
2000	N4b N10b N11b	N5b N20b N21b N22b N23b	N6b N44b N45b N46b N47b
2050	N7b N24b N25b N26b N27b	N8b N40b N41b N42b N43b	N9b N28b N29b N30b N31b

As mentioned above, the number of local FE-analyses is controlled by the number of defect geometries to be analyzed. For every global analysis, four local FE-analyses are performed (using sub-models that contain surface cracks). Then, a total of $43 \cdot 4 = 172$ local FE-analyses are needed to define the limit state functions corresponding to the selected critical events (using an approximation since only 43 global analyzes were performed of the 81 required to completely define the limit state functions).

When performing the local FE-analyses, see section 4.2, the largest sub-models were not sufficiently accurate in the originally intended location for the sub-models. Therefore a new location was chosen and the results were compared with the original location (for smaller cracks). Because of this, a total of ($43 \cdot 3$ (original location) + $43 \cdot 4$ (new location)) = 301 local FE-analyses were actually performed within the project.

After including these new sub-models, the sets of global and local analyses were considered to be sufficient to get a better approximation of the limit state surfaces and a reliable result in the subsequent probabilistic analysis.

4   DETERMINISTIC FE-ANALYSIS OF BWR CANISTER INSERTS IN THE CASE OF A ROCK SHEAR LOAD

In order to get the parameters needed in the probabilistic analysis, i.e. the *J*-values and the strain values, the FE-analysis described in section 3.4 has to be performed. First global FE-analyses are performed, including bentonite and boundary conditions between the buffer and the rock, to get the displacements, strains and stresses in the canister. These analyses are reported in [7] and the results are used as input to new global FE-analyses performed within this project (see Section 4.1). Using the results from the new global FE-analyses, local FE-analyses are performed (see Section 4.2). These calculations use sub-models that contain different defects (surface cracks).

4.1   Global FE-analysis

A complete 3D model of the canister with the possibility to insert cracks at arbitrary surface positions of the iron insert has been created with ABAQUS [17], using information from the symmetry model of the canister that is used in [7]. This symmetry model has been mirrored to give a complete 3D model of the canister. Since the complete canister is modeled without using symmetry, the orientation of the iron insert relative to the direction of the shear load could be arbitrarily chosen.

All information regarding the symmetry model is found in [7]. A summary taken from [7] is given below:

- Due to symmetry only one half of the canister has been modeled.
- The mesh is generated by 3-dimensional solid elements, mainly 8-noded hexahedral (most of them using full integration technique) and a few 6-noded wedge elements.
- The model size is defined by about 126,000 elements and 160,000 nodes (total number of variables about 650,000).
- The insert made of nodular cast iron has been simplified regarding the square tubes which are assumed to be tied to the nodular cast iron insert and thus these contribute as added material to the insert.
- The copper shell surrounds the insert and interacts with the insert. The canister has been modeled rather accurately in order to catch "hot spots" where large strains are expected, e.g. the fillets at the bottom and top (the lid). The lid is welded to the flange and lid and canister will act as one part.
- The material model for the insert is based on a von Mises material model with elastic behavior defined by Young's modulus and the Poisson's ratio and the plastic behavior defined through yield surface (true stress) versus plastic strain (defined as logarithmic strain).
- All the boundaries of the copper shell, the insert and the insert lid interact through contact surfaces allowing finite sliding. All contact surfaces have friction at sliding with no cohesion and the friction coefficient 0.1.
- Total pressure for the buffer is defined to simulate the swelling pressure plus 500 meter water pressure when using an elastic-plastic material model without pore pressure. The initial pressure has to be tuned for the different densities and has therefore been applied as initial pressure which gives about the right total pressure before the shearing starts.
- The numerical calculations are performed using the FE-code ABAQUS [17] assuming non-linear geometry and material definitions. This means that all non-linearities defined by the input will be considered, such as large displacements, large deformations, non-linear interactions (contact) and non-linear materials.

The global models used within this project have then been created using information from the symmetry model of the canister that is used in [7]. This symmetry model has been mirrored to give a complete 3D-model of the canister (see Fig. 4-1 to 4-2).

Figure 4-1. Global model of the canister (complete 3D-model).
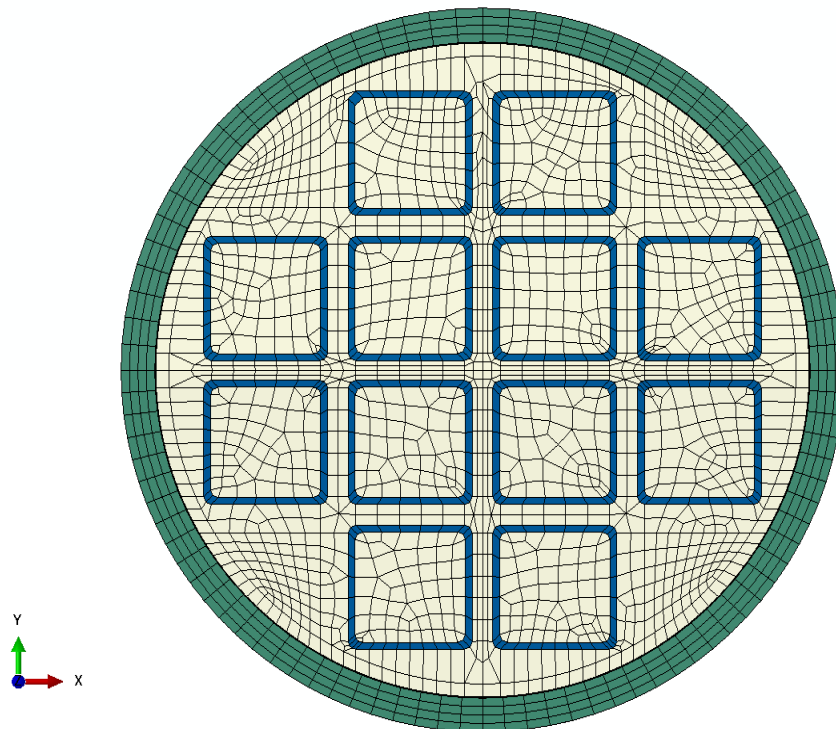
Figure 4-2. Global model of the canister (a section through the canister).

Given the results from [7], loads are applied as displacement history at the outer boundary of the copper canister. The loading history corresponds to the shear of the BWR canister including the buffer. All the load steps are applied corresponding to 0, 1, 2, 3, 4, 5, 6, 7, 8, 9 and 10 cm of shear (in the first step there exist initial stresses corresponding to the swelling pressure plus 500 meter water pressure).

The results obtained from the global models in this report are compared with the results obtained in [7]. The comparison in Figure 4-3 shows very small differences (using stresses in the axial direction). The differences (between 0 and 2%, when checking all the global models) are explained by the fact that the results are dependent on the loading history. The time increment with which the displacement history is applied is somewhat different as compared to [7]. The differences are considered to be small and not to influence the results significantly.

Fe-model N8b
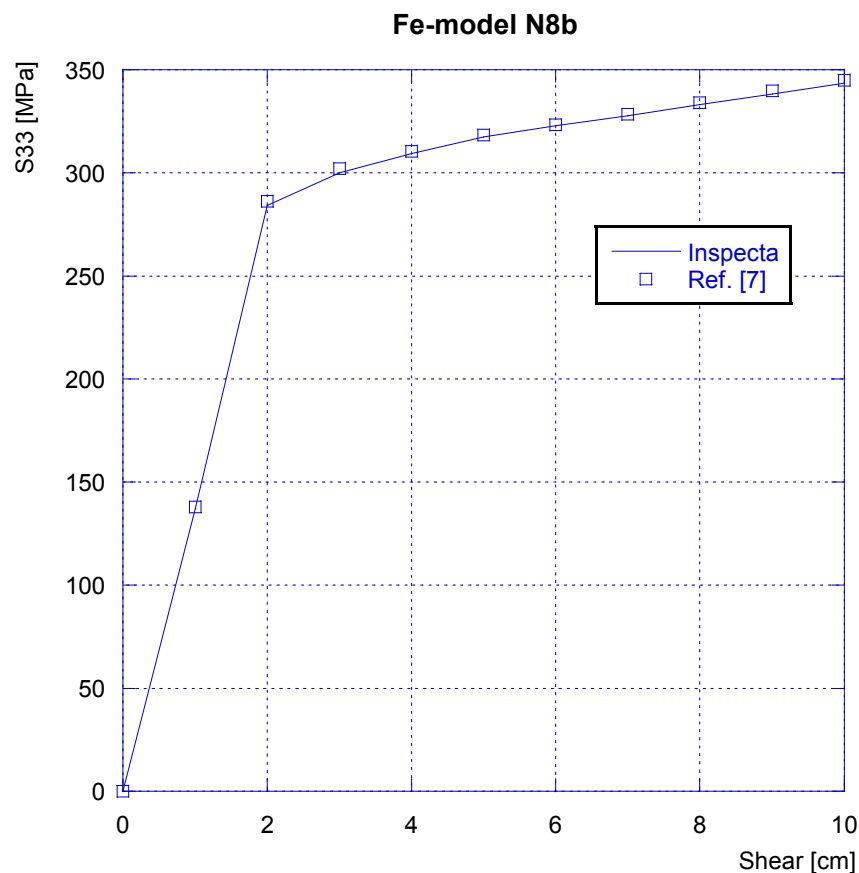
Figure 4-3. Highest stresses in the axial direction of the insert (using the case N8b).

The results from the global model are then investigated to decide where to introduce the defect. The location where the max principal stress is the highest is identified. This governs the location in the canister at which sub-models containing the defects are going to be introduced (see section 4.2).

4.2   Local FE-analysis using sub-models with surface defects

As given above, the analyses of the BWR canister are conducted with the FE program ABAQUS [17]. A sub-modelling technique is used to introduce different surface defects in the BWR insert. When using a sub-modelling technique, a global model is first used to get the stresses and displacements of the canister (see section 4.1). From these global results, the areas of interest are identified (where the max principal stresses are found). In these areas the sub-models containing the defects are introduced (see Fig. 4-4 to 4-5). The deformations from the global model are applied at the boundary of the sub-model. From the sub-model the J-integral results are then obtained.
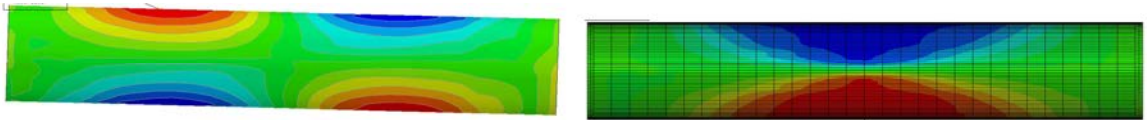
Figure 4-4.   Identification of areas where the max principal stresses are found (the location are mainly dependent on the position of the rock shear plane, two different positions are given in this figure).
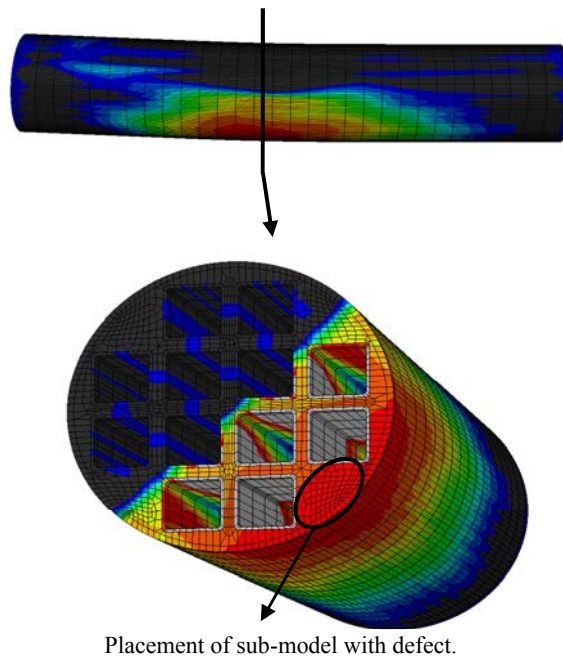
Placement of sub-model with defect.

Figure 4-5.   Identification of areas where the max principal stresses are found (where the sub-models containing the defects are introduced).

Only surface defects are modelled, with four different crack depths (see Sect. 3.4.4). All sub-models are made up by standard 20 node brick elements (C3D20). To check this choice, a comparison was made using the elements C3D20, C3D20R (using reduced integration) and C3D20H (using a hybrid displacement/pressure formulation interpolation scheme). When comparing the calculated J-values, the difference is quite small. In some cases the C3D20R elements introduced problems at the

crack tip front. All sub-models use the same material models as their respective global model [7]. Below, the modelling of the different defects is described. A large-displacement formulation is used in all analyses.

Since the sub-models containing surface defects are placed at the outer boundary of the cast iron insert, part of the copper canister is also modelled for the sub-model. This is done not to neglect any influence from the contact between the copper and iron surfaces. All sub-models are created as two rectangular blocks, one for the copper canister and one for the cast iron casing. The models are also curved to match the radius of the canister (see Fig. 4-6). The element mesh is focused towards the crack tip and the crack tip is modelled with a small notch. Examples of the sub-models used are shown in Fig. 4-7 to 4-9.
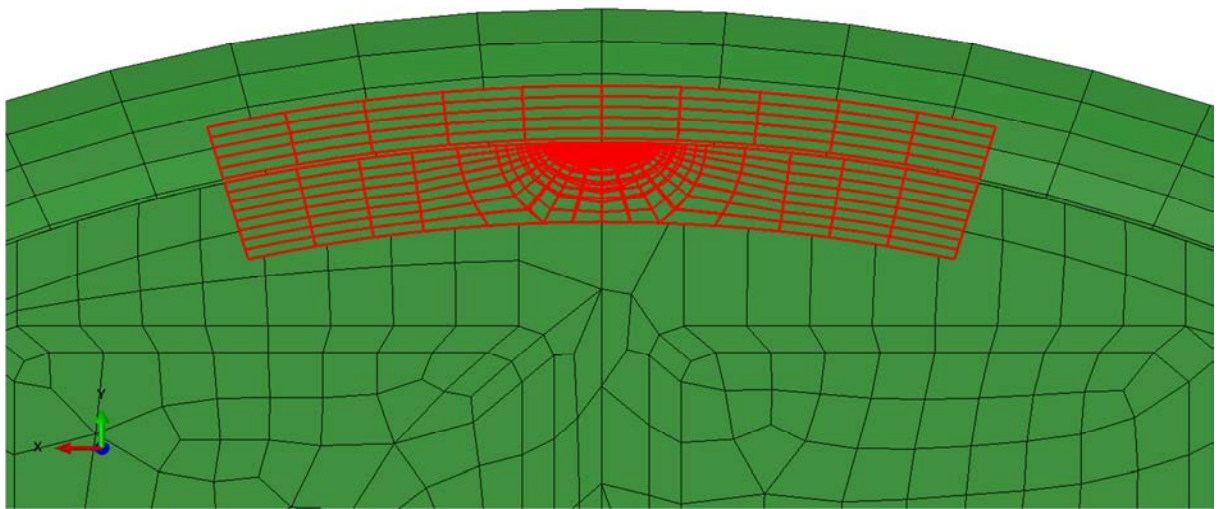
Figure 4-6.   Example of location of the sub-model where one can see that the sub-model is curved to match the radius of the canister.
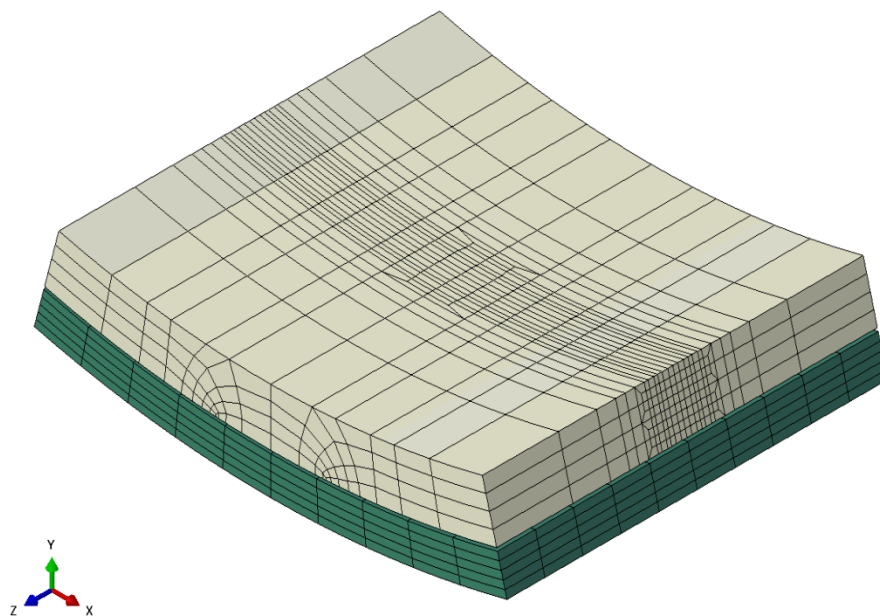
Figure 4-7. A typical sub-model used in the analysis (copper canister is shown in green).
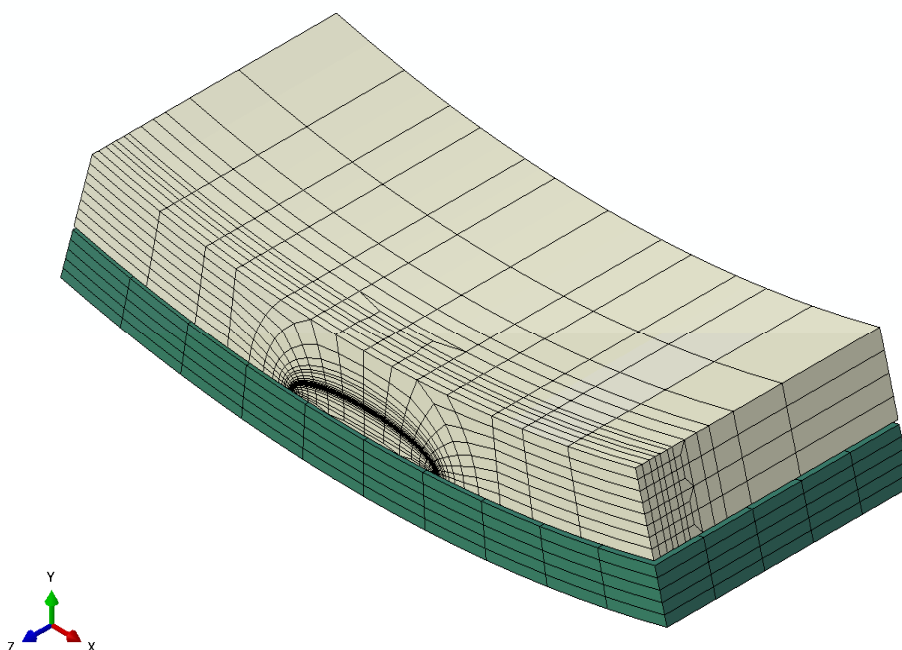
Figure 4-8.   A typical sub-model used in the analysis (a sectional view in the circumferential direction to see how the crack front is modeled).
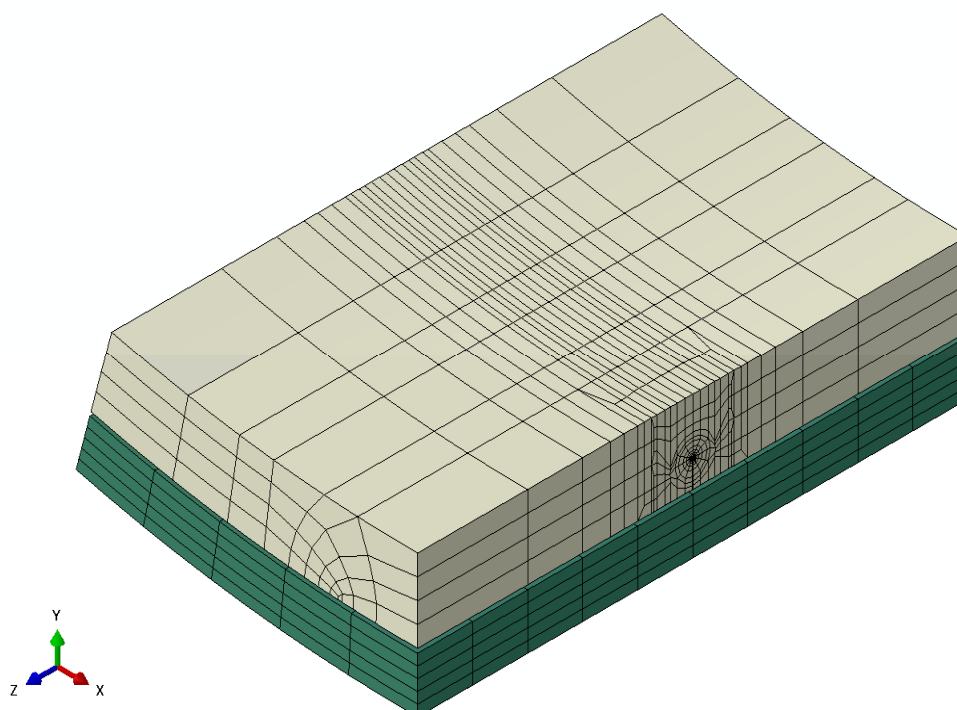
Figure 4-9.   A typical sub-model used in the analysis (a sectional view in the axial direction to see how the crack tip is modeled).

Boundary conditions and loading for the sub-model consist of displacements on the boundary obtained from the global model. These are automatically extrapolated from the global model to the boundary of the sub-model and hence it is very important that the placement of the sub-model relative to the global model is correct (see Fig. 4-6). To check the correctness of the transferred displacements from the global model to the sub-model, a model without a crack was used. The stresses through the thickness were compared with the corresponding stresses in the global model. The results showed a good agreement between the global model and the sub-model.

It was also possible to check the *J*-values obtained from a series of three sub-models (for the case N8b) with an earlier analysis using similar input data [4]. There are some differences in the assumed stress-strain curves for the insert (if this analysis is compared with the one given in [4]) and this means that the reported J values will not be identical. The comparison is presented in Fig. 4-10. As seen, there is a very good agreement between this analysis and the one given in [4].
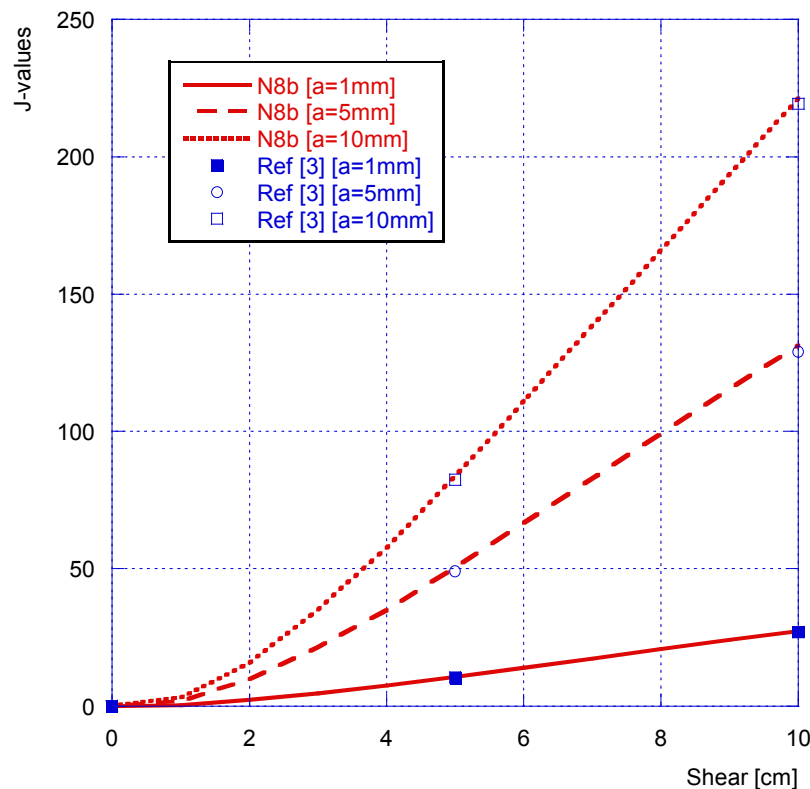
Figure 4-10.   Comparison between the *J*-values obtained in this analysis (for the case N8b) and those obtained from [4].

The governing parameter for both initiation of crack growth and 2 mm stable crack growth are the *J-values* given from the local FE-analysis of sub-models that contain surface cracks. The *J*-values obtained using the different global models (see Table 3-2) together with the different sub-models are given in appendix A (the maximum *J*-value for the different sub-models). ABAQUS domain integral method is used to calculate the *J*-integral [17].

The governing parameter for global plastic collapse is the strain values given from global FE-analyses of the canister insert. The strain values obtained using the different global models (see Table 3-2) are given in appendix B.

Finally, using the *J*-values presented in Fig. 4-10, a deterministic damage tolerance analysis could be performed (using similar data as the one presented in [4]) and the results from a typical analysis are presented in Fig. 4-11.
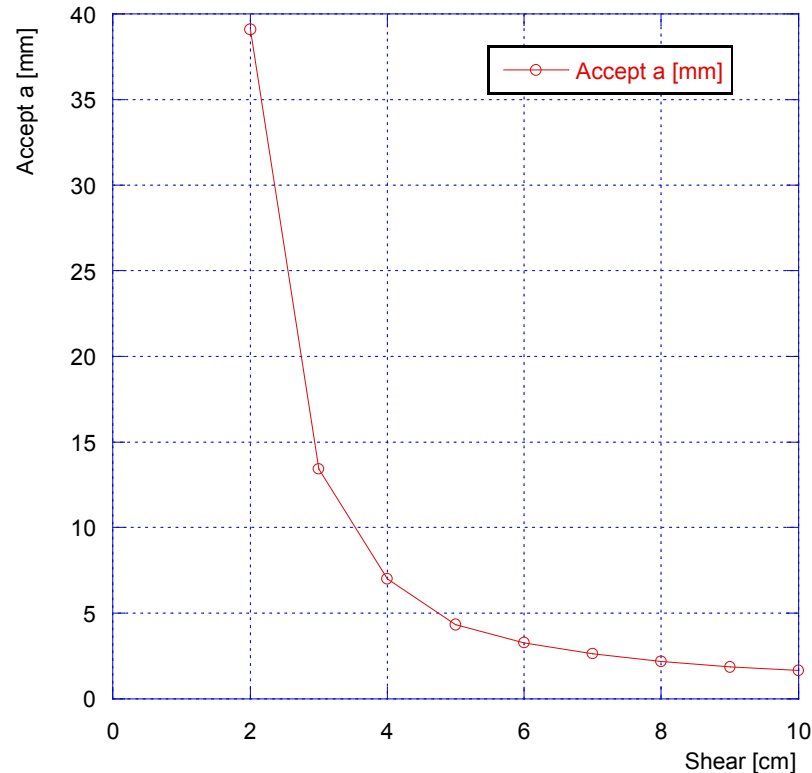
Figure 4-11.   Acceptable defect depths as a function of the size of the rock shear displacement (using fracture toughness at 2 mm stable crack growth and a bentonite density of 2050 kg/m^3).

In the damage tolerance analysis with postulated defects, the critical defect size is given using the failure criteria $J = J_{mat}$ and the acceptable defect size is given using the criteria $J = J_{mat}/SF_J$. In these equations, J is the applied *J*-value, J_{mat} is the fracture toughness (with or without some stable crack growth). SF_J is the safety factor used when calculating the acceptable defect size.

Recently, new fracture toughness data for PWR-inserts has been analyzed [18] and it is therefore possible to compare deterministic results using data from BWR- or PWR-inserts. The new PWR-data (from tests conducted in air) is much better than the old BWR-data (from tests conducted in water). The fracture toughness at 2 mm stable crack growth is 88 kN/m (BWR-data with 90% confidence) and 155 kN/m (PWR-data with 90% confidence). A deterministic damage tolerance analysis using J_{2mm}-data from BWR- or PWR-inserts is presented in Fig. 4-12.
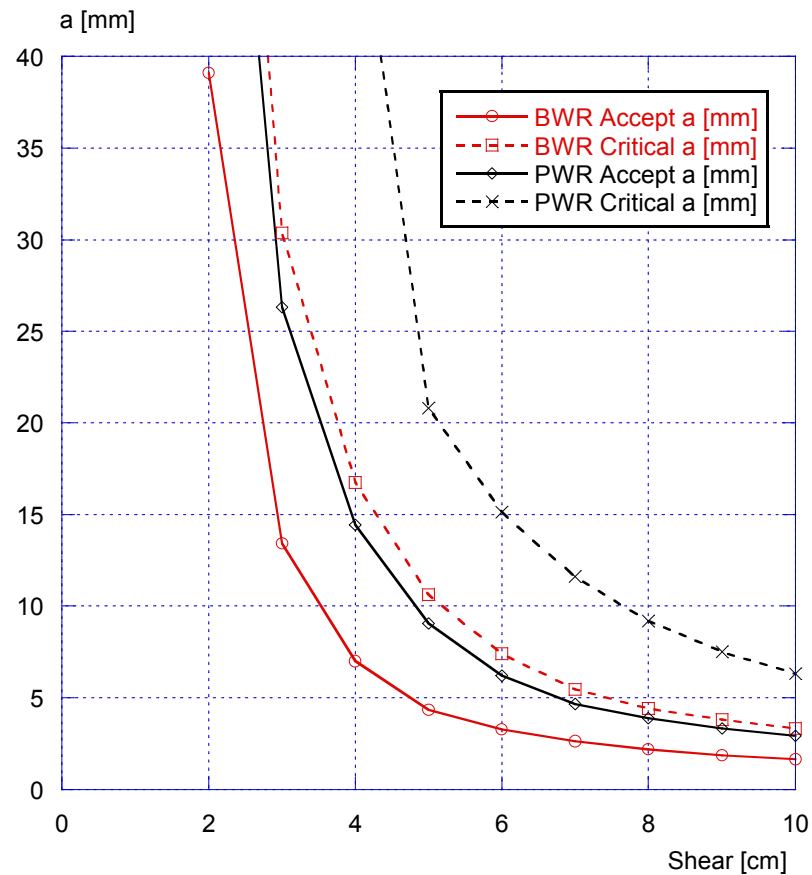
Figure 4-12.   Acceptable and critical defect depths as a function of the size of the rock shear displacement using fracture toughness at 2 mm stable crack growth and a bentonite density of 2050 kg/m^3. In this figure, a comparison is made using J_{2mm}-data from BWR- or PWR-inserts.

As shown in Fig. 4-12, there is a large difference in resulting acceptable and critical defect depths when using fracture toughness data from BWR- or PWR-inserts.

5   PROBABILITY OF INITIATION OF CRACK GROWTH OR STABLE CRACK GROWTH

In this section, the results for the (conditional) probability of initiation of crack growth and the (conditional) probability of 2 mm stable crack growth (given the existence of a surface crack) are given using the input data presented in section 2. First, the results using only two probabilistic parameters are presented and then it is shown how the results differ when more probabilistic parameters are used. Presenting the results in this manner gives an additional insight on how the different parameters influence the calculated probabilities.

5.1   Probability of initiation of crack growth or stable crack growth using two probabilistic parameters

In this analysis the <u>fracture toughness</u> and the <u>defect depth</u> are treated as probabilistic parameters. When calculating the probabilities, the mean values of the yield stress and ultimate tensile strength are used and a shear plane position at 75% from the base of the canister. In Fig. 5-1 the probability of initiation of crack growth is plotted as a function of the size of the rock shear displacement, using constant values regarding the bentonite density. In Fig. 5-2, the probability of 2 mm stable crack growth is plotted using equivalent assumptions.

Figure 5-1.   Probability of initiation of crack growth as a function of the size of the rock shear displacement for 3 different bentonite densities.
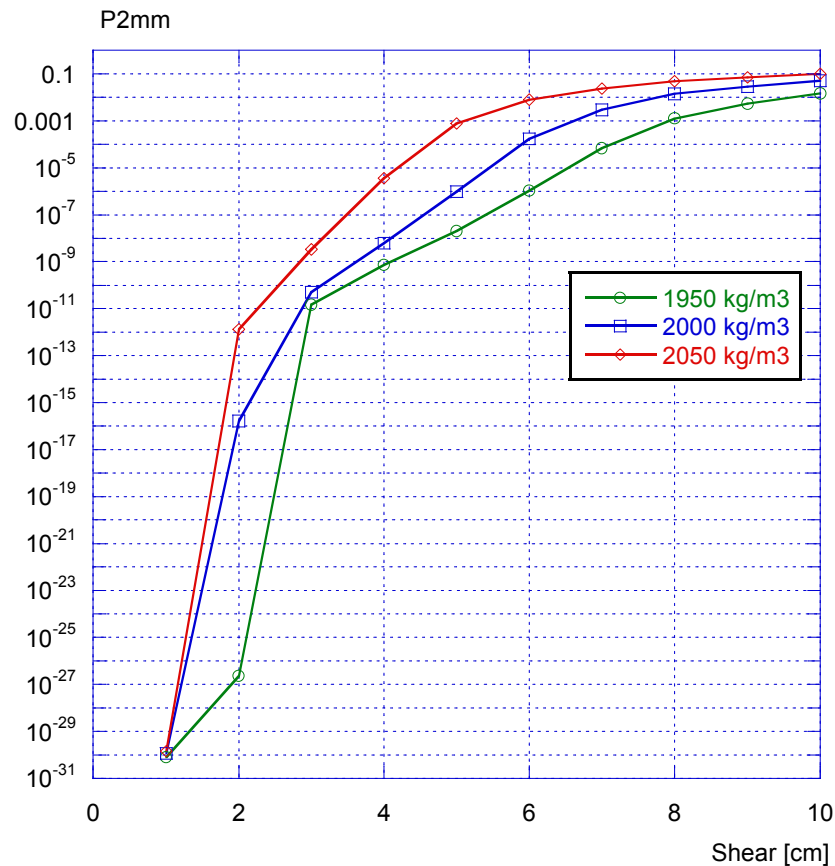
Figure 5-2.   Probability of 2 mm stable crack growth as a function of the size of the rock shear displacement for 3 different bentonite densities.

As shown above, both probabilities (P_i and P_{2mm}) have a similar behavior when investigating the dependence of the shear displacement and the bentonite density (but with different absolute values). At small values of shear displacement (1 cm and below) the resulting probabilities seem independent of the assumptions regarding bentonite density, which will be obvious when investigating the cause of this in a sensitivity analysis with more probabilistic parameters (see Section 5.3). When investigating the trends the results show that the probability is rapidly decreasing down to very small values for values of shear displacement below 3 cm. Also, for values of shear displacement above 10 cm the probability values are asymptotically approaching one (at even larger values of shear displacement).

In the deterministic damage tolerance analysis presented in the design analysis [1], the acceptable defect sizes are calculated using a bentonite density of 2050 kg/m^3 and 2 mm stable crack growth as a critical event. To display the differences between different assumptions regarding bentonite density and chosen critical event a comparison is made in Fig. 5-3.
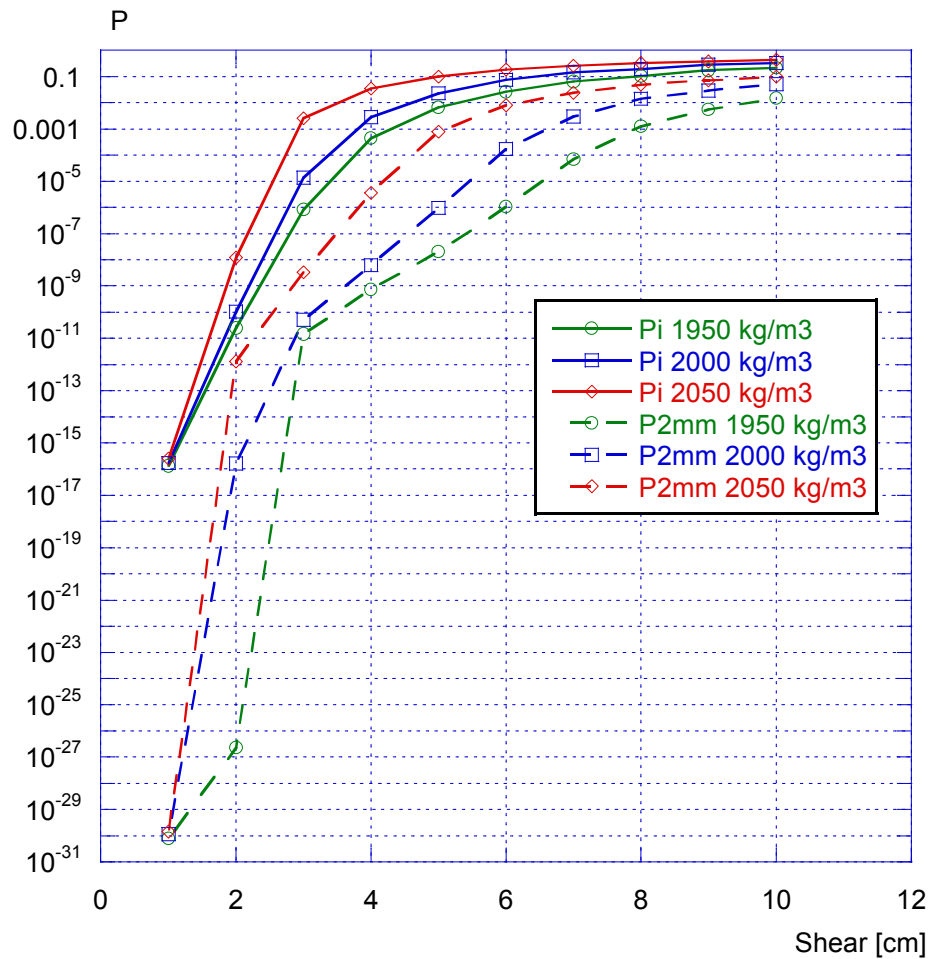
Figure 5-3.   Comparison between probability of initiation and probability of 2 mm stable crack growth as a function of the size of the rock shear displacement (at 3 different bentonite densities).

As shown in Fig. 5-3, the resulting stable crack growth probabilities are much smaller than the initiation probabilities for values of shear displacement of approximately 6 cm and below (starting with a factor of 1000, which quickly increases using a shear displacement below 4 cm).

Also shown in Fig. 5-3 is that many probabilities are extremely low (most importantly for the probability of 2 mm stable crack growth). This means that the resulting probabilities are dependent either on the low end tails of the fracture toughness distribution or the high end tail of the defect depth distribution. The absolute values will be different if another distribution is used or if the given distribution is truncated. If the defect depth distribution is truncated at $a = 20$ mm, lower probability values are expected and the present analysis could be considered to be pessimistic.

All the calculations presented above have been done using a constant value for the shear plane position (at 75% from the base of the canister). This is the position used in the design analysis [1] when calculating acceptable defect sizes. To check the influence of this parameter, a sensitivity analysis is presented in Fig. 5-4 (using a bentonite density of 2050 kg/m^3).
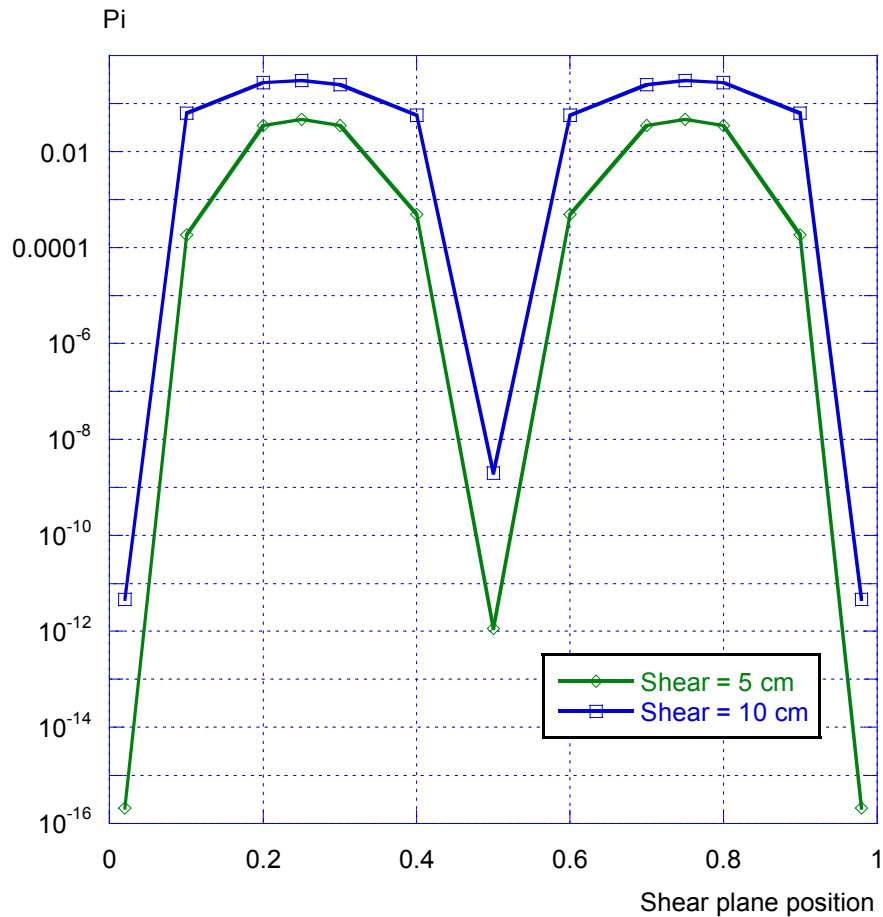
Figure 5-4.   Probability of initiation of crack growth as a function of the shear plane position (bentonite density = 2050 kg/m^3).

A few observations are made. First, the results are symmetrical with respect to the position 50%, which has been verified in [7] by using different values of the shear plane position. Secondly, the probabilities decrease rapidly at a shear plane position close to the base (0%), middle (50%) and top (100%) part of the canister. Also, the initiation probability is almost constant around a shear plane position of 25% (75%). This is more pronounced at higher values of shear displacement.

In order to further investigate the dependence of the shear plane position, the next step is to model this as a probabilistic parameter (see section 5.2).

5.2 Probability of initiation of crack growth or stable crack growth using three probabilistic parameters

In this analysis, the fracture toughness, defect depth and the shear plane position are treated as probabilistic parameters. When calculating the probabilities, the mean values of the yield stress and ultimate tensile strength are used. In Fig. 5-5 the probability of initiation of crack growth is plotted as a function of the size of the rock shear displacement (using a bentonite density = 2000 kg/m^3). In Fig. 5-6, the probability of 2 mm stable crack growth is plotted. Also, a comparison is made between the two cases with either two or three probabilistic parameters.
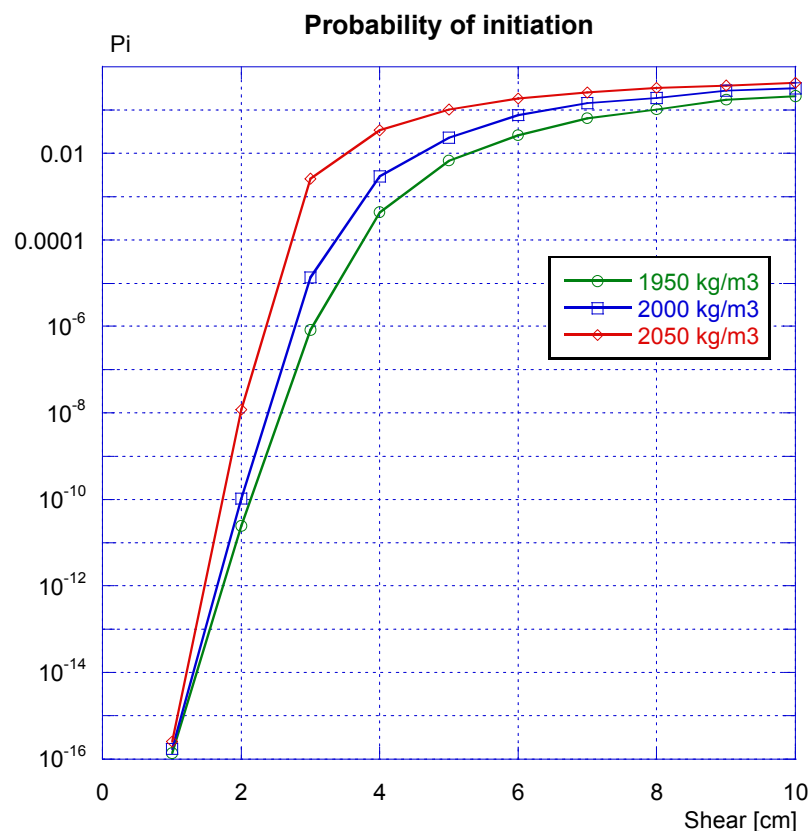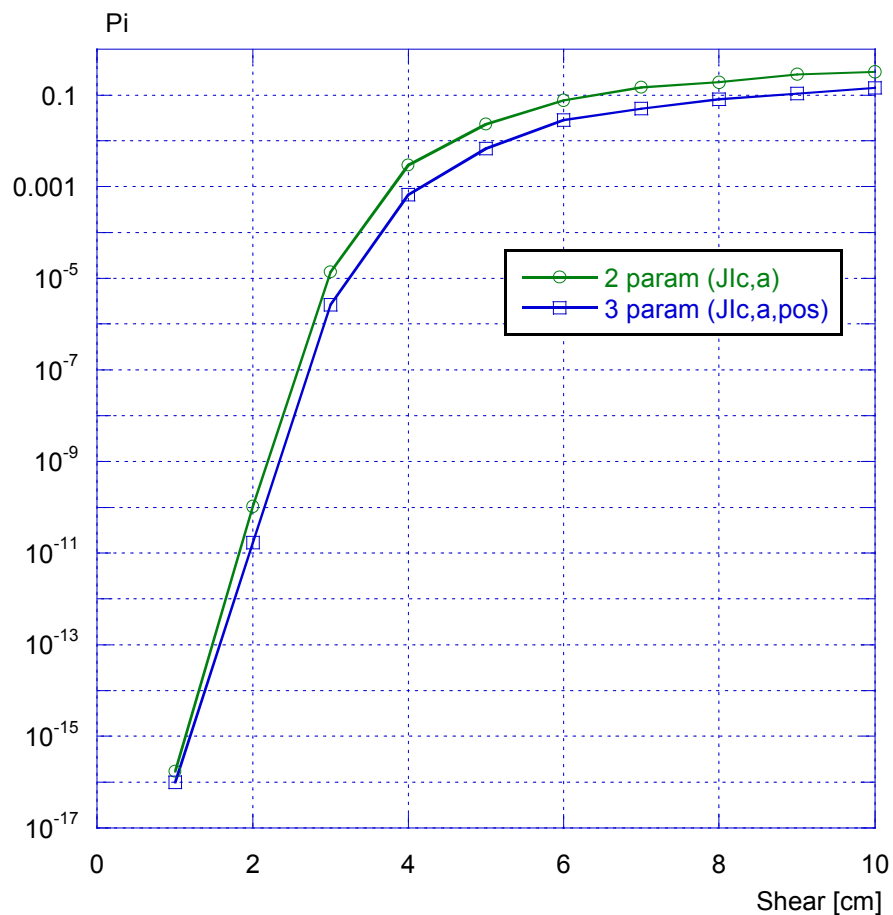

Figure 5-5.   Probability of initiation of crack growth as a function of the size of the rock shear displacement (with constant bentonite density = 2000 kg/m^3). A comparison is made between the cases with either two or three probabilistic parameters.
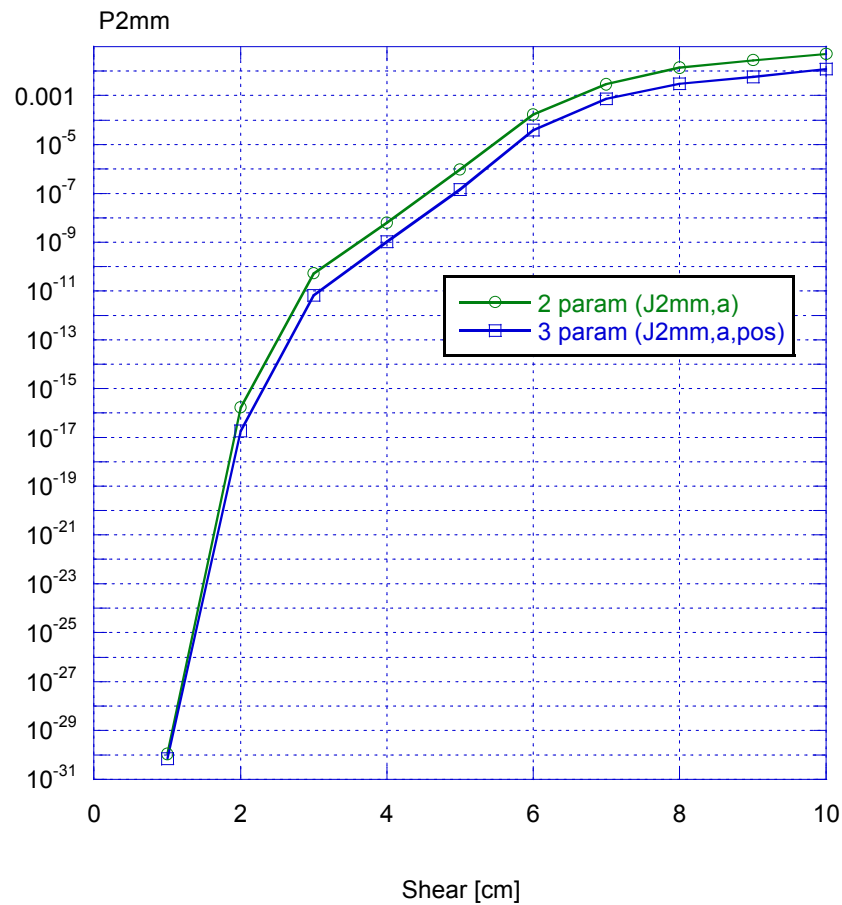
Figure 5-6.   Probability of 2 mm stable crack growth as a function of the size of the rock shear displacement (with constant bentonite density = 2000 kg/m^3).

As seen above, there is a small difference in the resulting probabilities between the two assumptions with or without using the shear plane position as a probabilistic parameter. When investigating Fig. 5-4, it is obvious that the probabilities will be lower when including the shear plane position as a probabilistic parameter (since the maximum value was used when treating the shear plane position as a deterministic parameter). However, the difference will be small since the values around a shear plane position of 25% or 75% are almost constant (see Fig. 5-4).

In order to investigate the influence of using more probabilistic parameters in the analysis, probabilistic assumptions regarding the bentonite density are introduced in section 5.3.

Report No.: 50014130-1   Revision No.: 5

5.3 Probability of initiation of crack growth or stable crack growth using four probabilistic parameters

In this analysis, the <u>fracture toughness</u>, <u>defect depth</u>, <u>shear plane position</u> and the <u>bentonite density</u> are treated as probabilistic parameters. When calculating the probabilities, the mean values of the yield stress and ultimate tensile strength are used. In Fig. 5-7-1, the probability of initiation of crack growth is plotted as a function of the size of the rock shear displacement (using different assumptions regarding the bentonite density).

It is important to remember that the assumption regarding the bentonite density that is used in this analysis does not represent the design condition of the buffer, but it may be used as an example of a realistic statistical distribution of the bentonite density (informed or non-informed). As given in section 2.7, two different density distributions were assumed. The first choice is a non-informed uniform distribution that is generally used to study the influence of the chosen parameter when there is no information regarding the data. The second choice is a more informed normal distribution based on data from the production report for the buffer [12]. These calculations are then compared with the earlier analysis that treated the bentonite density as a deterministic parameter (see Fig. 5-7-1).
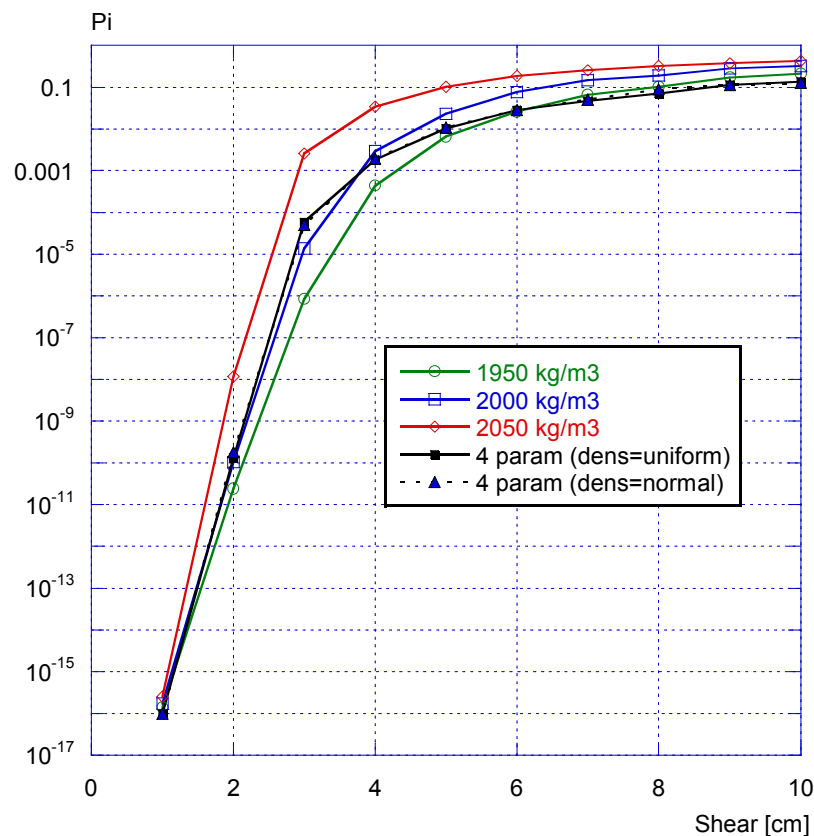
Figure 5-7-1.   Probability of initiation of crack growth as a function of the size of the rock shear displacement (using different assumptions regarding the bentonite density).

As seen above, when the shear displacement is below 4 cm the probability values are close to or slightly above the values obtained when using a constant bentonite density = 2000 kg/m^3. When the shear displacement is above 4 cm the probability values are close to the values obtained when using a constant bentonite density = 1950 kg/m^3 (independent of the chosen bentonite density distribution).

Report No.: 50014130-1   Revision No.: 5

Also, the results show that when treating the density as a probabilistic parameter, the probability of initiation values at shear values larger than 6 cm are lower than when the density is a deterministic parameter with density = 1950 kg/m^3. Since the comparison is made between the results presented in Fig. 5-1 (using two probabilistic parameters) and the results in this section using four probabilistic parameters (shear plane position and bentonite density are included), the reason that the probability values falls below the deterministic density values are the shear plane position which lowers the probability values. This is shown in Fig. 5-5.

Finally, in Fig. 5-7-2, the probability of 2 mm stable crack growth is plotted as a function of the size of the rock shear displacement (using different assumptions regarding the bentonite density).
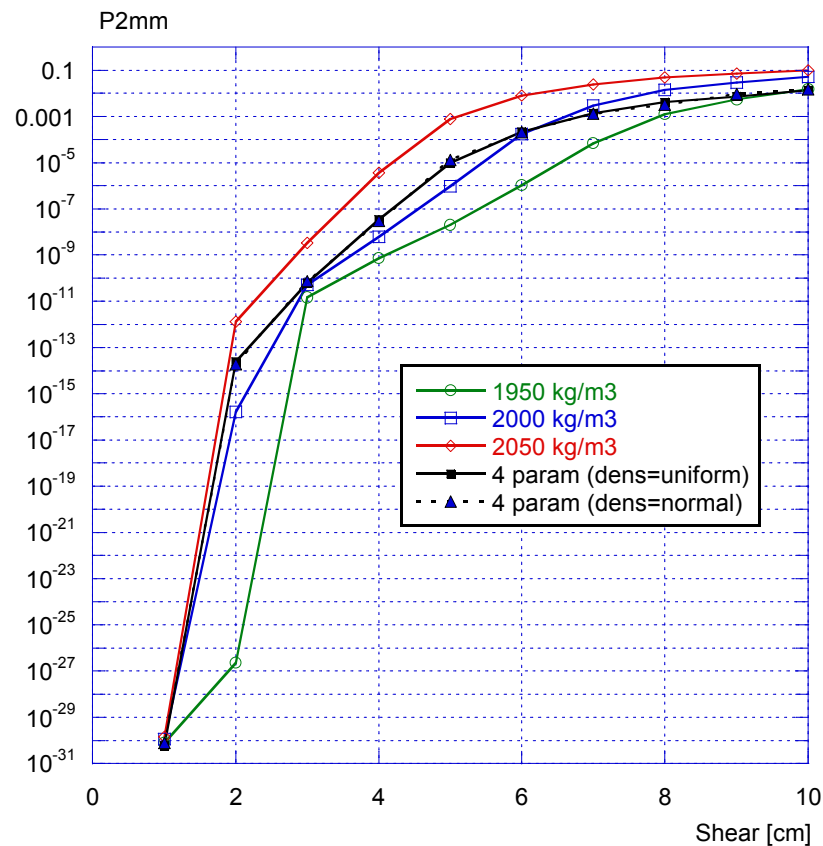
Figure 5-7-2.   Probability of 2 mm stable crack growth as a function of the size of the rock shear displacement (using different assumptions regarding the bentonite density).

A comparison of Fig. 5-7-1 and Fig. 5-7-2 shows that the behavior is similar when plotting the probability of initiation of crack growth or the probability of 2 mm stable crack growth.

5.3.1   What parameter contributes the most to the calculated probabilities?

A large benefit when conducting a probabilistic analysis is the fact that it is possible to investigate the dependence of the different probabilistic parameters included in the analysis. This section starts by an evaluation of what parameter that contributes the most to the calculated probabilities. This is done by using importance factors as presented and defined in section 3.2.4. These importance factors are used to get a <u>qualitative understanding</u> of the different parameters relative importance in a probabilistic analysis. <u>When a parameter has an importance factor close to one, it dominates the analysis</u> and most of the contribution to the calculated probabilities then comes from this parameter. When a parameter has an importance factor close to zero, it has a minor contribution to the calculated probabilities. In Fig. 5-8 to 5-9 the importance factors are plotted using two different assumptions regarding the bentonite density distribution (uniform or normal).

Figure 5-8.   Importance factors, related to the calculated initiation probabilities, using four probabilistic parameters (a uniform bentonite density distribution).

Figure 5-9.   Importance factors, related to the calculated initiation probabilities, using four probabilistic parameters (with a normal bentonite density distribution).

As seen above, the fracture toughness contributes the most to the calculated initiation probabilities when the shear displacement is below ~2.5 cm. When the shear displacement is above ~2.5 cm, the defect depth contributes the most to the calculated initiation probabilities. When the shear displacement is close to 10 cm, the shear plane position starts to be equally important. The bentonite density is of less importance among the four parameters considered in this analysis.

The results presented in Fig. 5-8 and Fig. 5-9 will change if a lower limit is introduced in the fracture toughness distribution (given in Sect. 2.2). Since the fracture toughness contributes the most to the calculated initiation probabilities (when the shear displacement is below ~2.5 cm), introducing a lower limit for the fracture toughness means that the defect depth will get a larger importance factor.

5.3.2 What parameter change has the most influence on the calculated probabilities?

In this section, the evaluation of what parameter change that has the most influence on the calculated probabilities is presented. The purpose of the evaluation is to study the impact on the calculated probabilities of a small change in the input data. This is done by using the procedure presented and defined in section 3.2.5, i.e. by differentiating the initiation probability with respect to different parameter (mean values and standard deviation). The results are normalized against the probabilities to get a better understanding of the interaction between the calculated sensitivities. In Fig. 5-10 to 5-11 these sensitivities are plotted with respect to the chosen mean value and standard deviation.

Note: Logarithmic scale in this plot.

Figure 5-10.   Sensitivity analysis, changes in the mean values and how it will affect the calculated initiation probabilities (linear and logarithmic scales).

As shown above, a small change in the mean value of the shear plane position will have a large impact on the calculated probabilities. This is independent of the assumed shear displacement. According to Fig. 5-4, the mean value represents a local minimum and a small deviation from this value will give a large increase in the calculated probabilities.

The second most important parameter in this sensitivity analysis is the defect depth, because it contributes the most to the calculated initiation probabilities (as shown in Fig. 5-8).

Finally, when the shear displacement is below 1 cm, the fracture toughness becomes the most important parameter. This is also related to the fact that it contributes the most to the calculated initiation probabilities (as also shown in Fig. 5-8).

Report No.: 50014130-1   Revision No.: 5

Figure 5-11.   Sensitivity analysis, changes in the standard deviation values and how it will affect the calculated initiation probabilities (linear and logarithmic scales).

As shown above, the behavior of the standard deviation values is similar to the behavior of the mean values in Fig. 5-10. The largest difference is related to the defect depth, which is more sensitive to changes in the standard deviation values.

5.4   Probability of initiation of crack growth or stable crack growth using five probabilistic parameters

In this analysis, the fracture toughness, defect depth, shear plane position, bentonite density and rock shear displacement are treated as probabilistic parameters. When calculating the probabilities, the mean values of the yield stress and ultimate tensile strength are used. In Fig. 5-12 the probability of initiation of crack growth and the probability of 2 mm stable crack growth are plotted as a function of the mean value of the rock shear displacement.

It is important to remember that the assumptions regarding the rock shear displacement that is used in this analysis do not represent the real conditions in the repository. They may be described as examples of statistical distributions with mean values of the same order of magnitude as the shear movements of significance in this study (as given in section 2.8).
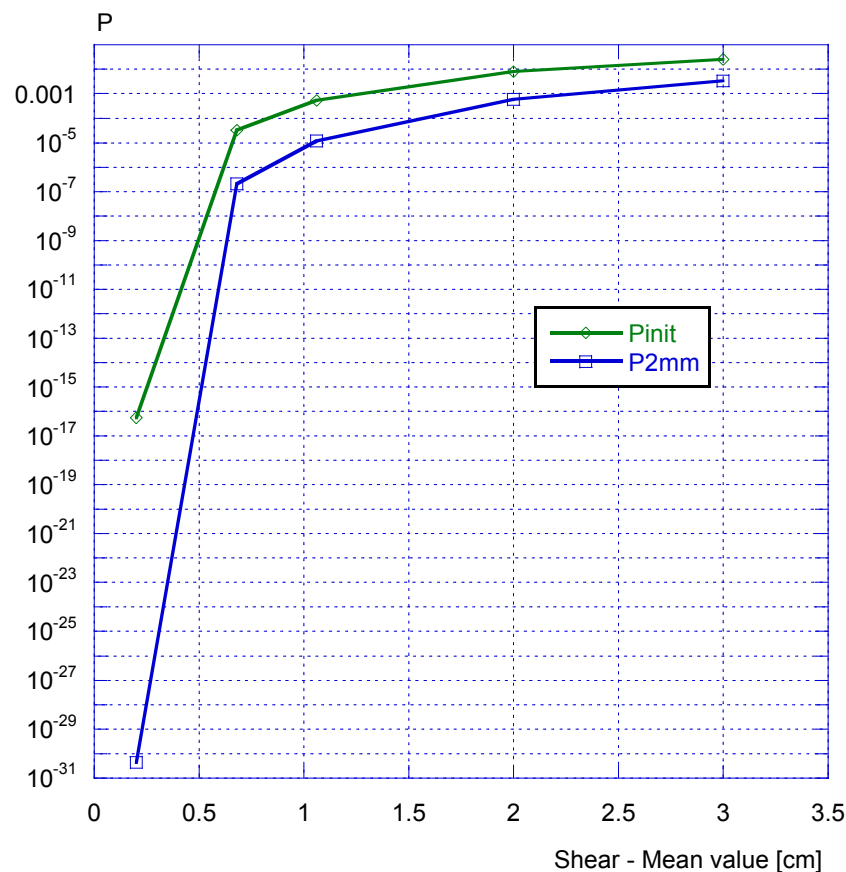
Figure 5-12.   Probability of initiation of crack growth and probability of 2 mm stable crack growth as a function of the mean value of the rock shear displacement.

As shown above, as the mean value decreases below 1 cm (and using an exponential distribution), the probability quickly approaches very small values and the impact of an earthquake induced rock shear load becomes insignificant. As the mean value increases above 1 cm, the calculated probabilities increase. The changes are not as rapid as for lower values of the mean, but an increase from e.g. 1 to 2 cm still implies a change in probability by more than an order of magnitude.

5.4.1   What parameter contributes the most to the calculated probabilities?

In this section it is investigated what parameter that contributes the most to the calculated probabilities (now using five probabilistic parameters). This is done by using importance factors plotted as a function of the mean value of the rock shear displacement (see Fig. 5-13).
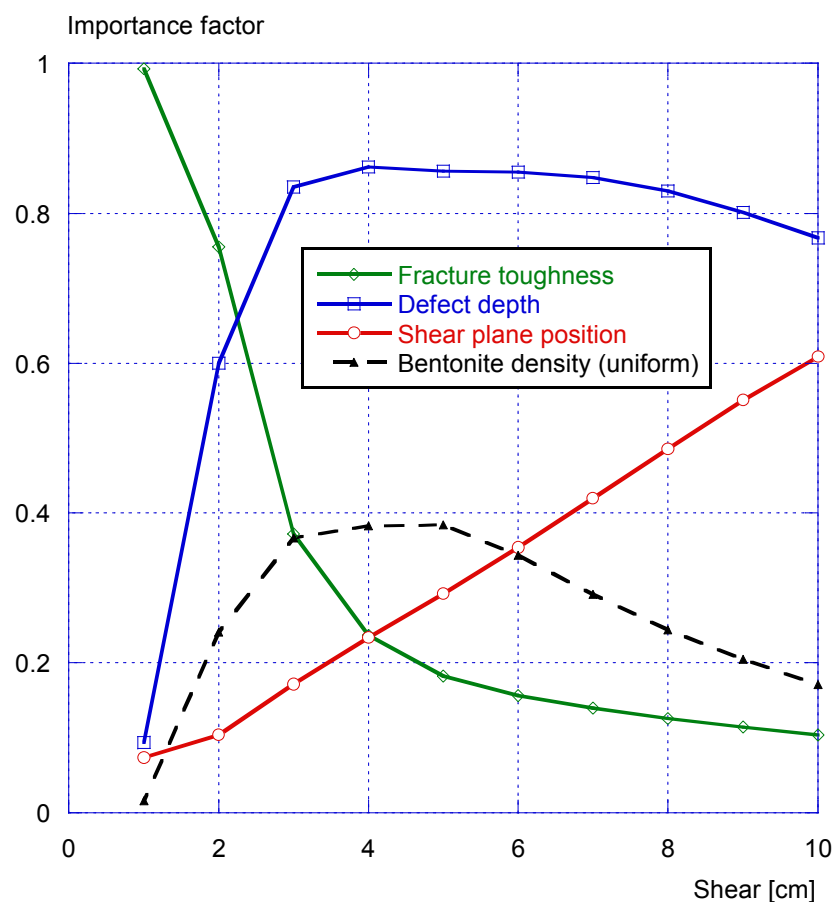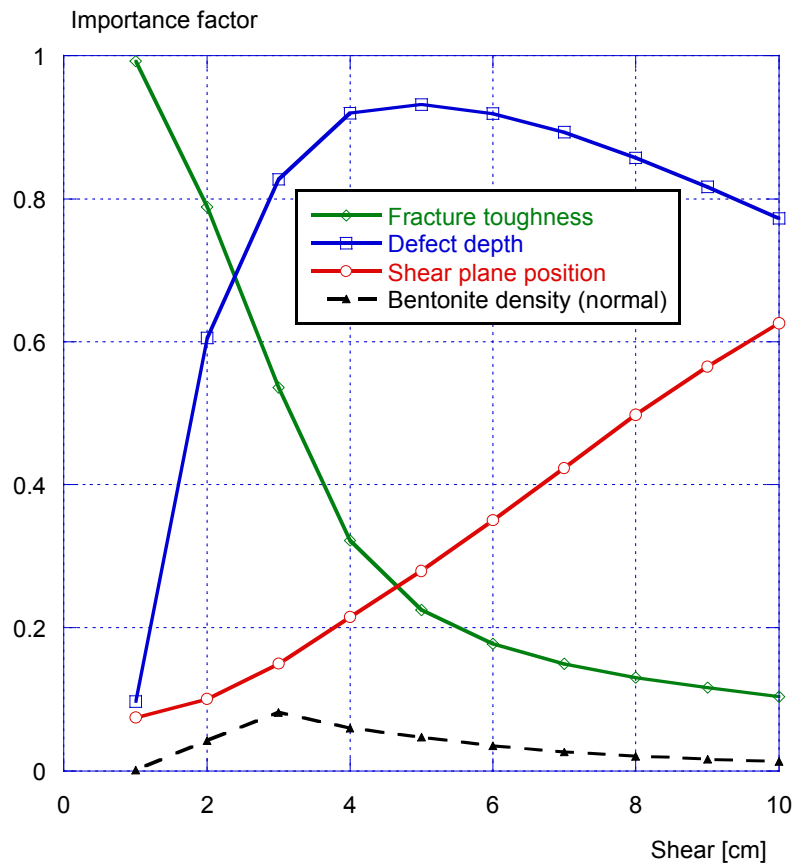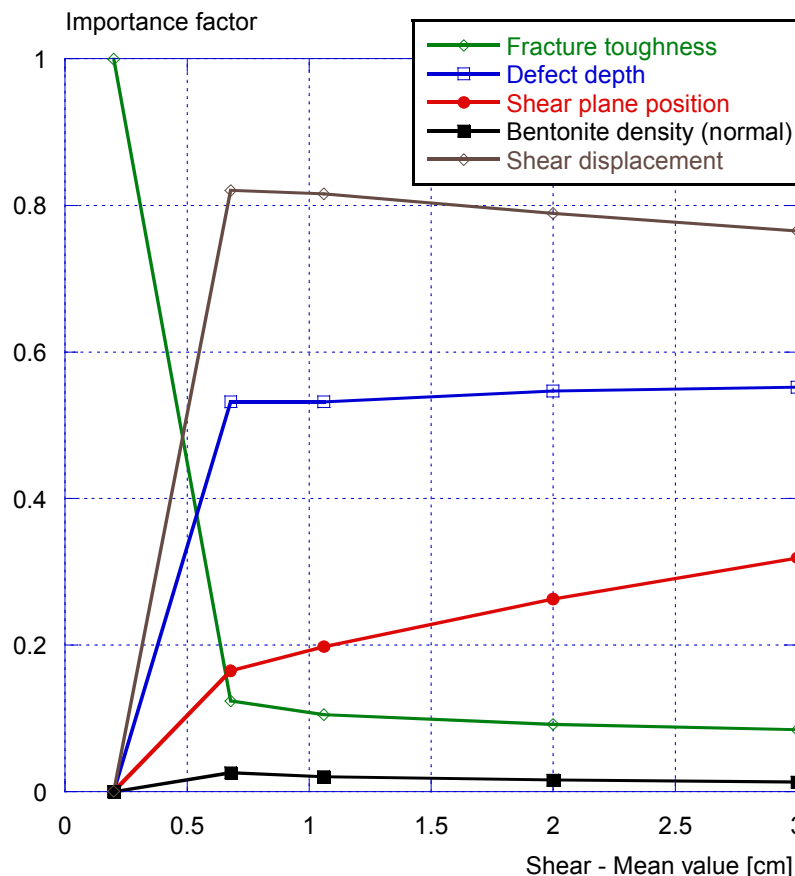

Figure 5-13.   Importance factors, related to the calculated initiation probabilities, using five probabilistic parameters.

As shown above, if the mean value of the rock shear displacement is above 0.5 cm, it also contributes the most to the calculated initiation probabilities. When the mean value of the rock shear displacement is below 0.5 cm, the fracture toughness contributes the most to the calculated initiation probabilities.

It is also interesting to compare Fig. 5-13 with Fig. 5-9 showing a plot of importance factors using four probabilistic parameters. The two figures are very similar, but with the introduction of the rock shear displacement, all the other parameters are not as important when the mean value of the rock shear displacement is above 0.5 cm. This shows the significance of the assumptions regarding the rock shear displacement.

6   PROBABILITY OF GLOBAL PLASTIC COLLAPSE AND A COMPARISON WITH THE PROBABILITY OF INITIATION OF CRACK GROWTH OR STABLE CRACK GROWTH

In this section, the results for the probability of global plastic collapse are given using the input data presented in section 2 (the limit state function is related to a critical strain measure, see section 3.1.3). The results are presented using three probabilistic parameters.

In this analysis, the elongation at fracture, shear plane position and the bentonite density are treated as probabilistic parameters. The defect depth is not included in this analysis, since it doesn't contribute to plastic collapse. When calculating the probabilities, the mean values of the yield stress and ultimate tensile strength are used and a uniform distribution is used for the bentonite density. In Fig. 6-1, the probability of global plastic collapse is plotted as a function of the size of the rock shear displacement (assumed to be deterministic in this analysis).
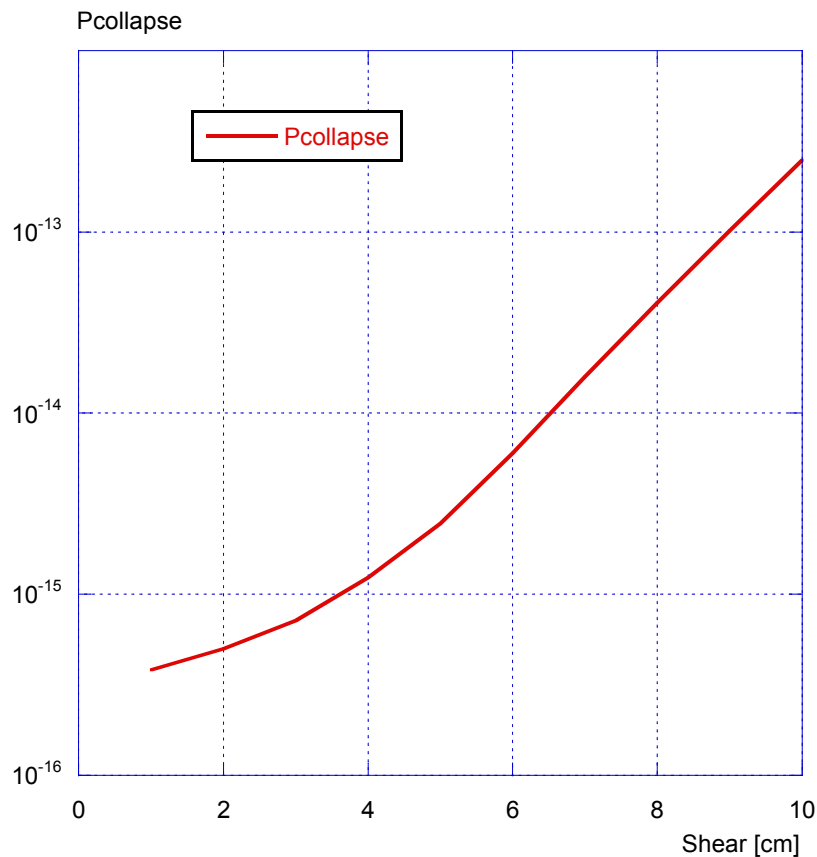
Figure 6-1.   Probability of global plastic collapse as a function of the size of the rock shear displacement.

As shown above, the probability of global plastic collapse is very small independent of the assumption regarding the rock shear displacement. It would be interesting to compare these probabilities with the earlier calculations where the existence of a surface crack is assumed; this is done in Fig. 6-2 below.
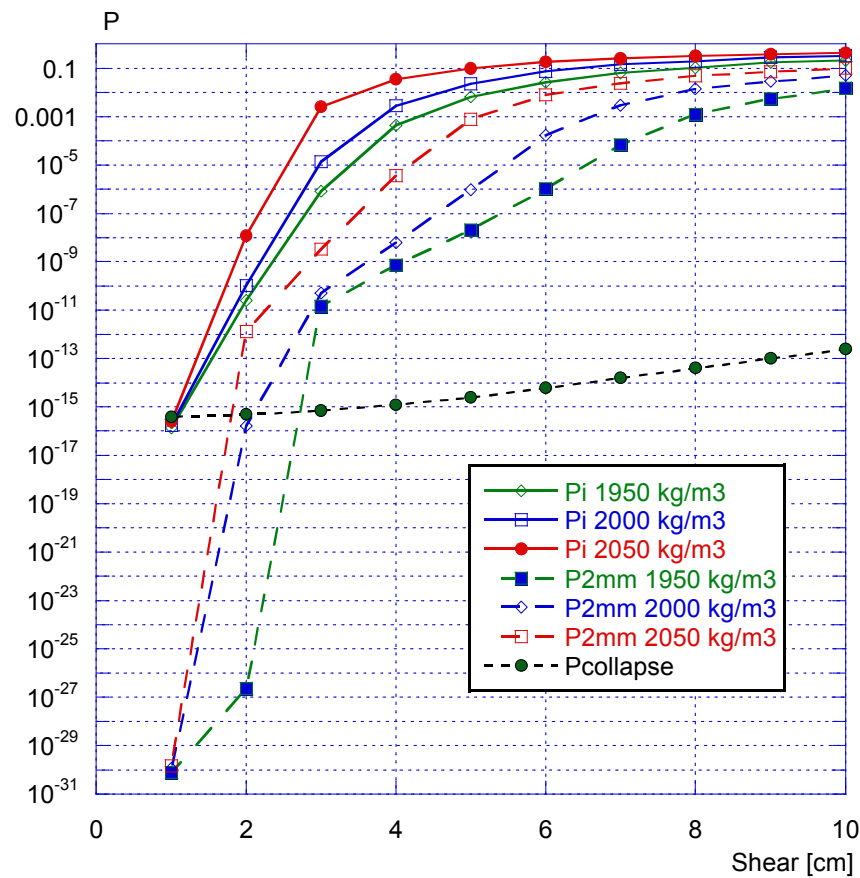
Figure 6-2.   Comparison between the probability of global plastic collapse, probability of initiation and probability of 2 mm stable crack growth as a function of the size of the rock shear displacement (P_i and P_{2mm} with 3 different bentonite densities).

As shown above, the global plastic collapse is of less importance as compared to the initiation of crack growth (or 2 mm stable crack growth).

7   MORE SENSITIVITY ANALYSIS

When the results in Section 5 were presented, a number of sensitivity analyses were also included as a natural part of the result presentation. This section concentrates on a number of sensitivity analyses to describe other relationships in a probabilistic analysis.

7.1   Comparison with different assumed defect depth distributions

In the probabilistic analysis, the existence of one crack-like defect was assumed, and the size (depth) of this defect is characterized by an exponential distribution (same assumption as in the earlier study [2]). The choice of defect depth distribution is quite important when performing a probabilistic analysis; therefore a sensitivity analysis using either a lognormal or a Weibull defect depth distribution (as recommended in [5]) would be of interest. A comparison between an exponential and a lognormal distribution is shown in Fig. 7-1.
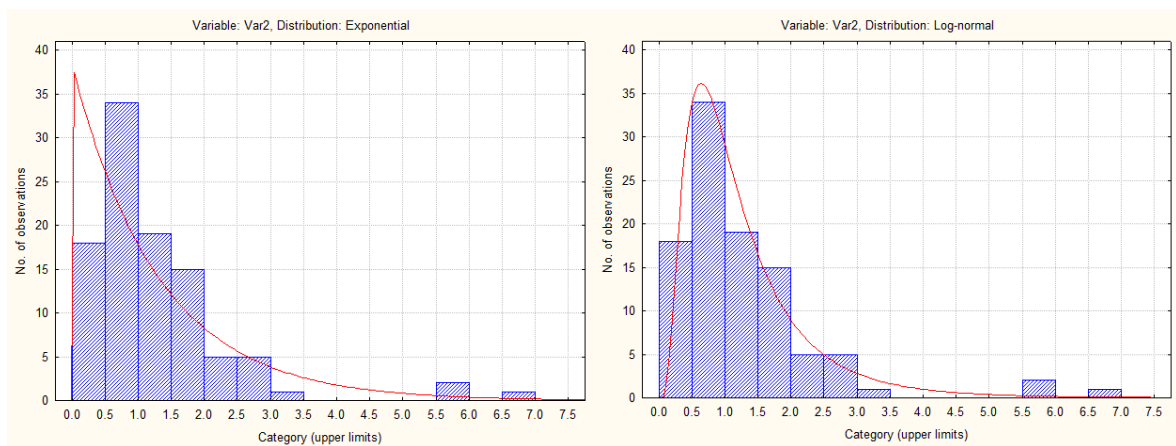
Figure 7-1. Comparison between an exponential and lognormal defect depth distribution.

Even though the lognormal distribution has a better fit to the data, it often underestimates the number of small defects that exists (but not included in the data).

Another comparison between an exponential, lognormal and Weibull distribution is shown in Fig. 7-2 to 7-3.
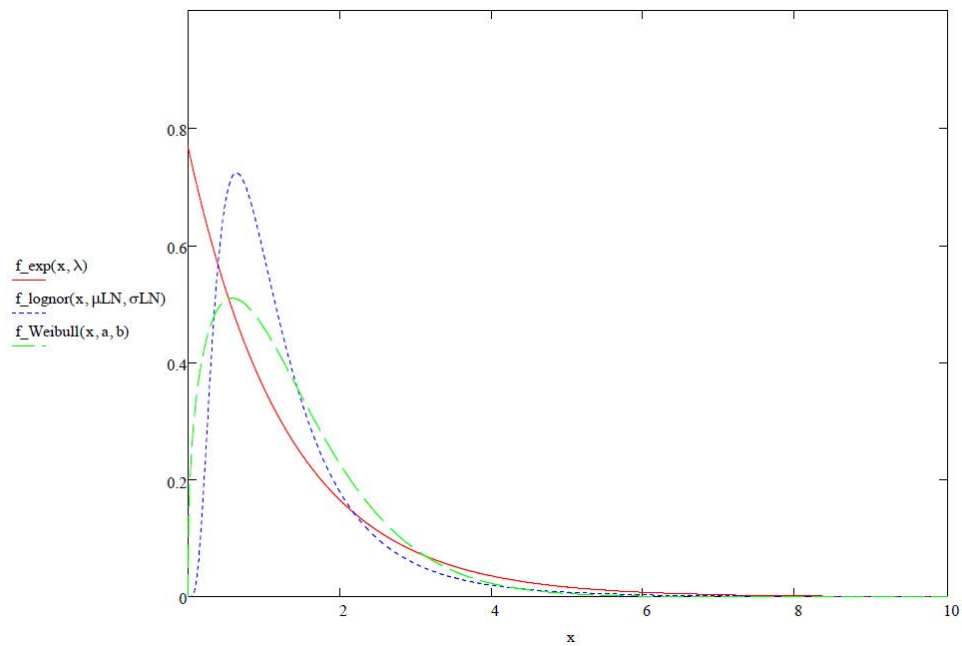
Figure 7-2.   Comparison between an exponential, lognormal and Weibull defect depth distribution (linear scale).
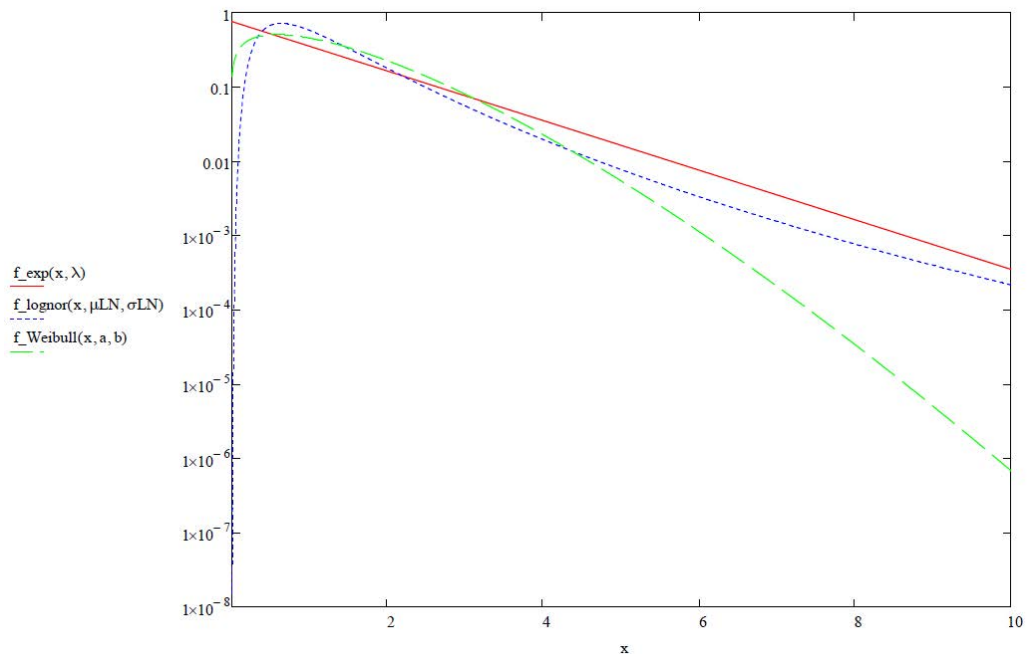
Figure 7-3.   Comparison between an exponential, lognormal and Weibull defect depth distribution (logarithmic scale).

As shown in Fig. 7-2 to 7-3, there is only a minor difference between the exponential and lognormal distribution for defects larger than ~1 mm (depth, but a major difference for defects smaller than ~1 mm. The largest difference between the Weibull distribution and the others is for defects larger than ~6 mm. However, in practice, the Weibull distribution is seldom used to model crack like defects in materials that do not behave in a brittle manner.

When fitting the data to the different distributions there are some differences in the mean values and standard deviation (see Table 7-1).

Table 7-1. Comparison between an exponential, lognormal and Weibull defect depth distribution.

Distribution	Mean	Stadev
Exponential	1.30	1.30
Lognormal	1.29	0.99
Weibull	1.32	0.95

To identify the impact of the choice of defect distribution, a sensitivity analysis was conducted that calculated the probability of 2 mm stable crack growth (see Fig. 7-4).
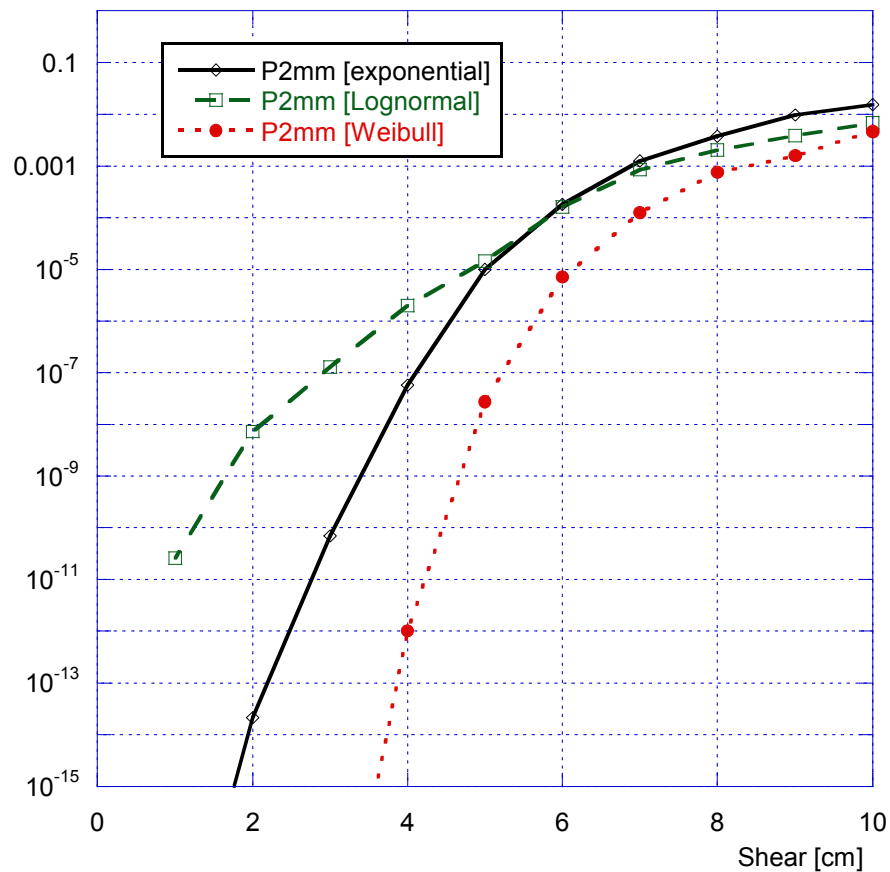
Figure 7-4.   The probability of 2 mm stable crack growth, sensitivity analysis using different defect depth distributions.

As shown in Fig. 7-4, the probabilities using a Weibull distribution are always below the probabilities with the other distributions. Also, the difference between the exponential and lognormal distribution is quite small when the shear displacement is above 5 cm.

Finally, it is of interest to compare the defect frequency (from data) with the probability to have defects which are larger than a specific defect depth using the three distributions (see Fig. 7-5). As before, the Weibull distribution gives probabilities that are below those with the other distributions and the actual data follows the exponential and lognormal distribution.
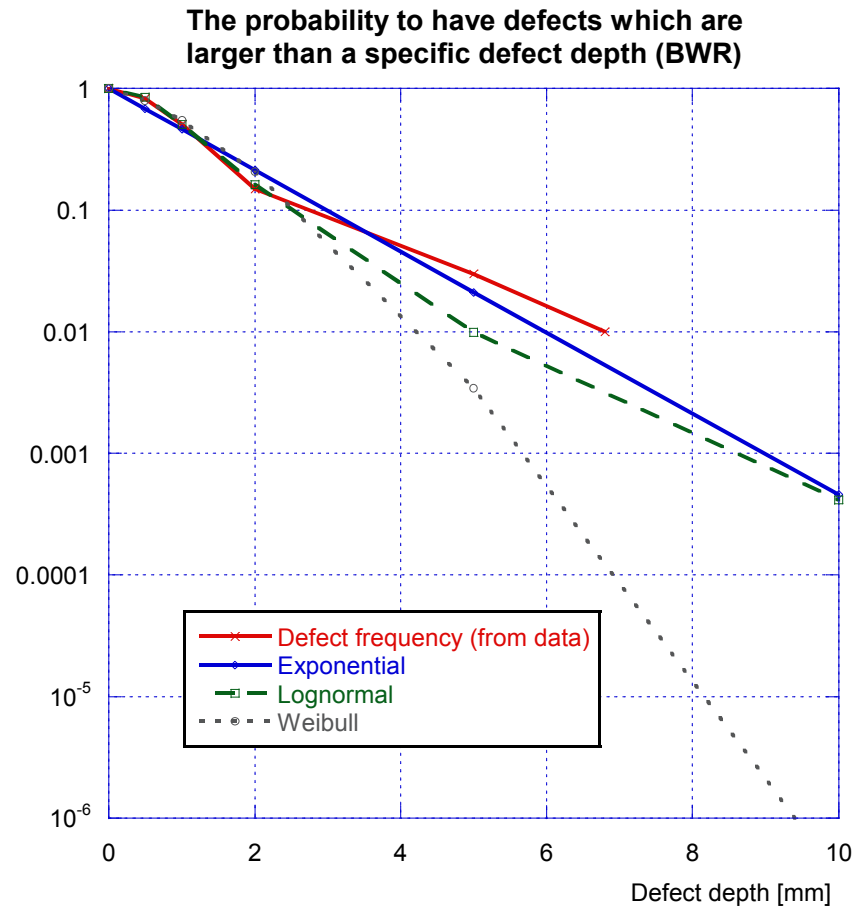
Figure 7-5.   Comparison of the defect frequency (from data) with the probability to have defects which are larger than a specific defect depth.

7.2 Investigation of the link between probabilities and defect size

Another interesting analysis is to check what defect size that contributes the most to the calculated probabilities. This could be done by investigating the link between initiation probabilities and defect size, i.e. to check the most probable point of failure (initiation of crack growth) from a FORM analysis. The analysis used in this study is presented in section 5.3 and the most probable point of failure from this analysis is plotted in Fig. 7-6.
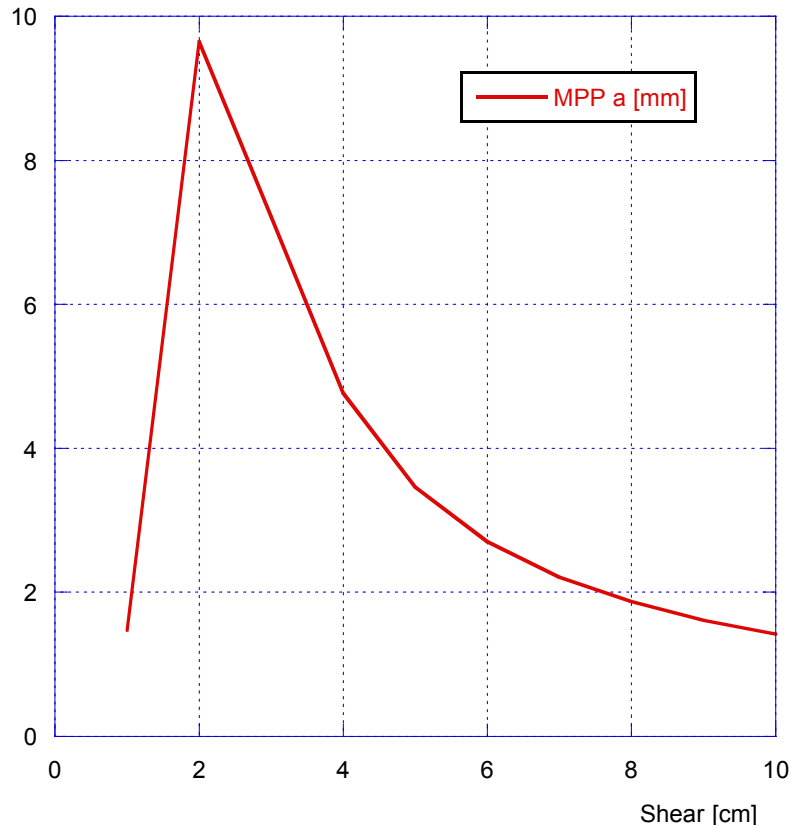
Figure 7-6.   The most probable point of failure (defect depth) using four probabilistic parameters and initiation of crack growth as a critical event.

As shown in Fig. 7-6, the most probable point of failure is located at smaller defect depths as the shear displacement increases. This means that smaller defects suffice to obtain initiation of crack growth. When the shear displacement is below 2 cm, there is a discontinuity in the curve representing the most probable point of failure. The reason for this is found in Fig. 5-8 and Fig. 5-9 (importance factors for this case) where the defect depth contributes the most to the calculated initiation probabilities (when the shear displacement is above ~2.5 cm).

Since the defect depth contributes the most to the calculated initiation probabilities (when the shear displacement is above ~2.5 cm) it is of interest to compare the most probable point of failure (defect depth) and the critical defect depth from a deterministic analysis (shear = 5 cm).

-     The critical defect depth = 3.3 mm (using the fracture toughness at initiation [4]).
-     The most probable point of failure/initiation (defect depth) = 3.5 mm.

Since the defect depth dominates the analysis at 5 cm shear displacement, it is reasonable that these values coincide.

7.3   Comparison using data from PWR inserts

All the probabilistic calculations presented earlier in the report uses data from BWR-inserts. Recently, new defect data [11] and fracture toughness data [18] for PWR-inserts has been analyzed and it is therefore possible to compare the probabilistic calculations using data from PWR-inserts.

First, a comparison is made, using defect distributions evaluated from BWR- or PWR-data. As given in Sect. 2.4, the BWR defect data follows an exponential distribution with a mean defect depth value of 1.3 mm. In [11], PWR-defect data are analyzed and this data follows an exponential distribution with a mean defect depth value of 0.8 mm. Obviously the PWR-data is better than the BWR-data and how this influences the calculated probability of 2 mm stable crack growth is given in Fig. 7-7.
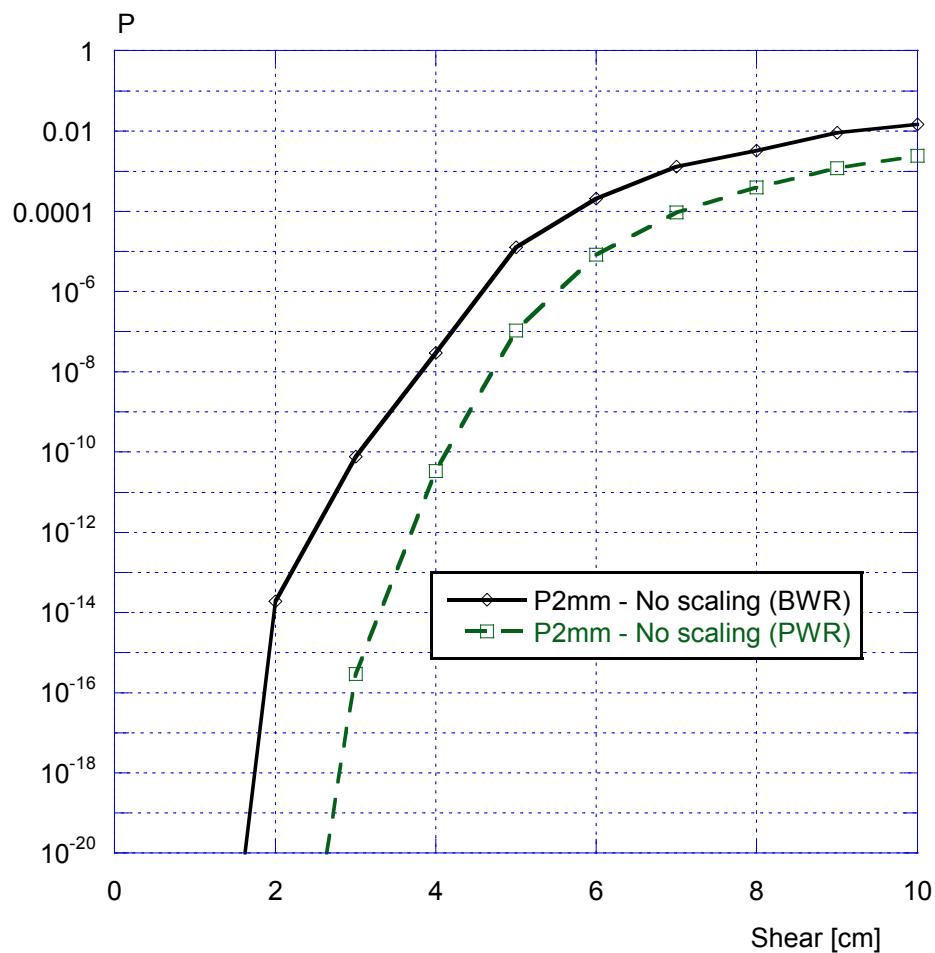
Figure7-7.   Probability of 2 mm stable crack growth as a function of the rock shear displacement (sensitivity analysis using defect distributions from BWR- or PWR-inserts).

As shown in Fig. 7-7, the probability of 2 mm stable crack growth is much lower using defect data from PWR-inserts as compared to BWR-inserts. As an example, using a rock shear displacement of 5 cm, the difference is a factor of 100.

Next, a comparison is made between using fracture toughness data from BWR- and from PWR-inserts. As given in Sect. 2.1, the BWR fracture toughness data at 2 mm stable crack growth follows a normal distribution with a mean value of 90.8 kN/m. According to [18], PWR fracture toughness data at 2 mm stable crack growth follows a normal distribution with a mean value of 159.7 kN/m. Obviously the PWR-data is much better than the BWR-data and how this influences the calculated probability of 2 mm stable crack growth is shown in Fig. 7-8 (combined with the analysis presented in Fig. 7-7).
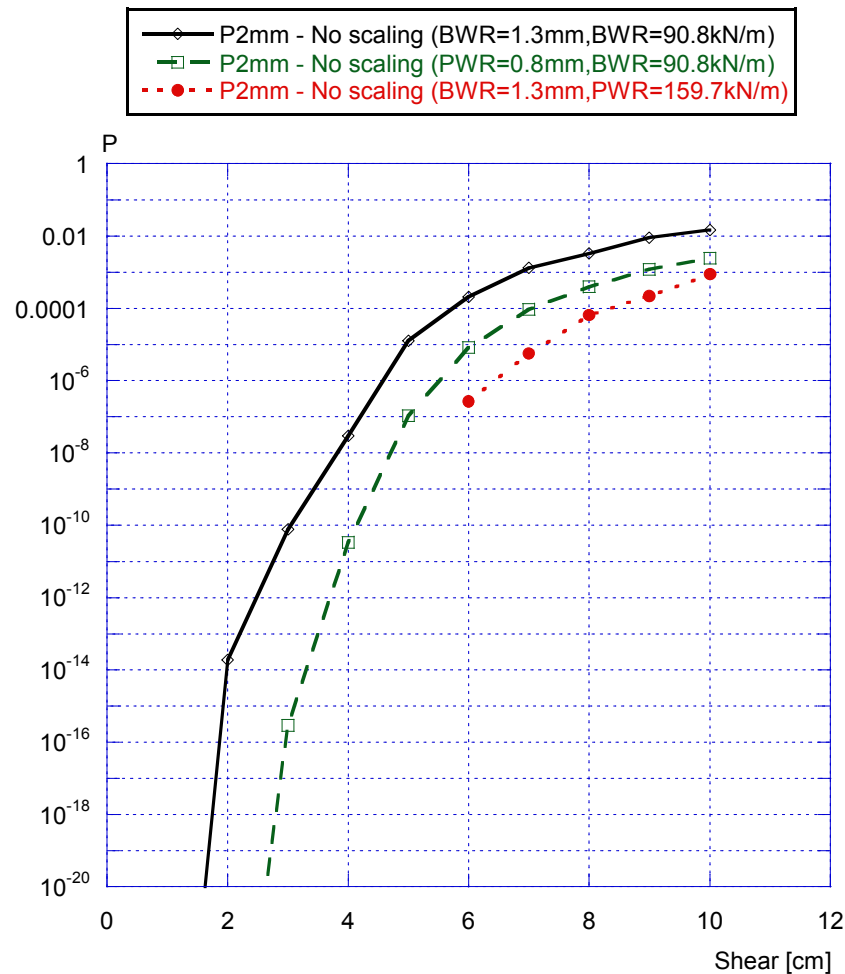
Figure7-8.   Probability of 2 mm stable crack growth as a function of the rock shear displacement (sensitivity analysis using different fracture toughness data and defect distributions from BWR- or PWR-inserts).

As shown in Fig. 7-8, the probability of 2 mm stable crack growth is much lower using fracture toughness data from PWR-inserts as compared to BWR-inserts. It is also shown that an analysis with fracture toughness data from PWR-inserts has a larger impact on the calculated probabilities than using defect distributions from PWR-inserts.

In Fig. 7-8, the results using fracture toughness data from PWR-inserts is only given with a shear displacement of 6 cm up to 10 cm. The reason for this is that the probabilistic calculations have problems with convergence for lower values of shear displacement. This is related to the approximation of the limit state functions (surfaces) which were developed using BWR-data. When using fracture toughness data from PWR-inserts, very large cracks are needed to fulfill the limit state and the extrapolation required is not valid for these large cracks.

7.4   Comparison using random parameters that are correlated

In the calculations presented in Sect. 5-6, all the random parameters are treated as not being correlated with one another. To check this assumption a simple sensitivity analysis was performed using one case presented in Sect. 5.1 (i.e. probability of initiation of crack growth using two probabilistic parameters and a bentonite density of 2050 kg/m^3). In general, a weak correlation (e.g. with a correlation coefficient = 0.1-0.2) can usually be ignored and the variables be treated as being independent. A strong correlation (e.g. with a correlation coefficient = 0.8-1.0) can usually be treated as fully dependent with one of the two variables replaced by the other.

Three cases are compared:

- In the baseline case, the assumption is that the fracture toughness and the defect depth are not correlated (as in the calculations presented in Sect. 5-6).

- In the second case, a weak correlation is introduced between the fracture toughness and the defect depth.

- In the third case, a strong correlation is introduced between the fracture toughness and the defect depth.

The correlation is introduced somewhat arbitrarily so that the correlation coefficient is larger than zero. The results are presented in Fig. 7-9.
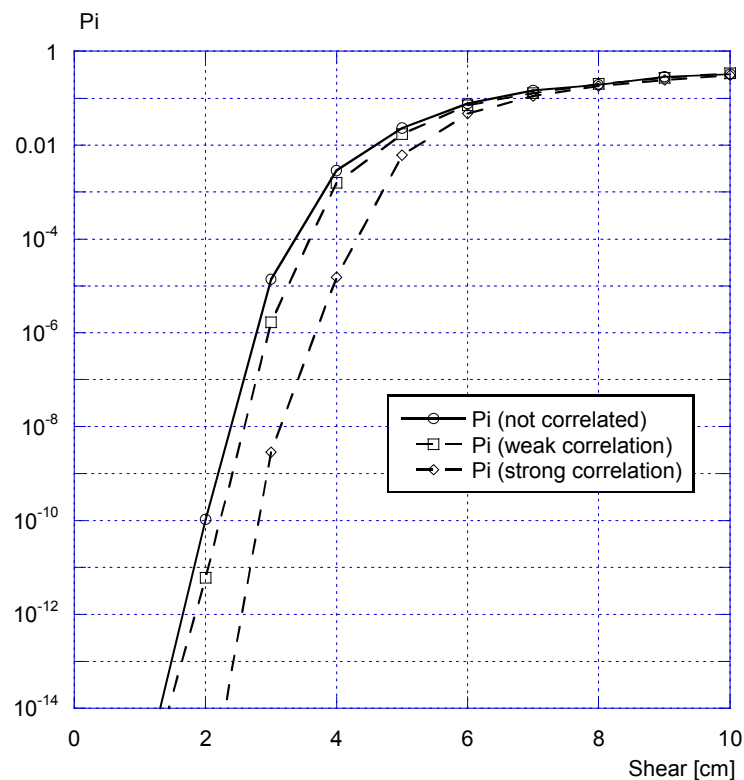
Figure 7-9.   Probability of initiation of crack growth as a function of the rock shear displacement (sensitivity analysis using different assumptions regarding the correlation between fracture toughness and defect depth).

As shown in Fig. 7-9, a weak correlation between the fracture toughness and the defect depth has a minor impact on the resulting initiation probabilities. A strong correlation has larger impact when the rock shear displacement is below 5 cm.

7.5 Investigation of the link between the given probabilities and a deterministic damage tolerance analysis

In Sect. 4.2 (Fig. 4-11), a deterministic damage tolerance analysis was presented using similar data as the one presented in [4] (fracture toughness at 2 mm stable crack growth, a shear plane position at 75% from the base of the canister and a bentonite density of 2050 kg/m^3). It is now possible to link this damage tolerance analysis with the probabilities presented in Sect. 5.3 (i.e. using four probabilistic parameters) and given in Fig. 5-7-2 (probability of 2 mm stable crack growth as a function of the size of the rock shear displacement). The different calculations are linked using an equivalent shear displacement and presented in Fig. 7-10 (the scaling defined in Sect. 8.1 is also included in the plot).
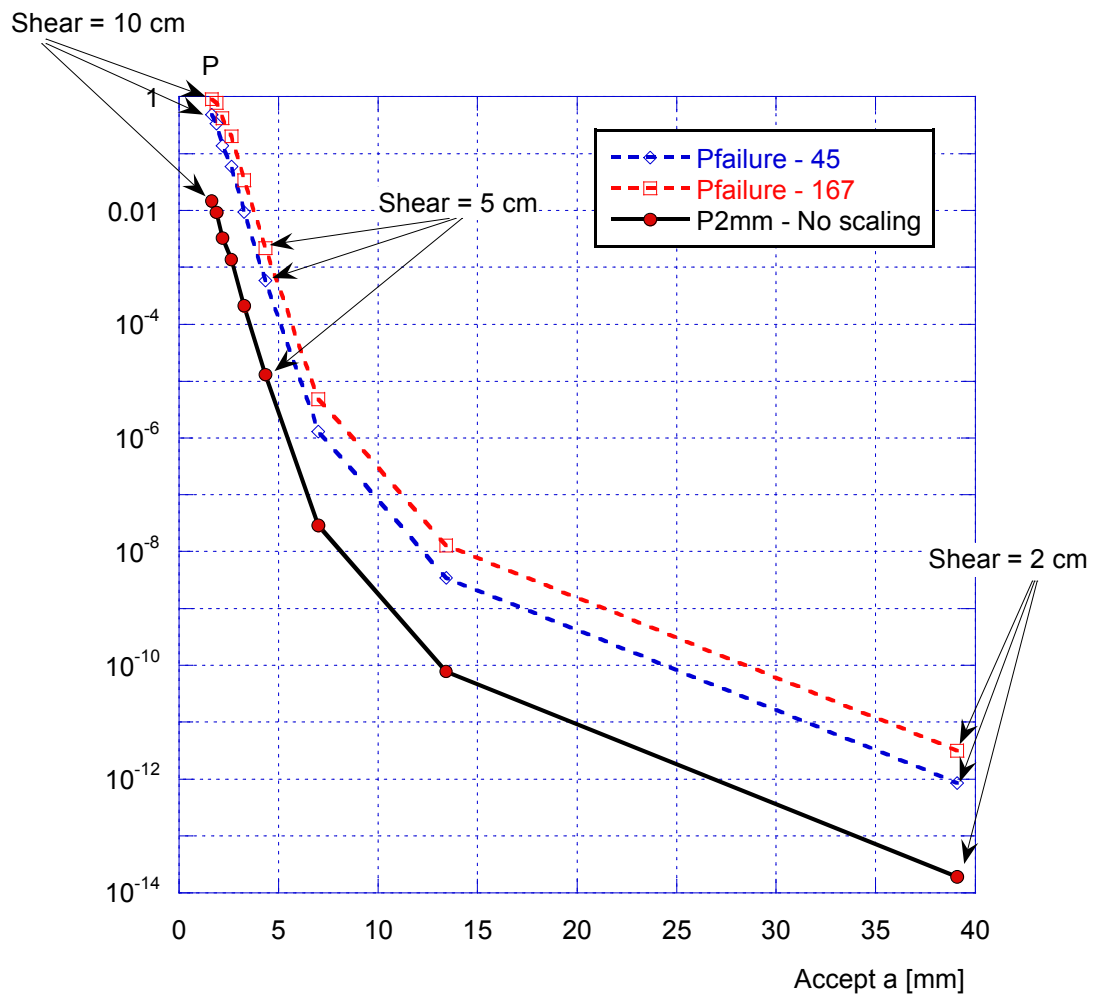
Figure 7-10.   Probability of 2 mm stable crack growth as a function of the acceptable defect depth given from a deterministic damage tolerance analysis. Also shown is the size of the equivalent rock shear displacement at three locations in the plot. Finally, the scaling defined in Sect. 8.1 is included in the plot (using $n = 45$ and $n = 167$).

8 ESTIMATE IF A CANISTER INSERT FAIL IN THE CASE OF AN EARTHQUAKE INDUCED ROCK SHEAR LOAD

In section 5, the results for the probability of initiation of crack growth and the probability of 2 mm stable crack growth are given using the assumption that there exists a surface crack with a derived depth distribution. This means that the calculated probabilities are related to the existence of one crack-like defect.

Using the analysis presented in section 5, it is possible to calculate the combined probability of initiation of crack growth (or the probability of 2 mm stable crack growth) for an entire insert. To perform this analysis a simple scaling argument has to be applied.

8.1 Number of surface defects in the insert

8.1.1 Number of surface defects using fractographic data from the broken test specimens

The fractographic data from the broken test specimens [8-10] are utilized to estimate the surface density of defects. There are 90 such specimens, with a total of 100 defects observed on the fracture surfaces, i.e. on average 1.1 defects per surface area, or 0.0072 defects/mm^2 since the surface area of the broken test specimens is around 154 mm^2 (see Fig. 8-1). This measure can, however, not be directly used as an estimate of the surface density of defects since the defects play an important role in initiating the fracturing of the test specimens. If the fracture is initiated by a defect, this defect will always be observed on the fracture surface, meaning that the fracture surface is not representative of the average conditions in the bulk of the test specimen.

$d = 14$ mm
$L_0 = 70$ mm
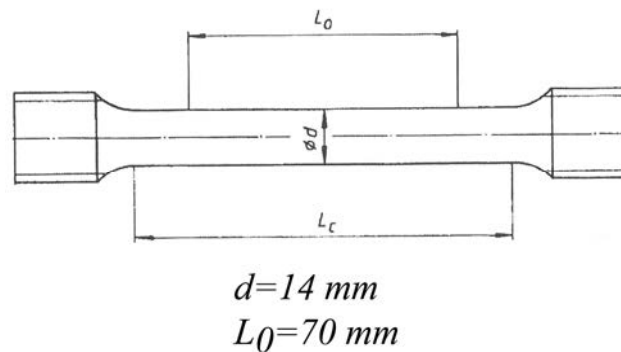
Figure 8-1. Tensile test specimen.

Examination of the fractographic data [8-10] reveals that, out of the 90 samples

- no defects are observed on 34 surfaces.
- 1 defect is observed on 28 surfaces.
- >1 defects are observed on 28 surfaces.

It is, furthermore, noted that the occurrence of more than one defect on a surface is predominantly observed on specimens taken from the top and the bottom of the insert, whereas specimens taken from the main part of the insert predominantly exhibit no defects or one defect. This indicates clustering at the top and bottom parts of the insert and there is currently not enough data to address clustering in the estimate of an overall surface density of defects. The following analysis, therefore, is not valid for the top and bottom parts of the canister insert, whereas it does cover the main part of the insert.

Since the specimens with two or more defects are associated with the top and the bottom, these specimens are excluded from the data set. Hence the 28 surfaces with one defect and the 34 surfaces with no defects are considered in the following. It is, furthermore, assumed that the specimens with no observed defects on the fracture surfaces are entirely free from defects (otherwise the fracture would be initiated by the defect and it would hence be observed).

It is reasonable to assume that the number of defects in a test specimen is Poisson distributed. If the mean value of this distribution is denoted λ, then the probability of finding no defects in a specimen, $p(0)$, is $e^{-\lambda}$. Since 34 out of the 34+28 samples had no defects on their fracture $p(0)$ is estimated at 34/62 and hence $\lambda \approx -\ln(34/62) \approx 0.60$ defects/specimen.

The relevant volume of each specimen is $70 \cdot 154$ mm^3 (see Fig. 8-1), meaning that the volume density of defects, ρ_V is obtained as $0.60/(70 \cdot 154) \approx 5.6 \cdot 10^{-5}$ defects/mm^3.

The defects are observed as ellipses with a mean value of their minor axes of 1.3 mm (see Sect. 2.4) and a mean aspect ratio of 1.7 [8-10], meaning that the mean value of the major axis is estimated at 2.2 mm. The average defect may then be approximated by a circle of radius r_d equal to half the geometric mean of the major and minor axes, yielding $r_d \approx 0.875$ mm. The relationship between ρ_V and ρ_S can now be written

$$\rho_S = 2 \cdot r_d \cdot \rho_V \tag{8.1}$$

since, on average, defects with their center located within a distance $\pm r_d$ from the surface would be observed. This way of estimating the surface density of defects yields $\rho_S \approx 9.8 \cdot 10^{-5}$ defects/mm^2.

The critical part of the insert mantle area is estimated as a relevant length of the insert multiplied by a relevant part of the circumference of insert. This critical part of the insert should be chosen to be the part of the insert where large tensile stresses from the rock shear displacement occur. The maximum length, in the axial direction, is approximately 50% of the entire length of the insert (see Fig. 8-2). This length is equal to $0.5 \cdot 4573 = 2286.5$ mm.
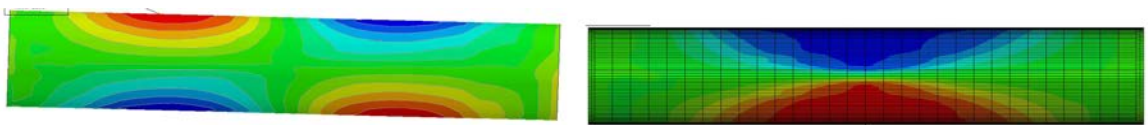
Figure 8-2.   Identification of the part of the insert, in the axial direction, where large tensile stresses are found (the location are mainly dependent on the position of the rock shear plane). The part of the insert with large tensile stresses is identified with a red color.

Next, the length in the circumferential direction should be identified. As shown in Fig. 8-3, the part of the insert where large tensile stresses from the rock shear displacement occur is approximately a sector with an angle of 90°.
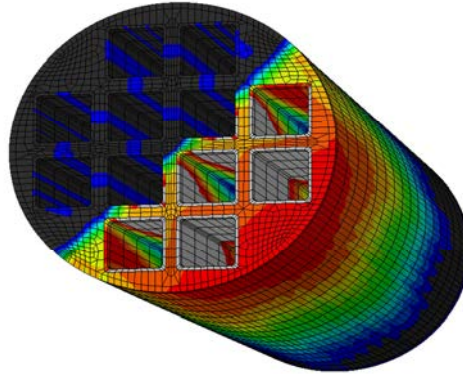
Figure 8-3.   Identification of the part of the insert, in the circumferential direction, where large tensile stresses are found (the part of the insert with large tensile stresses is identified with a red color).

The length in the circumferential direction is then given using the outer radius (474.5 mm) of the insert, $2 \cdot \pi \cdot 474.5 \cdot \frac{1}{4}$ mm ≈ 745 mm.

The critical part of the insert mantle area is thus $745 \cdot 2286.5$ mm$^2 \approx 1.7 \times 10^6$ mm^2. With $\rho_S \approx 9.8 \cdot 10^{-5}$ defects/mm^2 according to the above, this yields the total number of defects on the surface as n ≈ 167.

In summary, a rough estimate of the number of defects on the most exposed area on the canister insert yields a value of n ≈ 167. This method assumes that there is no clustering of defects and the result is, therefore, not representative for the top and bottom parts of the canister where there is indications of clustering.

8.1.2   Number of surface defects using data from non-destructive testing of the inserts

SKB has conducted non-destructive testing (magnetic particle testing) of the complete surface of three PWR inserts [19-22]. The number of reportable defects found on the surface were between two and nine defects (all defects are assumed to be crack like defects which is a pessimistic assumption). The found defects had a defect length between 2 mm and 4 mm (the inspection should report any indications of a length of 1.5 mm or larger). Assuming that the defect depth is equal to the measured defect length, the maximum number of surface defects in an insert is nine with a defect depth of 2 mm or larger. Using the defect depth distribution, given in sect. 2.4, approximately 20 % of the defects are larger than 2 mm. Using this assumption, the scale factor 9/0.20 = 45 surface defects are obtained in the insert (which is larger than the relevant part of the insert).

Table 8-1. Number of surface defects in the insert (scale factor n).

Assumption	Scale factor n
Using data from the tensile test specimens	167
Using data from non-destructive testing	45

8.2   Does the insert fail in the case of an earthquake induced rock shear load?

Since it is now known how many defects that is present on the surface of the insert, it is possible to calculate if an insert will fail in the case of an earthquake induced rock shear load. The calculations are based on the critical event that was used in the deterministic damage tolerance analysis of an earthquake induced rock shear load [4], i.e. 2 mm stable crack growth.

Assuming statistical independence, the combined probability of failure will be

$$P_{failure}^{combined} = 1 - \left(1 - P_{failure}\right)^{n} , \tag{8.2}$$

where $P_{failure}$ is related to the given critical event (2 mm stable crack growth) and n is the scale factor as given in Table 8-1.

As a basis, the probabilistic analysis presented in section 5.3 with four probabilistic parameters (fracture toughness, defect depth, shear plane position and the bentonite density) is used. In Fig. 8-4, the baseline case (with no scaling) is compared with the probability of failure of an insert (using two different scale factors).
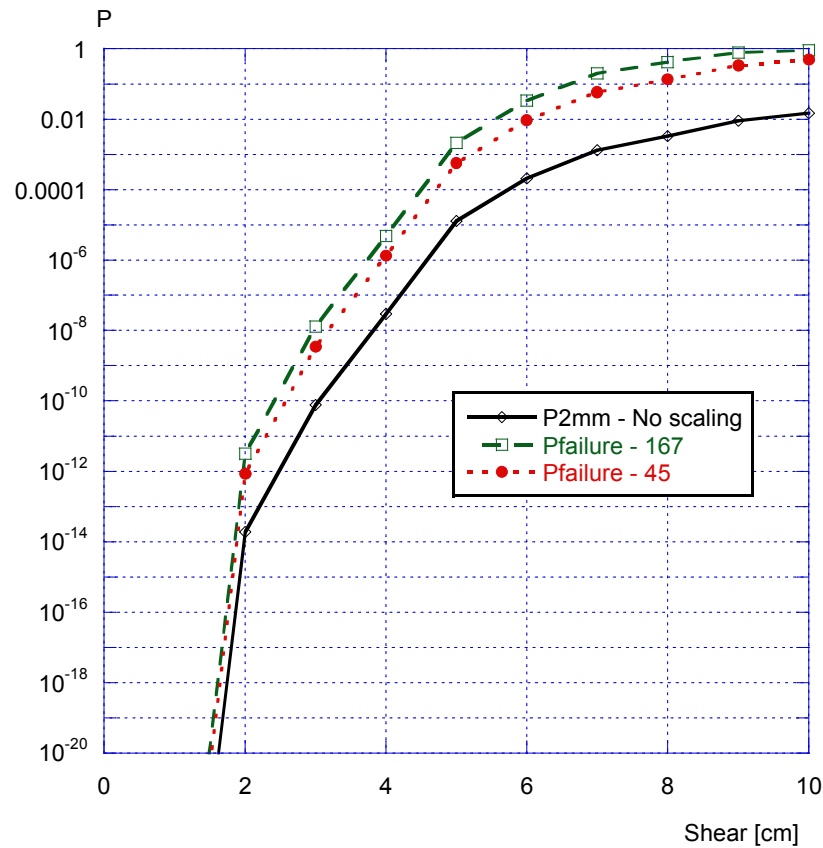
Figure 8-4.   Probability of failure of an insert compared with the baseline case (with no scaling) as a function of the size of the rock shear displacement.

As shown in Fig. 8-4, the probability of failure of an insert, using a rock shear displacement of 5 cm, is between $5.83 \cdot 10^{-4}$ (n=45) and $2.16 \cdot 10^{-3}$ (n=167).

In the analysis presented above, there is no link between the size of the rock shear displacement and the probability of occurrence of a shear of that size (for any given canister/insert). The probability of occurrence of a rock shear displacement is equal to one, independent of the size of the rock shear displacement.

In the safety assessment SR-Site it was assumed that shear up to 5 cm does not cause failure of a canister and all movements above 5 cm do. It could be interesting to compare the results from Fig. 8-4 with the assumption from SR-Site. Such a comparison is presented in Fig. 8-5 to Fig. 8-6.
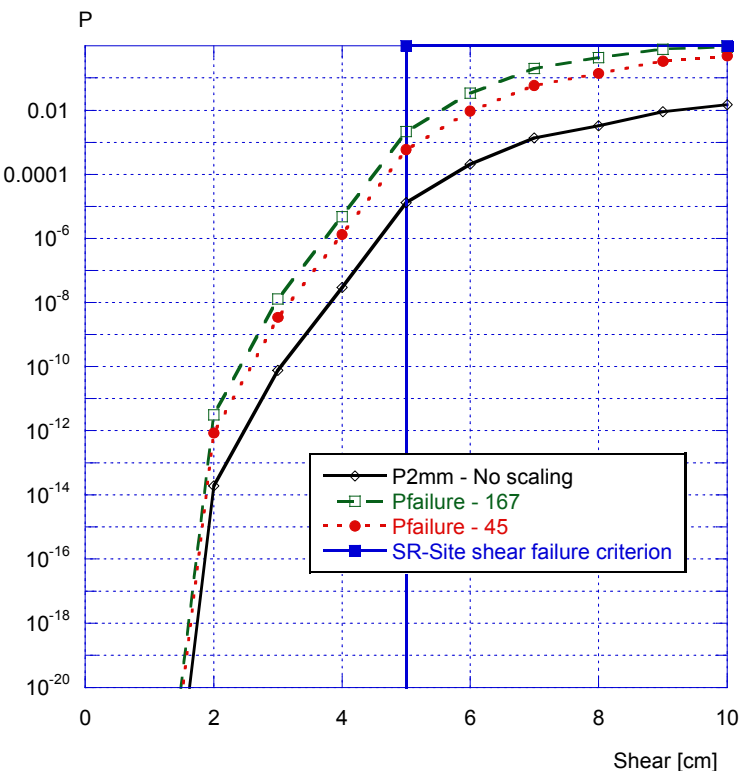
Figure 8-5.   Probability of failure of an insert compared with the baseline case (with no scaling) and the failure criterion from SR-Site as a function of the size of the rock shear displacement (logarithmic scale).
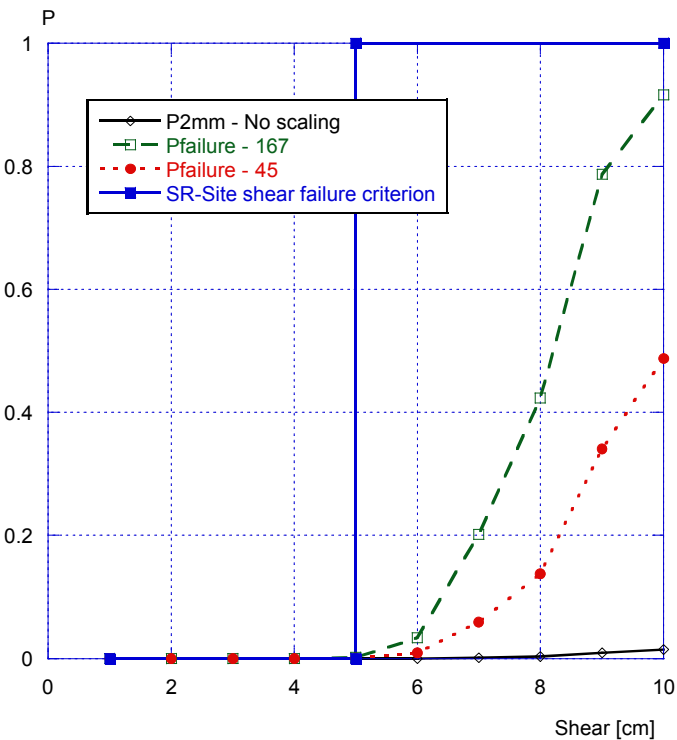
Figure 8-6.   Probability of failure of an insert compared with the baseline case (with no scaling) and the failure criterion from SR-Site as a function of the size of the rock shear displacement (linear scale).

In Sect. 7.3, a comparison was made between using defect distributions evaluated from BWR- and from PWR-data. This comparison is also of interest here, to see how it influences the calculated probability of failure of an insert (given in Fig. 8-7).
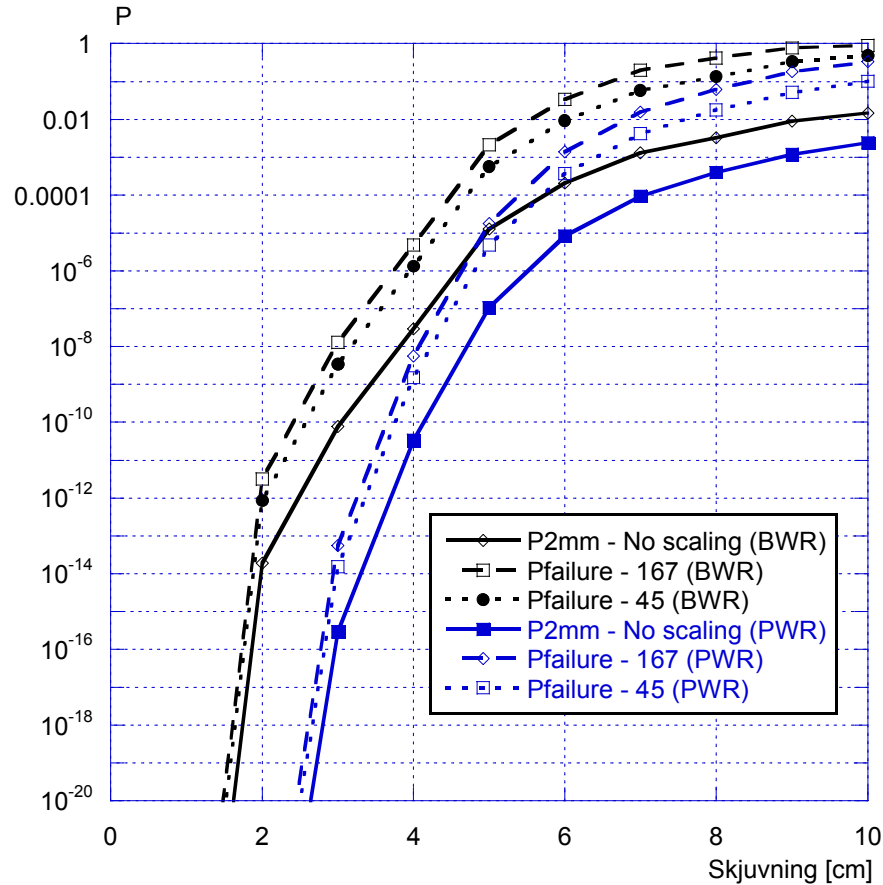
Figure 8-7.   Probability of failure of an insert compared with the baseline case (with no scaling) as a function of the size of the rock shear displacement (sensitivity analysis using defect distributions from BWR- or PWR-inserts).

In theory, this means that if all 6000 canisters in the final repository would be subjected to a 5 cm shear load, then three inserts will fail if $n = 45$ (using data from non-destructive testing) and 13 inserts will fail if $n = 167$ (using data from tensile test specimens). However, these figures are not really meaningful since on average less than one canister out of the 6000 is expected to experience a 5 cm shear movement during one million years [23].

9   CONCLUSIONS

In this report a probabilistic analysis of canister inserts for spent nuclear fuel, that is subjected to an earthquake induced rock shear through a deposition hole, is presented. The analysis is performed using BWR data (canister insert geometry and material's data). First, the important parameters that influence the calculated failure probabilities are identified. Then, a probabilistic analysis is performed for a postulated defect in the region of the insert that experiences the highest impact of a shear movement. These results are subsequently scaled so that results representative for an entire insert are obtained.

A large benefit when conducting a probabilistic analysis is the fact that it is possible to investigate the dependence of the different probabilistic parameters included in the analysis. Several sensitivity studies are presented in order to investigate what parameter that contributes the most to the calculated probability. Also a comparison is made using defect distributions and fracture toughness data from PWR-inserts.

The main conclusions from this study are:
- If the bentonite density is treated as a probabilistic parameter, its importance decreases as compared with the deterministic damage tolerance analysis.
- The shear plane position has no dominant contribution in the probabilistic analysis.
- Assumptions regarding the shear displacement have a large impact on the analysis.
  - When the shear displacement is treated as a deterministic parameter, the fracture toughness and defect size contributes the most to the calculated probabilities.
  - When the shear displacement is treated as a probabilistic parameter, the shear displacement and defect size contributes the most to the calculated probabilities.
- The probability of global plastic collapse is much smaller than the probability of initiation of crack growth and the probability of 2 mm stable crack growth.
- The probability of failure of an insert, using a rock shear displacement of 5 cm, is between $5.8 \cdot 10^{-4}$ and $2.2 \cdot 10^{-3}$.
- The calculated probabilities are much lower using defect distributions and fracture toughness data from PWR-inserts as compared to BWR-inserts.

10   REFERENCES

[1]   RAIKO, H., SANDSTRÖM, R., RYDÉN, H. and JOHANSSON, M., (2010-04), "Design analysis report for the canister", SKB Technical Report TR-10-28, Swedish Nuclear Fuel and Waste Management Co.

[2]   DILLSTRÖM, P., (2005-10), "Probabilistic analysis of canister inserts for spent nuclear fuel", SKB Technical Report TR-05-19, Swedish Nuclear Fuel and Waste Management Co.

[3]   DILLSTRÖM, P., (2013-12-05), "Probabilistisk analys av skjuvlastfallet", Inspecta PM 50011100-1, Rev. 1, Inspecta Technology AB, SKBdoc 1336557, Ver. 2.0.

[4]   DILLSTRÖM, P. and BOLINDER, T., (2010-10), "Damage tolerance analysis of canister inserts for spent nuclear fuel in the case of an earthquake induced rock shear load", SKB Technical Report TR-10-29, Swedish Nuclear Fuel and Waste Management Co.

[5]   DILLSTRÖM, P., et. al., (2008), "A combined deterministic and probabilistic procedure for safety assessment of components with cracks – Handbook", SSM Research Report 2008:01, Swedish Radiation Safety Authority.

[6]   CLAESSON, S., (2011-02-18), "Test of mechanical properties on cast iron inserts for encapsulation of spent nuclear fuel, summary report", SKB Public Report, DocID 1207576, Ver. 2.0, Swedish Nuclear Fuel and Waste Management Co.

[7]   HERNELIND, J., (2013-09-30), "Global simulation of copper canister – final deposition", SKBdoc 1339902, Ver. 1.0, Swedish Nuclear Fuel and Waste Management Co.

[8]   FOURLAKIDIS, V., (2012-08-22), Investigation report 20459 I TOP, Swerea SWECAST AB, SKBdoc 1356755, Ver. 1.0.

[9]   FOURLAKIDIS, V., (2012-08-22), Investigation report 20458, Swerea SWECAST AB, SKBdoc 1356630, Ver. 1.0.

[10]   FOURLAKIDIS, V., (2012-08-22), Investigation report 20459-II-BOTTOM, Swerea SWECAST AB, SKBdoc 1356753, Ver. 1.0.

[11]   DILLSTRÖM, P., and L. ALVERLIND, (2013-12-04), "Defect distributions for BWR- and PWR-insert material", Inspecta Technical Report 50017480-1, Rev. 0, Inspecta Technology AB, SKBdoc 1417759, Ver. 1.0.

[12]   BÖRJESSON, L., GUNNARSSON, D., JOHANNESSON, L-E., and E. JONSSON., (2010-12), "Design, production and initial state of the buffer", SKB Technical Report TR-10-15, Swedish Nuclear Fuel and Waste Management Co.

[13]   —, (2009-11), "Design premises for a KBS-3V repository based on results from the safety assessment SR-Can and some subsequent analyses", SKB Technical Report TR-09-22, Swedish Nuclear Fuel and Waste Management Co.

[14]   HEDIN, A., (2010), "Stereological Method for Reducing Probability of Earthquake-Induced Damage in a Nuclear Waste Repository", Mathematical Geosciences, 43(1), pp 1-21.

[15]   BRICKSTAD, B., (2009-03-17). "Analys av driftinducerade skador i svenska kärntekniska anläggningar", Utredningsrapport 2008/232, Strålsäkerhetsmyndigheten.

[16]   HERNELIND, J., (2010-08), "Modelling and analysis of canister and buffer for earthquake induced rock shear and glacial load", SKB Technical Report TR-10-34, Swedish Nuclear Fuel and Waste Management Co.

[17]   —, (2009-2011), ABAQUS Software, Dassault Systèmes Simula Corp.

[18]   SHIPSHA, A., (2013-12-03), "Statistical data analysis of cast iron properties for PWR-inserts from tension, compression and fracture toughness testing", Inspecta Technical Report 50017490-1, Rev. 1, SKBdoc 1414800, Ver. 1.0.

[19]   GRANKVIST, J., (2012-06-25), "IP23 Topp Magnetic Particle Testing Report", Heavycast Karlstad AB, SKBdoc 1366412, Version 1.0, Svensk Kärnbränslehantering AB.

[20] GRANKVIST, J., (2012-10-16), "IP24 Magnetic Particle Testing Report", Heavycast Karlstad AB, SKBdoc 1366422, Version 1.0, Svensk Kärnbränslehantering AB.

[21] GRANKVIST, J., (2013-01-24), "IP25 Magnetic Particle Testing Report", Heavycast Karlstad AB, SKBdoc 1378224, Version 1.0, Svensk Kärnbränslehantering AB.

[22] GRANKVIST, J., (2013-02-13/14), "Magnetpulverprovning IP 23 / IP 24", SKBdoc 1384432, Ver. 1.0, Svensk Kärnbränslehantering AB.

[23] —, (2011-03), "Long-term safety for the final repository for spent nuclear fuel at Forsmark, Main report of the SR-Site project", SKB Technical Report TR-11-01, Swedish Nuclear Fuel and Waste Management Co.

[24] FÄLTH, B., HÖKMARK, H., and R. MUNIER., (2010-06), "Effects of large earthquakes on a KBS-3 repository. Evaluation of modelling results and their implications for layout and design.", SKB Technical Report TR-08-11, Swedish Nuclear Fuel and Waste Management Co.

11   TABLE OF REVISIONS

Rev.	Activity / Purpose of this revision	Handled by	Date
0	—	Peter Dillström	2013-11-20
1	- All sections / Major revision after review from SKB.	Peter Dillström	2013-12-08
2	- Revised list of references. - Included a deterministic damage tolerance analysis, comparing fracture toughness data from BWR- or PWR-inserts (in Sect. 4.2). - New sensitivity analysis, comparing both defect distributions and fracture toughness data from BWR- or PWR-inserts (new Sect. 7.3, in Sect. 8.2). - New conclusion, comparing data from BWR- and PWR-inserts.	Peter Dillström	2013-12-19
3	- The report is revised according to the review comments in SKBDoc 1420300 Ver. 0.1. - New sensitivity studies introduced in Sect. 7 (new Sect. 7.4 and 7.5).	Peter Dillström	2014-02-26
4	- The report is revised according to the review comments in SKBDoc 1420300 Ver. 0.11.	Peter Dillström	2014-03-08
5	- The report is revised according to the review comments in SKBDoc 1431620 Ver. 0.3.	Peter Dillström	2014-03-13

12   APPENDIX A – *J*-VALUES FROM THE LOCAL FE-ANALYSIS

A complete 3D model of the canister, with the possibility to insert cracks at arbitrary surface positions of the iron insert, was created (see section 4.1) using information from the symmetry model of the canister. This symmetry model was mirrored to give a complete 3D model of the canister. Since the complete canister is modeled without using symmetry the orientation of the iron insert relative to the direction of the shear load could be arbitrarily chosen.

When performing the local FE-analyses, see section 4.2, the largest sub-models were not sufficiently accurate in the original intended location (no rotation of the global model). Therefore a new location was chosen (the global model was rotated 45°) and the results were compared with the original location (for smaller cracks).

The *J*-values obtained using the different global models (rotated 45°) together with the different sub-models are given below (the maximum *J*-value along the crack front).

	Sub-model	1 cm	2 cm	3 cm	4 cm	5 cm	6 cm	7 cm	8 cm	9 cm	10 cm
N1b	a=1mm	0.024	0.083	0.1407	0.1876	0.224	0.2518	0.2743	0.2935	0.3098	0.3243
	a=5mm	0.1191	0.4124	0.6994	0.9326	1.113	1.251	1.363	1.458	1.539	1.611
	a=10mm	0.2233	0.7745	1.313	1.749	2.085	2.343	2.551	2.729	2.88	3.014
	a=20mm	0.4107	1.452	2.498	3.378	4.041	4.546	4.958	5.302	5.595	5.854
N2b	a=1mm	0.2313	1.127	2.701	4.066	5.647	7.296	9.203	11.35	13.62	15.92
	a=5mm	1.178	5.189	12.22	18.87	26.48	34.36	43.6	54.08	65.05	76.15
	a=10mm	2.097	8.909	19.43	30.66	43.43	56.74	72.37	89.96	108.3	126.9
	a=20mm	3.62	15.1	32.77	54.23	77.04	101.8	130.9	162.9	195	226.7
N3b	a=1mm	0.1094	0.436	0.9268	1.857	2.553	3.248	3.826	4.35	4.931	5.604
	a=5mm	0.5226	2.188	4.617	8.077	11.9	15.1	18.3	21.42	24.63	28.11
	a=10mm	0.9279	3.881	8.053	13.09	18.75	24	29.2	34.25	39.35	44.92
	a=20mm	1.614	6.72	13.63	21.45	30.77	40.71	50.02	58.89	67.56	76.79
N4b	a=1mm	0.0414	0.1607	0.3064	0.4511	0.5771	0.6808	0.7657	0.8367	0.8996	0.9554
	a=5mm	0.1897	0.7471	1.429	2.099	2.684	3.161	3.55	3.879	4.173	4.424
	a=10mm	0.3307	1.319	2.525	3.705	4.727	5.55	6.223	6.787	7.293	7.728
	a=20mm	0.5555	2.268	4.365	6.39	8.102	9.455	10.54	11.44	12.24	12.93
N5b	a=1mm	0.3086	1.28	3.127	5.036	7.278	9.913	12.81	15.79	18.83	21.78
	a=5mm	1.449	5.999	14.36	23.61	34.33	47.09	61.15	75.54	90.12	104.5
	a=10mm	2.581	10.33	23.2	38.87	56.93	78.41	101.9	126.1	150.8	175.5
	a=20mm	4.504	17.96	39.84	68.69	102	141.8	183.9	225.3	265.7	304.3

Inspecta

Report No.: 50014130-1   Revision No.: 5

	Sub-model	1 cm	2 cm	3 cm	4 cm	5 cm	6 cm	7 cm	8 cm	9 cm	10 cm
N6b	a=1mm	0.1606	0.6289	1.297	2.381	3.167	3.962	4.883	5.858	6.847	7.934
	a=5mm	0.7532	2.961	6.03	10.33	14.44	18.3	22.74	27.38	32.09	33.63
	a=10mm	1.342	5.28	10.5	16.62	23.39	29.88	37.32	45.09	51.42	55.86
	a=20mm	2.352	9.286	18.05	27.59	39.91	52.24	65.64	79.58	86.87	96.96
N7b	a=1mm	0.0829	0.4135	0.7451	1.056	1.338	1.614	1.97	2.356	2.575	2.709
	a=5mm	0.3805	1.896	3.422	4.84	6.104	7.215	8.268	9.285	10.29	11.17
	a=10mm	0.6625	3.305	5.956	8.392	10.46	12.2	13.73	15.1	16.37	17.5
	a=20mm	1.118	5.479	9.938	13.96	17.27	19.99	22.37	24.46	26.38	28.06
N8b	a=1mm	0.3455	2.289	4.621	7.411	10.64	13.99	17.35	20.75	24.07	27.31
	a=5mm	1.736	9.763	21.51	34.87	50.51	66.73	82.92	99.23	115.5	131.4
	a=10mm	3.146	15.75	35.11	57.56	83.8	111.1	138.5	166	193.8	221.3
	a=20mm	5.26	25.45	61.07	102.6	149.8	196.7	241.7	285	327	366.9
N9b	a=1mm	0.1754	0.7867	2.089	3.125	4.238	5.425	6.806	8.393	10.05	11.74
	a=5mm	0.8858	3.994	9.746	15.22	21.2	27.52	34.75	43.24	52.31	61.55
	a=10mm	1.562	6.968	15.21	24.2	33.79	43.91	55.67	69.39	83.76	98.28
	a=20mm	2.69	11.95	24.5	41.2	57.84	74.87	93.95	115.6	137.3	158.2
N10b	a=1mm	0.0415	0.1615	0.3092	0.4598	0.5911	0.7048	0.8045	0.8987	1.003	1.123
	a=5mm	0.1899	0.7505	1.442	2.135	2.744	3.254	3.686	4.067	4.427	4.749
	a=10mm	0.3309	1.323	2.541	3.74	4.787	5.634	6.331	6.921	7.456	7.916
	a=20mm	0.5557	2.267	4.383	6.408	8.105	9.443	10.52	11.42	12.24	12.94
N11b	a=1mm	0.0415	0.1615	0.3093	0.4602	0.5934	0.7056	0.8055	0.9002	1.005	1.126
	a=5mm	0.1899	0.7508	1.443	2.137	2.747	3.258	3.691	4.073	4.433	4.758
	a=10mm	0.3309	1.323	2.542	3.742	4.79	5.637	6.335	6.925	7.459	7.919
	a=20mm	0.5557	2.267	4.384	6.407	8.102	9.435	10.51	11.41	12.21	12.91
N12b	a=1mm	0.0425	0.1306	0.2195	0.2931	0.3482	0.3903	0.4247	0.4535	0.4781	0.4994
	a=5mm	0.1924	0.6001	1.012	1.353	1.608	1.803	1.962	2.096	2.208	2.309
	a=10mm	0.3321	1.051	1.776	2.374	2.821	3.163	3.44	3.673	3.87	4.045
	a=20mm	0.536	1.738	2.956	3.98	4.748	5.332	5.8	6.191	6.523	6.815
N13b	a=1mm	0.038	0.122	0.2074	0.2786	0.3313	0.3715	0.4041	0.4314	0.4547	0.4751
	a=5mm	0.172	0.5614	0.9583	1.289	1.534	1.721	1.872	2	2.108	2.203
	a=10mm	0.297	0.9844	1.684	2.266	2.699	3.029	3.297	3.521	3.712	3.88
	a=20mm	0.4766	1.635	2.823	3.817	4.564	5.134	5.593	5.98	6.31	6.6

	Sub-model	1 cm	2 cm	3 cm	4 cm	5 cm	6 cm	7 cm	8 cm	9 cm	10 cm
N14b	a=1mm	0.038	0.1223	0.2083	0.2804	0.334	0.375	0.4083	0.4363	0.4604	0.4815
	a=5mm	0.1721	0.5625	0.9619	1.296	1.544	1.734	1.888	2.019	2.13	2.227
	a=10mm	0.2971	0.9857	1.688	2.274	2.711	3.044	3.315	3.542	3.735	3.906
	a=20mm	0.4767	1.636	2.826	3.822	4.572	5.143	5.604	5.989	6.316	6.604
N15b	a=1mm	0.0425	0.1303	0.2184	0.2909	0.3449	0.3861	0.4194	0.4474	0.471	0.4918
	a=5mm	0.1923	0.5987	1.008	1.344	1.595	1.787	1.942	2.072	2.182	2.279
	a=10mm	0.332	1.049	1.771	2.364	2.807	3.145	3.418	3.648	3.842	4.013
	a=20mm	0.5358	1.736	2.953	3.975	4.738	5.32	5.788	6.183	6.517	6.814
N16b	a=1mm	0.1072	0.4074	0.8617	1.667	2.208	2.763	3.184	3.645	4.151	4.682
	a=5mm	0.5277	2.067	4.27	7.428	10.33	12.96	15.45	18.04	20.73	23.52
	a=10mm	0.9344	3.675	7.395	11.81	16.45	20.71	24.73	28.89	33.2	37.68
	a=20mm	1.608	6.334	12.37	19.04	27.31	35.03	42.15	49.46	56.85	64.33
N17b	a=1mm	0.1178	0.4467	0.9105	1.56	2.648	3.3	3.932	4.593	5.142	5.68
	a=5mm	0.5815	2.28	4.673	7.599	11.59	15.33	18.49	21.84	25.14	28.21
	a=10mm	1.03	4.085	8.249	13.11	18.57	24.2	29.35	34.75	39.99	44.89
	a=20mm	1.763	7.009	14	21.63	29.73	39.05	48.53	57.94	66.87	75.09
N18b	a=1mm	0.1024	0.3975	0.8594	1.637	2.152	2.871	3.43	4.074	4.777	5.544
	a=5mm	0.4917	1.993	4.21	7.48	10.19	13.8	16.91	20.27	23.95	28.06
	a=10mm	0.8753	3.534	7.244	11.77	16.27	22.22	27.26	32.67	38.62	45.23
	a=20mm	1.535	6.119	12.19	19.33	28	38.9	47.98	57.39	67.36	78.22
N19b	a=1mm	0.1084	0.4112	0.8155	1.308	2.17	3.191	3.893	4.69	5.171	5.539
	a=5mm	0.5337	2.085	4.15	6.564	9.534	14.5	17.73	21.14	24.53	27.58
	a=10mm	0.9456	3.714	7.34	11.42	15.81	22.85	28.26	33.88	39.38	44.44
	a=20mm	1.626	6.394	12.57	19.11	25.84	36.63	46.92	56.99	66.49	75.09
N20b	a=1mm	0.2266	0.9554	2.376	4.052	6.07	8.371	10.76	13.11	15.47	17.74
	a=5mm	1.126	4.757	11.51	19.76	29.77	41.23	52.99	64.64	76.29	87.67
	a=10mm	2.105	8.627	19.74	33.88	50.98	70.44	90.53	110.8	131.1	151.1
	a=20mm	4.057	16.27	37.39	64.24	96.76	133.6	170.2	205.9	240.9	274.1
N21b	a=1mm	0.2253	0.9104	2.134	3.933	5.884	8.112	10.79	13.6	16.46	19.25
	a=5mm	1.119	4.567	10.47	19.09	28.7	39.56	52.76	66.63	80.55	94.31
	a=10mm	2.096	8.433	18.52	32.63	49.03	67.62	90.21	113.7	137.5	161.1
	a=20mm	4.05	16.18	33.95	60.7	90.68	124.1	164	204.5	244.3	282.8

Report No.: 50014130-1   Revision No.: 5

	Sub-model	1 cm	2 cm	3 cm	4 cm	5 cm	6 cm	7 cm	8 cm	9 cm	10 cm
N22b	a=1mm	0.3039	1.256	3.121	5.058	7.311	9.989	12.9	15.91	18.94	21.89
	a=5mm	1.427	5.896	14.32	23.7	34.53	47.43	61.61	76.04	90.65	105.2
	a=10mm	2.543	10.18	22.91	38.64	56.83	78.52	102.3	126.6	151.2	176
	a=20mm	4.442	17.75	39.25	68.16	101.4	141	182.8	223.7	263.4	301.6
N23b	a=1mm	0.2502	1.024	2.58	4.359	6.395	8.836	11.49	14.2	16.9	19.56
	a=5mm	1.228	5.078	12.29	20.97	30.8	42.81	55.89	69	82.25	95.36
	a=10mm	2.263	9.122	20.71	35.45	52.28	72.71	94.82	117.2	140	162.7
	a=20mm	4.258	17.05	38.06	66.61	99.04	138.1	179.7	220.4	260.4	298.7
N24b	a=1mm	0.0497	0.2725	0.586	0.9333	1.282	1.795	2.07	2.264	2.446	2.583
	a=5mm	0.2303	1.278	2.75	4.312	5.752	7.175	8.58	9.831	10.83	11.52
	a=10mm	0.406	2.264	4.831	7.482	9.749	11.74	13.54	15.27	16.93	18.12
	a=20mm	0.6993	3.978	8.221	12.5	16.11	19.2	21.93	24.63	27.65	30.04
N25b	a=1mm	0.0496	0.271	0.5826	0.9016	1.17	1.432	1.635	1.821	2.005	2.176
	a=5mm	0.2301	1.27	2.721	4.207	5.454	6.637	7.564	8.34	9.083	9.67
	a=10mm	0.4057	2.255	4.803	7.388	9.545	11.56	13.07	14.32	15.45	16.33
	a=20mm	0.699	3.975	8.203	12.57	16.13	19.38	21.79	23.76	25.56	26.93
N26b	a=1mm	0.0497	0.2725	0.5861	0.9323	1.279	1.828	2.091	2.288	2.472	2.615
	a=5mm	0.2303	1.277	2.748	4.307	5.743	7.325	8.784	10.04	11.01	11.71
	a=10mm	0.4059	2.264	4.829	7.478	9.743	11.95	13.82	15.64	17.31	18.53
	a=20mm	0.6993	3.95	8.223	12.58	16.2	19.63	22.5	25.4	28.56	31.05
N27b	a=1mm	0.0496	0.2709	0.5825	0.9014	1.17	1.43	1.633	1.818	2.002	2.17
	a=5mm	0.2301	1.27	2.719	4.203	5.448	6.63	7.555	8.332	9.071	9.656
	a=10mm	0.4057	2.255	4.802	7.384	9.539	11.55	13.06	14.31	15.45	16.32
	a=20mm	0.699	3.974	8.201	12.57	16.13	19.4	21.81	23.79	25.61	27
N28b	a=1mm	0.155	0.7209	1.823	2.775	3.846	5.085	6.531	8.207	9.996	11.79
	a=5mm	0.7281	3.432	7.804	12.74	17.94	23.95	30.83	38.92	47.61	56.34
	a=10mm	1.299	6.009	12.6	20.63	29.3	39.42	51.02	64.61	79.18	93.79
	a=20mm	2.258	10.59	20.97	35.81	51.6	70.41	91.8	116.4	142.9	169.7
N29b	a=1mm	0.0987	0.5016	1.034	1.712	2.754	3.895	5.11	6.336	7.707	9.336
	a=5mm	0.4909	2.496	5.154	8.496	13.14	18.65	24.64	30.63	37.31	45.2
	a=10mm	0.9218	4.671	9.562	15.33	22.58	31.7	41.78	51.95	63.33	76.77
	a=20mm	1.879	9.099	18.2	28.15	41.23	57.57	75.35	93.29	113.8	137.7

Inspecta

	Sub-model	1 cm	2 cm	3 cm	4 cm	5 cm	6 cm	7 cm	8 cm	9 cm	10 cm
N30b	a=1mm	0.155	0.7205	1.828	2.77	3.826	5.07	6.489	8.127	9.883	11.64
	a=5mm	0.728	3.429	7.79	12.68	17.81	23.75	30.51	38.42	46.94	55.46
	a=10mm	1.299	6.007	12.6	20.6	29.22	39.27	50.74	64.11	78.48	92.83
	a=20mm	2.258	10.59	21.03	35.98	51.88	70.78	92.29	117	143.7	170.6
N31b	a=1mm	0.0987	0.5014	1.034	1.708	2.735	3.863	5.051	6.254	7.595	9.173
	a=5mm	0.4908	2.494	5.149	8.48	13.12	18.58	24.48	30.37	36.91	44.54
	a=10mm	0.9218	4.669	9.557	15.32	22.55	31.6	41.58	51.65	62.86	76.01
	a=20mm	1.879	9.097	18.21	28.23	41.43	57.88	75.76	93.86	114.6	138.6
N36b	a=1mm	0.2336	1.209	2.677	4.081	5.707	7.642	9.804	12.06	14.3	16.54
	a=5mm	1.187	5.423	12.29	19.04	26.83	36.16	44.94	56.84	68.9	79.75
	a=10mm	2.109	9.111	19.87	31.23	44.38	57.07	73.45	92.95	112.8	133.4
	a=20mm	3.617	15.2	34.86	55.61	77.11	100.8	129.7	163	197.1	229.8
N37b	a=1mm	0.238	1.145	2.995	4.603	6.475	7.286	8.88	10.68	12.61	14.73
	a=5mm	1.19	5.366	12.68	21.01	30.01	33.8	41.27	49.83	59.64	70.06
	a=10mm	2.124	9.481	20.41	34.1	49.24	55.44	68.03	82.47	98.84	116.1
	a=20mm	3.675	16.49	33.91	58.83	85.42	95.35	118.3	144.5	173.9	203.9
N38b	a=1mm	0.2335	1.207	2.659	4.055	5.643	7.782	9.959	12.21	14.46	16.71
	a=5mm	1.186	5.413	12.24	18.91	26.58	36.87	47.43	58.26	69.21	80.2
	a=10mm	2.108	9.105	19.84	31.14	44.18	61.67	79.41	97.73	116.3	135.1
	a=20mm	3.617	15.22	35.05	55.97	78.45	114.2	147.4	179.2	209.8	240.4
N39b	a=1mm	0.2348	1.139	2.857	4.345	6.039	7.811	9.683	11.67	13.9	16.21
	a=5mm	1.189	5.338	12.13	19.94	28.19	36.65	45.36	55.29	66.15	77.37
	a=10mm	2.123	9.435	19.85	32.52	46.35	60.56	75.33	92.13	110.4	129.1
	a=20mm	3.709	16.44	32.97	56.1	81.02	105.8	133.1	164.2	197.2	229.8
N40b	a=1mm	0.35	2.371	4.607	7.352	10.38	13.49	16.61	19.68	22.68	25.59
	a=5mm	1.751	10.5	21.38	34.51	49.19	64.14	79.14	93.95	108.7	123.1
	a=10mm	3.14	16.42	35.09	57.06	81.75	106.9	132.4	157.5	182.9	207.9
	a=20mm	5.272	26.59	61.97	102.4	146.7	189.6	231	270.7	309.1	345.3
N41b	a=1mm	0.3398	1.825	5.015	8.126	11.49	15.25	19.07	22.82	26.52	30.02
	a=5mm	1.695	8.476	22.56	37.55	53.69	72.02	90.57	108.7	126.6	144
	a=10mm	3.055	14.22	36.48	61.62	88.93	119.7	150.7	181.4	211.7	241.6
	a=20mm	5.128	23.37	62.3	106.6	154.4	206.6	256.9	304.8	350.5	393.6

	Sub-model	1 cm	2 cm	3 cm	4 cm	5 cm	6 cm	7 cm	8 cm	9 cm	10 cm
N42b	a=1mm	0.3443	2.03	4.94	7.735	10.81	13.91	16.95	19.91	22.84	25.75
	a=5mm	1.712	9.742	21.01	35.77	50.75	65.78	80.5	95.06	109.4	123.7
	a=10mm	3.062	15.34	33.56	59.73	84.8	110.2	135.5	160.5	185.5	210.4
	a=20mm	5.12	25.28	57.64	105.7	153.5	198.7	241.8	283	322.2	359.6
N43b	a=1mm	0.3396	1.821	4.978	8.068	11.39	15.12	18.92	22.68	26.25	29.71
	a=5mm	1.694	8.464	22.45	37.32	53.33	71.5	89.9	107.9	125.6	142.6
	a=10mm	3.054	14.21	36.44	61.38	88.48	119.2	150.2	180.6	210.8	240.5
	a=20mm	5.128	23.41	62.72	107.6	156.4	209.9	262.1	311.7	359	403.4
N44b	a=1mm	0.1611	0.6343	1.554	2.354	3.16	4.03	5.053	6.091	7.256	8.524
	a=5mm	0.7544	3.006	6.378	10.71	14.54	18.71	23.58	28.62	31.85	37.68
	a=10mm	1.343	5.28	10.67	17.29	23.74	30.74	38.94	46.63	52.16	62.49
	a=20mm	2.354	9.295	18.08	29.57	41.53	54.09	69.78	79.01	91.43	109.4
N45b	a=1mm	0.1605	0.6282	1.257	2.126	3.195	3.997	4.849	5.801	6.758	7.699
	a=5mm	0.7522	2.957	5.89	9.516	14.29	18.15	22.27	26.83	31.4	35.89
	a=10mm	1.34	5.272	10.38	16.1	22.71	29.22	36.14	43.72	51.32	58.84
	a=20mm	2.351	9.274	18.06	27.27	37.23	49.29	62.64	76.02	89.25	97.01
N46b	a=1mm	0.161	0.634	1.546	2.339	3.133	4.157	5.168	6.295	7.547	7.547
	a=5mm	0.7542	3.003	6.446	10.71	14.56	19.44	24.28	28.53	32.22	38.09
	a=10mm	1.343	5.278	10.67	17.27	23.7	31.95	40.14	45.46	53.63	63.33
	a=20mm	2.354	9.295	18.12	29.72	41.84	56.84	72.65	80.42	96.29	112.8
N47b	a=1mm	0.1605	0.6279	1.252	2.157	3.184	4.166	5.134	6.205	7.295	8.405
	a=5mm	0.7521	2.956	5.882	9.495	14.3	19.07	23.76	28.91	34.09	39.36
	a=10mm	1.34	5.27	10.37	16.08	22.7	30.75	38.67	47.3	55.98	62.74
	a=20mm	2.351	9.272	18.07	27.35	37.43	52.6	67.75	83.07	98.29	105.4

Inspecta

13   APPENDIX B – STRAINS FROM THE GLOBAL FE-ANALYSIS

A complete 3D model of the canister was created (see section 4.1). The model was created using information from the symmetry model of the canister. This symmetry model was mirrored to give a complete 3D model of the canister. Since the complete canister is modeled without using symmetry, the orientation of the iron insert relative to the direction of the shear load could be arbitrarily chosen.

The strain values obtained using the different global models (not rotated) are given below (the maximum true strain in the axial direction which is equivalent to the maximum principal strain).

	1 cm	2 cm	3 cm	4 cm	5 cm	6 cm	7 cm	8 cm	9 cm	10 cm
N1b	2.56E-04	4.52E-04	5.75E-04	6.55E-04	7.09E-04	7.49E-04	7.81E-04	8.06E-04	8.27E-04	8.45E-04
N2b	7.00E-04	1.35E-03	1.93E-03	2.74E-03	3.63E-03	4.63E-03	5.95E-03	7.50E-03	9.14E-03	1.08E-02
N3b	5.05E-04	9.76E-04	1.35E-03	1.66E-03	2.00E-03	2.38E-03	2.80E-03	3.23E-03	3.65E-03	4.10E-03
N4b	2.73E-04	5.36E-04	7.18E-04	8.46E-04	9.37E-04	1.00E-03	1.06E-03	1.10E-03	1.14E-03	1.17E-03
N5b	7.23E-04	1.43E-03	2.21E-03	3.33E-03	4.62E-03	6.40E-03	8.47E-03	1.06E-02	1.28E-02	1.49E-02
N6b	5.34E-04	1.04E-03	1.44E-03	1.77E-03	2.21E-03	2.67E-03	3.20E-03	3.74E-03	4.31E-03	5.00E-03
N7b	3.79E-04	7.59E-04	1.02E-03	1.21E-03	1.35E-03	1.45E-03	1.53E-03	1.59E-03	1.65E-03	1.70E-03
N8b	8.26E-04	1.71E-03	3.10E-03	4.80E-03	6.97E-03	9.32E-03	1.17E-02	1.40E-02	1.62E-02	1.85E-02
N9b	6.52E-04	1.28E-03	1.79E-03	2.46E-03	3.28E-03	4.13E-03	5.13E-03	6.37E-03	7.74E-03	9.14E-03
N10b	2.73E-04	5.36E-04	7.18E-04	8.46E-04	9.37E-04	1.00E-03	1.06E-03	1.10E-03	1.14E-03	1.17E-03
N11b	2.73E-04	5.36E-04	7.18E-04	8.46E-04	9.37E-04	1.00E-03	1.06E-03	1.10E-03	1.14E-03	1.17E-03
N12b	2.56E-04	4.52E-04	5.75E-04	6.55E-04	7.09E-04	7.49E-04	7.81E-04	8.06E-04	8.27E-04	8.45E-04
N13b	2.51E-04	4.47E-04	5.69E-04	6.49E-04	7.02E-04	7.40E-04	7.71E-04	7.97E-04	8.18E-04	8.36E-04
N14b	2.51E-04	4.47E-04	5.69E-04	6.49E-04	7.02E-04	7.40E-04	7.71E-04	7.97E-04	8.18E-04	8.36E-04
N15b	2.56E-04	4.52E-04	5.75E-04	6.55E-04	7.09E-04	7.49E-04	7.81E-04	8.06E-04	8.27E-04	8.45E-04
N16b	4.84E-04	9.27E-04	1.27E-03	1.55E-03	1.91E-03	2.23E-03	2.61E-03	3.03E-03	3.44E-03	3.85E-03
N17b	5.04E-04	9.79E-04	1.35E-03	1.66E-03	1.93E-03	2.22E-03	2.61E-03	2.99E-03	3.35E-03	3.70E-03
N18b	4.98E-04	9.39E-04	1.28E-03	1.58E-03	1.95E-03	2.44E-03	2.94E-03	3.46E-03	4.02E-03	4.66E-03
N19b	4.87E-04	9.33E-04	1.28E-03	1.56E-03	1.79E-03	2.12E-03	2.50E-03	2.90E-03	3.26E-03	3.61E-03
N20b	7.16E-04	1.42E-03	2.33E-03	3.62E-03	5.25E-03	7.26E-03	9.38E-03	1.15E-02	1.36E-02	1.56E-02
N21b	7.16E-04	1.42E-03	2.06E-03	3.07E-03	4.16E-03	5.54E-03	7.41E-03	9.48E-03	1.16E-02	1.38E-02
N22b	7.16E-04	1.42E-03	2.20E-03	3.32E-03	4.61E-03	6.43E-03	8.54E-03	1.07E-02	1.29E-02	1.51E-02
N23b	7.16E-04	1.42E-03	2.19E-03	3.30E-03	4.57E-03	6.33E-03	8.36E-03	1.04E-02	1.25E-02	1.46E-02
N24b	2.88E-04	6.68E-04	9.49E-04	1.17E-03	1.32E-03	1.43E-03	1.53E-03	1.62E-03	1.71E-03	1.80E-03
N25b	2.88E-04	6.68E-04	9.49E-04	1.17E-03	1.32E-03	1.44E-03	1.53E-03	1.60E-03	1.66E-03	1.70E-03
N26b	2.88E-04	6.68E-04	9.49E-04	1.17E-03	1.32E-03	1.45E-03	1.54E-03	1.64E-03	1.74E-03	1.83E-03
N27b	2.88E-04	6.68E-04	9.49E-04	1.17E-03	1.32E-03	1.44E-03	1.53E-03	1.60E-03	1.66E-03	1.70E-03
N28b	5.17E-04	1.10E-03	1.54E-03	2.12E-03	2.81E-03	3.66E-03	4.66E-03	5.98E-03	7.42E-03	8.85E-03
N29b	5.10E-04	1.09E-03	1.53E-03	1.90E-03	2.38E-03	3.03E-03	3.68E-03	4.41E-03	5.28E-03	6.42E-03
N30b	5.17E-04	1.10E-03	1.54E-03	2.12E-03	2.80E-03	3.64E-03	4.61E-03	5.88E-03	7.26E-03	8.63E-03
N31b	5.10E-04	1.09E-03	1.53E-03	1.90E-03	2.38E-03	3.02E-03	3.66E-03	4.38E-03	5.23E-03	6.32E-03
N36b	7.00E-04	1.35E-03	2.08E-03	3.01E-03	4.13E-03	5.59E-03	7.31E-03	9.12E-03	1.09E-02	1.28E-02

Report No.: 50014130-1   Revision No.: 5

	1 cm	2 cm	3 cm	4 cm	5 cm	6 cm	7 cm	8 cm	9 cm	10 cm
N37b	6.76E-04	1.36E-03	1.96E-03	2.80E-03	3.72E-03	4.11E-03	4.94E-03	6.05E-03	7.38E-03	8.84E-03
N38b	7.00E-04	1.35E-03	2.08E-03	3.00E-03	4.09E-03	5.67E-03	7.41E-03	9.16E-03	1.09E-02	1.26E-02
N39b	6.92E-04	1.36E-03	1.93E-03	2.69E-03	3.54E-03	4.40E-03	5.43E-03	6.75E-03	8.20E-03	9.73E-03
N40b	8.26E-04	1.80E-03	3.35E-03	5.28E-03	7.61E-03	9.98E-03	1.23E-02	1.46E-02	1.68E-02	1.90E-02
N41b	8.26E-04	1.70E-03	2.92E-03	4.47E-03	6.40E-03	8.74E-03	1.12E-02	1.36E-02	1.61E-02	1.85E-02
N42b	8.26E-04	1.80E-03	3.33E-03	5.22E-03	7.47E-03	9.74E-03	1.20E-02	1.41E-02	1.62E-02	1.83E-02
N43b	8.26E-04	1.70E-03	2.92E-03	4.44E-03	6.33E-03	8.58E-03	1.09E-02	1.32E-02	1.55E-02	1.78E-02
N44b	5.34E-04	1.04E-03	1.44E-03	1.89E-03	2.36E-03	2.96E-03	3.64E-03	4.37E-03	5.25E-03	6.25E-03
N45b	5.34E-04	1.04E-03	1.44E-03	1.76E-03	2.06E-03	2.49E-03	2.96E-03	3.41E-03	3.86E-03	4.34E-03
N46b	5.34E-04	1.04E-03	1.44E-03	1.89E-03	2.35E-03	3.05E-03	3.73E-03	4.52E-03	5.46E-03	6.49E-03
N47b	5.34E-04	1.04E-03	1.44E-03	1.76E-03	2.06E-03	2.59E-03	3.11E-03	3.62E-03	4.14E-03	4.71E-03